Université catholique de Louvain
Faculté des sciences
Institute of Condensed Matter and Nanosciences
Louvain Drug Research Institute

Synthesis and pharmacological evaluation of lactams as Fatty Acid Amide Hydrolase inhibitors

Axel Morelle
Supervisors: Prof. Raphaël Robiette and Prof. Giulio Muccioli

Louvain-La-Neuve, 2025

"Success consists of going from failure to failure without loss of enthusiasm."

Winston Churchill

Jury composition

President of the jury:

Prof. Yann Garcia, Université catholique de Louvain (Belgium)

External members:

Prof. Catherine Michaux, Université de Namur (Belgium)

Dr Laurent Trembleau, University of Aberdeen (United Kingdom)

Prof. Stéphane Vincent, Université de Namur (Belgium)

Internal member:

Prof. Olivier Riant, Université catholique de Louvain (Belgium)

Supervisors:

Prof. Raphaël Robiette, Université catholique de Louvain (Belgium)

Prof. Giulio Muccioli, Université catholique de Louvain (Belgium)

Remerciements

Réaliser une thèse est un véritable marathon, une course d'endurance où chaque pas est important. Bien que ce soit souvent une aventure en solitaire, je n'aurais jamais pu franchir la ligne d'arrivée sans l'aide précieuse de nombreuses personnes qui ont gravité autour de moi tout au long de ces années. Leur soutien, qu'il soit discret ou important, a été inestimable. Arrêtons là les métaphores de course à pied, celles et ceux qui me connaissent bien savent que la course et moi, cela fait deux... et qu'en plus, je risquerais encore de me blesser ! Il est évidemment difficile de remercier tout le monde sans oublier personne, mais tentons de faire de notre mieux.

Tout d'abord, un immense merci à mon promoteur, le Prof. Raphaël Robiette. Merci de m'avoir accueilli dans votre laboratoire, pour votre suivi attentif, votre bienveillance, et pour avoir su me guider même quand mes angoisses atteignaient des sommets. Vos conseils et votre soutien m'ont souvent aidé à garder le cap durant les moments compliqués.

Je remercie également mon co-promoteur, le Prof. Giulio Muccioli. Merci d'avoir accepté le challenge de la co-promotion et d'avoir été toujours très accueillant lors de mes nombreuses visites impromptues. Grâce à vous, cette thèse a pu devenir le projet interdisciplinaire dont je rêvais.

Je tiens à remercier les membres de mon jury : le Prof. Yann Garcia pour avoir assuré la présidence, ainsi que les Professeurs Stéphane Vincent, Catherine Michaux, Olivier Riant et Laurent Trembleau pour avoir accepté de faire partie de ce jury. Merci pour vos relectures minutieuses et vos corrections avisées, qui ont grandement amélioré ce manuscrit.

Un grand merci à Gabriella et Alain pour leur aide précieuse en RMN, à Laurent pour son assistance avec les HPLC et les analyses de masse, à Catherine Michaux pour notre collaboration sur les études de *docking*, et à

Julien Mignon pour son aide lors des analyses de dichroïsme circulaire. Je remercie également Marc de Wergifosse et Robin Crits pour la réalisation de simulation de spectre de dichroïsme circulaire. Un merci tout particulier à Jessica, dont l'aide va bien au-delà du secrétariat ou du magasin Lavoisier.

Je tiens également à remercier le service Helpdesk pour leur aide précieuse et surtout pour leur patience face à mes problèmes informatiques souvent dignes d'une personne ayant deux fois mon âge.

Merci à tous les membres du labo, actuels ou anciens, qui ont fait en sorte que je me sente bien au quotidien : Stéphanie, Audrey, Julien, Thomas, Ugo, Alexis, Boris, Charles, Julinda, Julien, Arnaud, Madeline, Maxence, Simon, Lei, Juhans, Julien, Maximilien, Judith. Un grand merci à mon ancien encadrant de mémoire, Sébastien, qui m'a accueilli, formé, et fait découvrir la réalité du terrain.

Je tiens à remercier François Pierrard et Pierre Hubert qui ont participé à la relecture de ce manuscrit.

Je remercie mes anciens mémorants, Juhans et Simon, pour leur investissement, leur motivation et leur gentillesse tout au long de leur année à mes côtés.

Merci à toute l'équipe de didactique, anciens et actuels, à LLN : Antonin, Louise, Simon, Martin, Sébastien, Agnès, Catherine, Marine, Nicolas, Guillaume, Joffrey, Thomas, Pascale, Corentin, Justine, Robin, Chloé, Ulysse, Tommy, Jérôme, Gabriel, Nadia, Nadine, et bien sûr Édouard, mon "papa du labo", pour son soutien indéfectible et son amitié précieuse. À Woluwé : Mohamed, Esra, Juhans, Marine, Julien, je vous remercie également pour votre soutien.

À tous les étudiants et toutes les étudiantes à qui j'ai eu l'occasion d'enseigner, un grand merci. Vous m'avez aidé à me découvrir, à comprendre

mes capacités et mes aspirations. Merci aussi à Marc, Nathalie, Stéphanie et Roch, qui m'ont transmis leur passion de l'enseignement.

Ma famille occupe une place spéciale dans ces remerciements. Mes loulous : Benjamin, Gabin et Arthur, mes filleuls et neveu, Gaël et Athénaïs, merci pour tout. Marraine Sophie, je ne serais pas là sans toi, merci pour ton soutien constant et aussi pour ces tables de multiplication et conjugaisons recopiées maintes et maintes fois. Merci aussi à Mamie Thérèse, pour tous ces week-ends d'enfance passés à tes côtés. À ma sœur jumelle, Steffy, ma confidente, merci pour toutes ces heures de discussion et pour ton soutien inconditionnel.

Merci à mes amis de toujours : François R., Johan, François M., François B. Damien, Anita, Martin, Simon, François K., Jordan, Alex, Colin, Mémé, Merlin, François P., Pierre. Vous avez été des piliers durant ces années, et les moments passés ensemble sont autant de trésors.

Un grand merci à tous mes colocataires qui ont partagé ce long chemin avec moi : Aymeric, Alex, Damien, Joël, Baptiste, Léo, Justin et Nathan. Merci pour votre soutien quotidien, votre patience et votre capacité à vivre avec mon stress, surtout au cours des derniers mois de thèse. Un merci tout particulier à toi, Alex, pour ton soutien et tout ce que tu m’as apporté.

Merci à la Summer Holiday Team : François, Jordan et Alex, pour tous ces voyages et souvenirs inoubliables.

Enfin, je tiens à remercier Madame Hocepied, qui a su me transmettre sa passion pour la chimie, et Marc, Philippe et Marc, pour leur soutien de longue date.

Merci à vous tous d’avoir, de près ou de loin, rendu cette thèse possible.

Table of contents

Abstract

This thesis explores the development of lactam inhibitors of the enzyme FAAH (Fatty Acid Amide Hydrolase) using an interdisciplinary approach that combines organic synthesis, pharmacology, and docking studies. This project builds on the research of Marion Feledziak and Josephine Caruano, where M. Feledziak identified the β-lactam **35** as the most effective inhibitor after the study of a series of β-lactams (lead) (**Figure 1**).[1-2] The main objective of this thesis is to better understand the interactions between lactam compounds and FAAH in order to design more effective inhibitors.

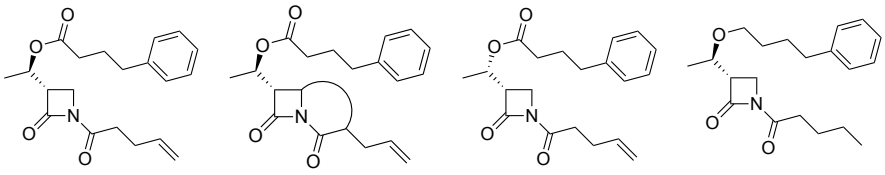

35 **55** **63** **117**

*Figure 1: Lead compound (**35**), bicyclic β-lactam scaffold (**55**), diastereomer (S,S) (**63**) and β-lactam with combined parameters (**117**).*

The first investigations focused on bicyclic compounds to lock the *syn* configuration and avoid the formation of *anti* products (see **Figure 1**). However, pharmacological tests revealed that the bicyclic inhibitors were not as effective as expected, suggesting the influence of other factors. Docking studies confirmed a different interaction mode for the monolactam compounds.

Another aspect of this project was the exploration of the (*S,S*) diastereomer **63** of the lead compound, created by inverting the configuration of the carbon bearing the ester (see **Figure 1**). The synthesis yielded mixtures of the lead compound's stereoisomers. The evaluation of

IC_{50} values for these mixtures, conducted as a preliminary measure, suggested a low influence of the asymmetric centres on inhibition.

Additionally, the thesis examined the influence of the lactam ring size on FAAH inhibition by considering γ-lactams and δ-lactams. Unfortunately, the synthesis of these derivatives could not be completed due to prioritisation issues.

The β-lactam **117**, which combines two parameters studied separately in the pharmacophore investigation, was synthesised and tested (see **Figure 1**).[2-3] This compound showed the best *in cellulo* properties. A docking study was also conducted to understand its mode of interaction with FAAH.

This thesis underscores the importance of an interdisciplinary approach. Docking studies guided the synthesis of new compounds and explained the variations in efficacy observed during pharmacological tests, while pharmacological results refined the docking models. This synergy overcame complex challenges and opened new avenues for the development of FAAH inhibitors.

Résumé

Cette thèse explore le développement d'inhibiteurs lactamiques de l'enzyme FAAH (Fatty Acid Amide Hydrolase) en utilisant une approche interdisciplinaire combinant synthèse organique, pharmacologie et études de *docking*. Ce projet s'inscrit dans la continuité des recherches de Marion Feledziak et Josephine Caruano, où M. Feledziak a identifié le β-lactame **35** comme étant l'inhibiteur le plus efficace après l'étude d'une série de β-lactames (*lead*) (**Figure 2**).[1-2] L'objectif principal de cette thèse est de mieux comprendre les interactions entre les composés lactamiques et la FAAH afin de concevoir des inhibiteurs plus efficaces.

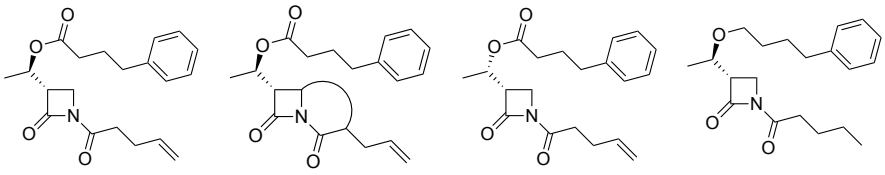

35 **55** **63** **117**

*Figure 2: Composé lead (**35**), Motif des β-lactames bicycliques (**55**), diastéréoisomère (S,S) (**63**) et β-lactames avec les paramètres combinés (**117**).*

Les premières investigations ont porté sur les composés bicycliques pour bloquer la configuration *syn* et éviter la formation de produits *anti* (voir **Figure 2**). Cependant, les tests pharmacologiques ont révélé que les inhibiteurs bicycliques n'étaient pas aussi efficaces qu'attendu, suggérant l'influence d'autres facteurs. Les études de *docking* ont confirmé un mode d'interaction différent des composés monolactames.

Un autre aspect de ce projet a été l'exploration du diastéréoisomère **63** (*S,S*) du lead, créé par inversion de la configuration du carbone portant l'ester (voir **Figure 2**). La synthèse a permis d'obtenir des mélanges de stéréoisomères du lead. L'évaluation des IC_{50} de ces mélanges, réalisés à titre

indicatif, a suggéré une faible influence des centres asymétriques sur l'inhibition.

De plus, la thèse a examiné l'influence de la taille du cycle lactame sur l'inhibition de la FAAH en considérant les γ-lactames et les δ-lactames. Malheureusement, la synthèse de ces dérivés n'a pas pu être achevée en raison de problèmes de priorisation.

Le β-lactame **117**, combinant deux paramètres étudiés séparément lors de l'étude du pharmacophore, a été synthétisé et testé (voir **Figure 2**).[2-3] Ce composé a montré les meilleures propriétés *in cellulo*. Une étude de *docking* a également été réalisée pour comprendre son mode d'interaction avec la FAAH.

Cette thèse souligne l'importance de l'approche interdisciplinaire. Les études de *docking* ont guidé la synthèse de nouveaux composés et expliqué les variations d'efficacité observées lors des tests pharmacologiques, tandis que les résultats pharmacologiques ont affiné les modèles de *docking*. Cette synergie a permis de surmonter des défis complexes et d'ouvrir de nouvelles perspectives pour le développement d'inhibiteurs de la FAAH.

Abbreviations List

Abbreviation	Full term
2-AG	2-arachidonoylglycerol
ABHD	α/β-hydrolase domain-containing 6
AC	Adenylate cyclase
ACB	Acyl chain binding channel
ACN	Acetonitrile
AEA	*N*-arachidonoylethanolamine (anandamide)
AIBN	Azobisisobutyronitrile
Alloc	Allyloxycarbonyl
AMP	Adenosine monophosphate
APCI	Atmospheric-pressure chemical ionisation
ATP	Adenosine triphosphate
BOC	*Tert*-butoxycarbonyl
BSA	Bovine serum albumin
CA	Cytoplasmic access channel
CAN	Cerium ammonium nitrate
cat.	Catalyst
CB	Cannabinoid
CBC	Cannabichromene
CBD	Cannabidiol
CBN	Cannabinol
CBZ	Benzyloxycarbonyl
CD	Circular dichroism
CNS	Central nervous system
CO	Carbonyl
COSY	Correlation spectrometry
DBU	1,8-Diazabicyclo[5.4.0]undec-7-ene
DCM	Dichloromethane

Abbreviation	Full term
DEPT-Q	Distortionless enhancement by polarisation transfer – quaternary
DIAD	Diisopropyl azodicarboxylate
DIBAL	Diisobutylaluminium hydride
DIPEA	*N*,*N*-diisopropylethylamine
DMAP	4-dimethylaminopyridine
DMEDA	*N*,*N*-dimethylethylenediamine
DMF	Dimethylformamide
DMSO	Dimethyl sulfoxide
DPPA	Diphenylphosphoride azide
EC_{50}	Median effective concentration
EDTA	Ethylenediaminetetracetic acid
EMT	Endocannabinoid Membrane transporters
ESI	Electrospray ionisation
FAAH	Fatty acid amide hydrolase
FBS	Fetal bovine serum
FDA	Food and drug administration
Gly	Glycine
GPR55	G protein-coupled receptor 55
*h/r*FAAH	Humanised rat fatty acid amide hydrolase
*h*FAAH	Human fatty acid hydrolase
HIV	Human immunodeficiency viruses
HMBC	Heteronuclear multiple bond correlation
HMPA	Hexamethylphosphoramide
HMQC	Heteronuclear multiple quantum coherence
HPLC	High performance liquid chromatography
HRMS	High-resolution mass spectrometry
HTS	High-throughput screening
IC_{50}	Half-maximal inhibitory concentration

Abbreviation	Full term
LDA	Lithium diisopropylamide
Leu	Leucine
LiHMDS	Lithium hexamethyldisilazide
LPS	Lipopolysaccharides
LSC	Liquid scintillation counting
LTQ	Linear trap quadrupole
Lys	Lysine
MAFP	Methyl arachidonoyl fluorophosphate
MAGL	Monoacylglycerol lipase
MAPK	Mitogen-activated protein kinase
Met	Methionine
MS	Mass spectrometry
Ms	Mesyl
NAAA	*N*-acylethanolamine acid amidase
NAE	*N*-acylethanolamine
NMR	Nuclear magnetic resonance
NOE	Nuclear Overhauser effect
NOESY	Nuclear Overhauser effect sprectrometry
OEA	Oleoylethanolamide
PBPs	Penicillin binding proteins
PEA	Palmitoylethanolamide
Phe	Phenylalanine
PMB	*Para*-methoxybenzyl
PMSF	Phenylmethylsulfonyl fluoride
PPAR	Peroxisome proliferator-activated receptor
R.T.	Room temperature
Rac	Racemic
Rf	Retardation factor
*r*FAAH	Rat fatty acid amide hydrolase

Abbreviation	Full term
SAR	Structure-activity relationship
SEA	Stearoylethanolamide
Ser	Serine
S_N	Nucleophilic substitution
SPE	Solid-phase extraction
TBAF	Tetra-*n*-butylammonium fluoride
TBDMS	*Tert*-butyldimethylsilyl
TFA	Trifluoroacetic acid
THF	Tetrahydrofurane
TLC	Thin layer chromatography
TMAD	Tetramethylazodicarboxamide
TMEDA	Tetramethylethylenediamine
TMS	Tetramethylsilane
TMSCl	Trimethylsilyl chloride
tPSA	Topological polar surface area
TRPV1	Transient receptor potential cation channel subfamily V member 1
Ts	Tosyl
TTMSS	Tris(trimethylsilyl)silane
UV	Ultraviolet
Val	Valine
α_D	Specific optical rotation
Δ^9-THC	Δ^9-tetrahydrocannabinol
μw	Microwave

Usage of AI tools

This manuscript has been partially written using generative AI tools to reformulate and/or translate parts of the text initially written by the author, in accordance with UCLouvain guidelines. The AI-generated content served as inspiration and was subsequently reworked by the author.

Chapter 1: Introduction

1.1 Exogenous cannabinoids

Since the 2nd century AD, cannabis has garnered interest for its medicinal properties.[4] It was quickly observed that its consumption could reduce pain,[5] provide an anti-inflammatory effect, and stimulate appetite.[6] Some accounts report its use dating back to 3000 BC.[6] The main active molecule responsible for these effects is Δ^9-tetrahydrocannabinol **1** (Δ^9-THC), a benzopyran derivative first isolated and characterised in 1964 by Y. Gaoni and R. Mechoulam (**Figure 3**).[7] Although Δ^9-THC has proven therapeutic benefits, its use for medical purposes remains difficult and controversial due to its psychotropic effects. These effects include mood changes (euphoria), alterations in auditory and visual perceptions, hallucinations, depersonalisation disorders, and loss of time perception.[8] Nevertheless, Δ^9-THC is still used in the treatment of some conditions, often in the absence of effective alternatives.

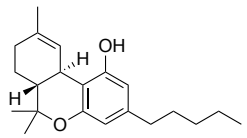

1

*Figure 3: Δ^9-tetrahydrocannabinol (Δ^9-THC) **1**.*

It is important to note that, although Δ^9-THC is the main molecule responsible for the activity of cannabis, the plant contains about 140 cannabinoids.[9] Most of these compounds do not have psychotropic effects. Cannabidiol **2** (CBD) is the most well-known among them,[10] but others such as cannabinol **3** (CBN) and cannabichromene **4** (CBC) also deserve mention (**Figure 4**). However, their mechanisms of action and pharmacological effects are still not well understood.[11-12]

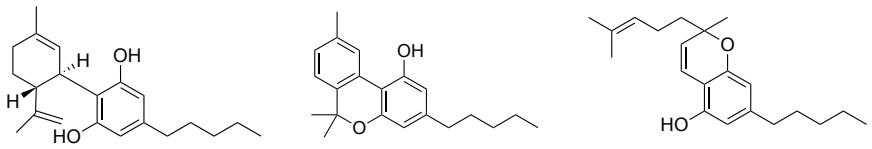

2 **3** **4**

*Figure 4: Cannabidiol (CBD) **2**, cannabinol (CBN) **3**, Cannabichromene (CBC) **4**.*

1.2 Cannabinoid receptors

The study of Δ^9-THC's mechanism of action revealed the existence of a system called the endocannabinoid system, where Δ^9-THC acts as an exogenous agonist and that comprises specific receptors, endogenous ligands (the endocannabinoids) and the associated enzymes responsible for their synthesis and degradation.

The main receptors of the endocannabinoid system are two G protein-coupled receptors named CB1 and CB2 cannabinoid receptors. These receptors have been isolated and their crystal structures elucidated.[13] Although CB1 and CB2 receptors are part of the same system and share many endogenous ligands, they only have 48% structural similarity,[14-15] reaching 68% when considering only the transmembrane segment sequence.[16] Moreover, these receptors are not located in the same areas of the body, or at least not in the same proportions.

The CB1 receptors, named so because they were discovered first in 1988, are highly expressed in the central nervous system (CNS) and play a role in pain modulation and transmission.[17] They are also responsible for the psychotropic effects of Δ^9-THC.[18] The CB2 receptors, discovered in 1993, are mainly found in peripheral tissues, particularly the spleen and immune system cells.[19] They are involved in immune response and inflammation regulation. [20]

Being G protein-coupled receptors, CB1 and CB2 participate in signal transduction (**Figure 5**). They are mainly coupled to G0/i and therefore inhibit adenylate cyclase (AC) activity, which converts ATP into cyclic AMP, a crucial messenger for intracellular information transfer. Additionally, endocannabinoid receptors activate Mitogen-Activated Protein Kinases (MAPK), protein kinases that regulate numerous cell functions including cell differentiation and proliferation, as well as cell survival. Finally, CB1 and CB2 receptors cause cellular inhibition, but only CB1 can inhibit Ca^{2+} and K^{+} channels. [1, 21]

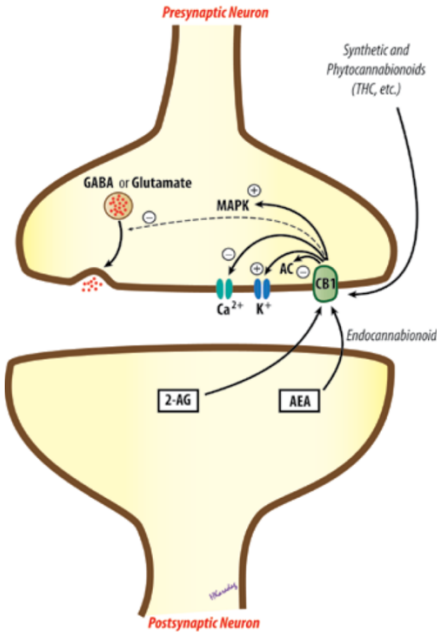

Figure 5: Simplified overview of signal transduction mechanisms for the CB1 Receptor. From [22].

Given the numerous beneficial effects associated with the activation of CB1 and/or CB2 receptors, the design and synthesis of new ligands for these receptors have been the subject of extensive research in medicinal chemistry.[23] However, most developed CB1 agonists have shown undesirable psychoactive effects due to CB1 activation in the central nervous

system.[24] Furthermore, the development of such drugs is complicated by the complexity of endocannabinoid system signalling and the unfavourable pharmacokinetic properties of ligands targeting CB receptors, which are highly lipophilic.[25] Nevertheless, the FDA has approved two cannabinoids: Δ^9-THC **1** (Marinol®) and nabilone **5** (Cesamet®), often used as a last resort to treat nausea and vomiting in chemotherapy patients,[26] and, in the case of Δ^9-THC, to stimulate appetite in HIV patients (**Figure 6**).[27] It is worth mentioning that there are also antagonist ligands for CB1 receptors (notably rimonabant), as well as ligands specific to CB2 receptors. The latter are numerous and have shown promising preclinical results. However, they will not be discussed in this manuscript.

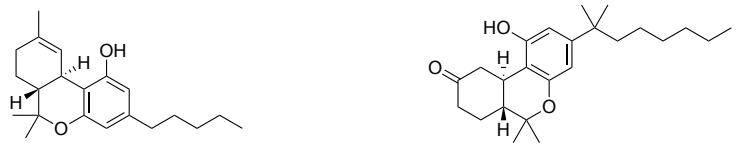

1 **5**

*Figure 6: Δ^9-THC (Marinol®) **1** and nabilone (Cesamet®) **5**. Nabilone is composed of a racemate of the two trans isomers.*

1.3 Endogenous ligands

In addition to exogenous ligands, CB1 and CB2 bind and are activated by endogenous ligands, namely the endocannabinoids. The two main endocannabinoids contain an arachidonic acid motif: *N*-arachidonoylethanolamine **6** (anandamide, AEA) and 2-arachidonoylglycerol **7** (2-AG) (**Figure 7**).[28] These endogenous ligands were discovered after the identification of cannabinoid receptors, which were initially known to bind cannabinoids without identified endogenous ligands.[25] Anandamide was isolated in 1992 from porcine brains,[29] while 2-AG was isolated in 1995 from canine intestinal tissues.[30] Other endogenous ligands such as 2-arachidonoyl-glyceryl-ether **8** and *O*-arachidonoylethanolamine **9** have been

identified, but their physiological importance still needs further clarification.[31]

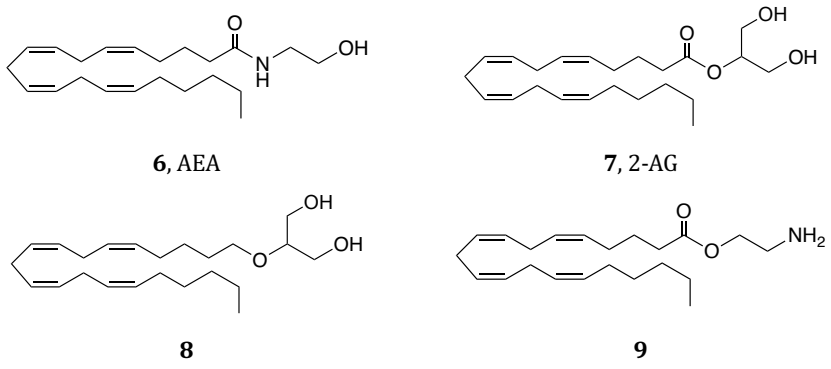

6, AEA **7**, 2-AG

8 **9**

*Figure 7: arachidonoylethanolamine (anandamide, AEA) **6**, 2-arachidonoylglycerol (2-AG) **7**, 2-arachidonoyl-glyceryl-ether **8** and O-arachidonoyl-ethanolamine **9**.*

The median effective concentration (EC_{50}) of anandamide and 2-arachidonoylglycerol is lower for CB1 than for CB2 (**Table 1**), indicating that these two ligands have a higher affinity for CB1 receptors.[32-34] In contrast, Δ^9-THC shows a lower EC_{50} for CB2 than for CB1. Nonetheless, Δ^9-THC has a higher affinity for cannabinoid receptors than the endogenous ligands. While these values are assay-dependent, they give an idea of the affinity of the molecules for the cannabinoid receptors.

*Table 1: EC_{50} values for AEA (**6**), 2-AG (**7**), and Δ^9THC (**1**) for CB1 and CB2.[32-34]*

Agonist	**EC_{50} (CB1)**	**EC_{50} (CB2)**
AEA (**6**)	61 – 89 nM	260 – 371 nM
2-AG (**7**)	58 nM	120 – 145 nM
Δ^9THC (**1**)	37 nM	20 nM

It is important to note that these agonists do not interact with the receptors in the same manner. AEA is a partial agonist for CB1 and a weak agonist for CB2, while 2-AG binds strongly to both CB1 and CB2, showing much higher maximal efficacy compared to AEA.[32-34]

The interaction of endogenous ligands with CB1 and CB2 produces therapeutic effects without the psychotropic effects associated with Δ^9-THC (with the exception of 2-AG, where a significant increase in the CNS (following MAGL inhibition) leads to hypo-locomotion in mice, indicating "psychotropic" effects). Although both Δ^9-THC and anandamide (AEA) are agonists of CB1 receptors, Δ^9-THC has a greater affinity for this receptor. This adds to the fact that AEA is a partial agonist and could explain the psychoactivity of Δ^9-THC. However, the therapeutic use of endogenous agonists is limited by their metabolism (see section 1.4).

In addition to these endogenous ligands, other bioactive lipids deserve mention, such as palmitoylethanolamide **10** (PEA), oleoylethanolamide **11** (OEA), and stearoylethanolamide **12** (SEA) (**Figure 8**).[35] These *N*-acylethanolamines, contrary to AEA, do not bind to cannabinoid receptors and are not considered endocannabinoid ligands.[36-37] However, they share common characteristics with the endocannabinoid AEA, such as biosynthesis, release, and regulation.[38] These lipids create a so-called “entourage effect” and can prolong the effects of endocannabinoids (more specifically anandamide) by delaying their degradation, occupying the common enzymatic cavities of endocannabinoids during their own degradation.[39]

10, PEA

11, OEA

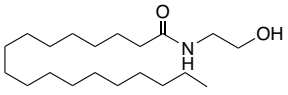

12, SEA

*Figure 8: palmitoylethanolamide (PEA) **10**, oleoylethanolamide (OEA) **11** and stearoylethanolamide (SEA) **12**.*

1.4 Metabolic pathways of the *N*-acylethanolamines

1.4.1 Introduction

Following the discovery of endogenous ligands, research has focused on the biosynthesis and degradation of these ligands by enzymes. In this project, we will focus on degradation.

The agonists of the CB1 and CB2 receptors are produced in an activity-dependent manner from phospholipid precursors present in the cell, and their degradation is controlled by a series of lipases that catalyse their hydrolysis. The endocannabinoids are suggested to be released outside the cell *via* Endocannabinoid Membrane Transporters (EMT) (see **Figure 9**).[1, 40] These EMT, that remain to be molecularly characterised, seem to facilitate the bidirectional transport of the endogenous ligands, as the enzymes responsible for the hydrolysis of 2-AG and AEA are located inside the cell, thereby terminating signal transduction.[41]

The primary enzymes responsible for the degradation of endocannabinoid molecules are Fatty Acid Amide Hydrolase (FAAH) and Monoacylglycerol Lipase (MAGL). AEA is mainly hydrolysed by FAAH, leading to the formation of arachidonic acid and ethanolamine (see **Figure 9**). In contrast, 2-AG is degraded by MAGL into arachidonic acid and glycerol.[1] It is also worth noting that other enzymes can degrade these endocannabinoids. For instance, NAAA can hydrolyse NAE's,[42] and ABHD6 can hydrolyse 2-AG.[43] While several studies have shown the interest of inhibiting these four enzymes (*i.e.* FAAH and NAAA as well as MAGL and ABHD6) to increase the endocannabinoid levels, the focus of the project was on developing FAAH inhibitors, thus in the following sections we will essentially focus on this enzyme and its inhibitors

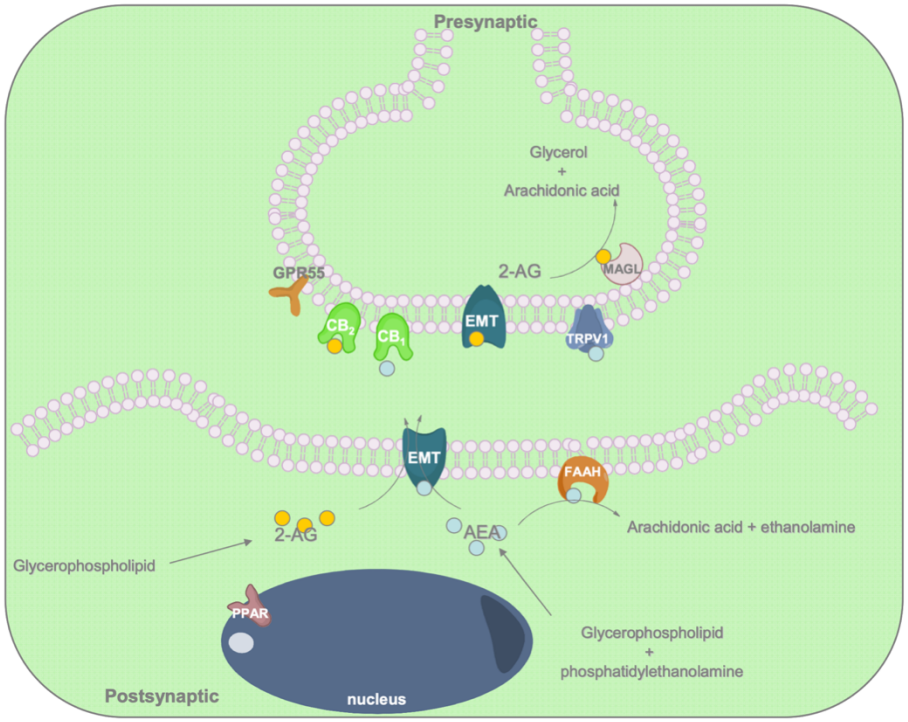

Figure 9: Simplified view of the endocannabinoid system. The diagram includes the two major endocannabinoids, anandamide (AEA) and 2-arachidonoylglycerol (2-AG), as well as their main degradation pathway. Endocannabinoid Membrane Transporter (EMT), G Protein-coupled Receptor 55 (GPR55), Transient Receptor Potential cation channel subfamily V member 1 (TRPV1), Peroxisome Proliferator-Activated Receptor (PPAR). From [1].

1.4.2 Fatty Acid Amide Hydrolase (FAAH)

FAAH is an entirely intracellular enzyme, expressed in a wide variety of tissues.[28, 44] However, its distribution varies among species. In rats, FAAH is primarily found in the liver, small intestine, brain, testes, uterus, kidneys, and spleen, but not in the heart and skeletal muscles.[45-46] In contrast, in humans, FAAH is predominantly present in the pancreas, brain, kidneys, skeletal muscles, and placenta, but less so in the liver.[47] The structure of rat FAAH (*r*FAAH) was first resolved in 2002 by Cravatt et al. with a resolution of 2.8 Å by reacting *r*FAAH with Methyl Arachidonoyl Fluorophosphate

(MAFP).[48] It was shown that the crystal structure of *r*FAAH complexed with MAFP forms a dimer (**Figure 10a**).[48] Analysis of the 3D structure also revealed the presence of two lipophilic channels: the acyl chain binding channel (ACB) which allows access to the catalytic triad from the membrane surface, and the cytoplasmic access channel (CA) which is in contact with the solvent and allows the evacuation of hydrolysis products from the enzyme (**Figure 10b**).[25] This latter channel could also allow the entry of water molecules into the catalytic pocket.[25] It is important to note that the 3D structure of human FAAH has not yet been determined by X-ray diffraction.[49]

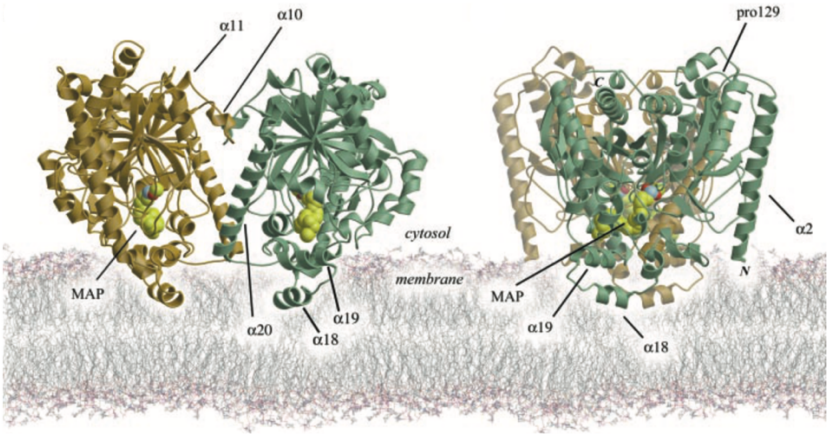

(a)

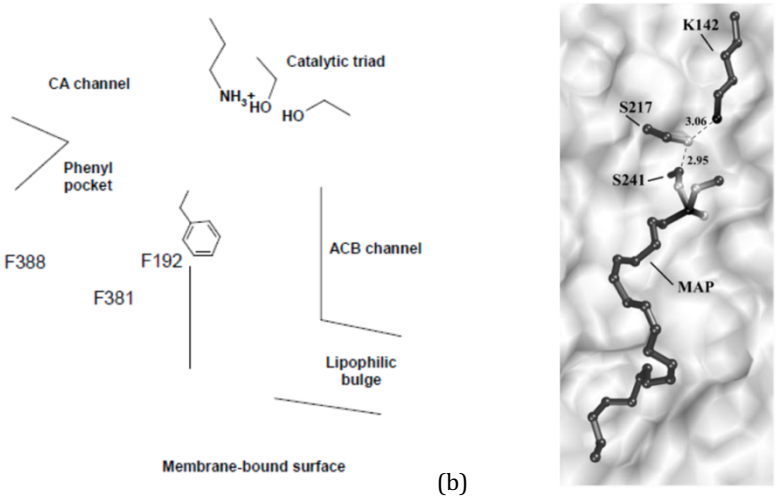

Figure 10: (a) Dimeric structure of rFAAH complexed with MAFP, from [48]; (b) Representation of the catalytic pocket showing the catalytic triad as well as the ACB and AC channels; (c) Catalytic triad of rFAAH, from [50].

FAAH is a membrane-bound enzyme (see **Figure 10a**) and is a serine hydrolase. Its catalytic triad is composed of Ser_{241}-Ser_{217}-Lys_{142} (see **Figure 10c**), enabling it to hydrolyse a wide range of bioactive lipids, including the NAE family, although it is primarily described as an enzyme degrading AEA.[19]

Once the substrate reaches the enzyme's catalytic centre, it interacts with it, allowing the degradation of anandamide. In 2008, Seierstad *et al.* proposed a mechanism for the hydrolysis of AEA by FAAH (**Scheme 1**).[51] First, the nucleophilic character of Ser_{241} is activated by a network of H-bonds with Ser_{217}, which in turn forms H-bonds with Lys_{142}. The alcohol of Ser_{241} then adds onto the carbonyl of anandamide, forming a tetrahedral intermediate (step 1). A subsequent elimination step produces ethanolamine and forms an acyl-enzyme linkage with Ser_{241} (step 2). The presence of a water molecule allows the hydrolysis of this acyl-enzyme bond *via* the formation of a new tetrahedral intermediate (step 3), followed by the elimination of arachidonic acid and the recovery of the intact catalytic triad,

ready for another enzymatic cycle (step 4).[25] Through this process, the concentration of anandamide (and other NAE's) is rapidly regulated in the body.[52]

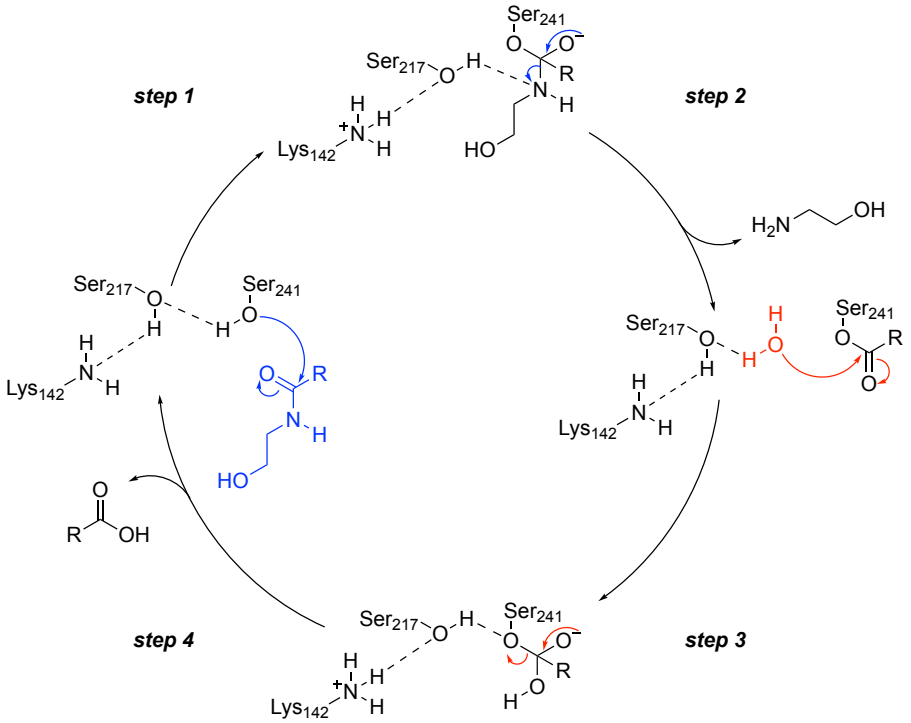

Scheme 1 : Enzymatic cycle for the hydrolysis of anandamide, inspired by [25].

1.5 FAAH inhibitors

1.5.1 Introduction

As previously mentioned, anandamide (AEA) **6** is a preferred substrate for FAAH. This enzyme readily degrades anandamide (and other NAEs) to regulate its concentration in the body. However, AEA has interesting therapeutic effects (analgesic, anti-inflammatory, reduction of anxiety and depression, stimulation of appetite and sleep).[53-55] Therefore, developing an effective FAAH inhibitor would allow for the control and increase of anandamide concentration.[56-57]

There are two types of inhibitors: reversible and irreversible. Reversible inhibitors can interact with their target *via* non-covalent interactions or by forming covalent bonds with an amino acid residue, where the acyl-enzyme bond can be broken, allowing the enzyme to regenerate intact.[58] Conversely, irreversible inhibitors form permanent covalent bonds with FAAH, preventing the enzyme from returning to its initial state and rendering it permanently inactive, hence their designation as "suicide inhibitors".[56]

There are also two generations of inhibitors. Sections 1.5.2 and 1.5.3 will describe these two generations, presenting a few non-exhaustive examples of molecules to illustrate the main characteristics of these inhibitors.

1.5.2 First-generation inhibitors

First-generation inhibitors are characterised by their extremely electrophilic functions, which allow them to interact effectively with the catalytic triad, rendering them irreversible. The first inhibitor of this family, is phenylmethylsulfonyl fluoride (PMSF, **13**), belonging to the sulfonyl family (**Table 2**, entry 1).[59] Molecule **13** has an interesting IC_{50} of 13 µM.[60] However, it lacks selectivity, as it also inhibits proteases.[61] Following this discovery, new inhibitors were developed. These inhibitors possess a motif similar to that of endogenous ligands, with an electrophilic function that allows for very effective interaction with the catalytic triad. Among this generation of inhibitors, several families stand out: fluorosulfonates like arachidonylsulfonyl fluoride **14** (IC_{50} of 0.1 nM)[62] (entry 2), fluorophosphonates such as methoxy arachidonyl fluorophosphonate **15** (MAFP, used for the X-ray resolution of FAAH) with an IC_{50} of 1-3 nM[62] (entry 3), and trifluoromethyl ketones as illustrated by arachidonyl trifluoromethyl ketone **16** with an IC_{50} of 7.5 µM (entry 4).[51]

Table 2: Examples of first-generation inhibitors.

Entry	Name	Structure	IC_{50}
1[60]	phenylmethylsulfonyl fluoride (PMSF)	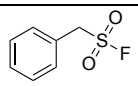 **13**	13 μM
2[62]	arachidonylsulfonyl fluoride	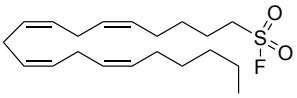 **14**	0.1 nM
3[62]	arachidonyl fluorophosphonate (MAFP)	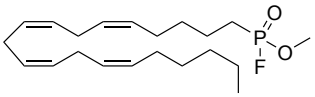 **15**	1-3 nM
4[51]	arachidonyl trifluoromethyl ketone	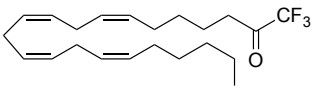 **16**	7.5 μM

However, these molecules are not the best candidates for the development of therapeutic inhibitors. Indeed, these inhibitors are highly reactive and lack selectivity, mainly due to the alkyl chain that increases affinity for other enzymes regulating endocannabinoid ligands (see section 1.4.1).[63] Additionally, these molecules have low water solubility, high plasma protein binding, and can accumulate in adipose tissues, which is not favourable from a biopharmaceutical perspective.[25]

Nevertheless, their study remains interesting as it has provided essential information for the development of new (second-generation) inhibitors, namely:

1. The efficacy of the inhibitor is mainly due to the electrophilicity of the electrophilic centre;
2. The presence of hydrogen bond acceptor groups on the inhibitor allows for favourable interactions with the enzyme;

3. The nature of the lipophilic group on the molecule has little impact on inhibition.[25]

1.5.3 Second-generation inhibitors

A second class of inhibitors was developed based on the lessons learned from first-generation inhibitors. It includes various chemical functions, with the main families being α-ketoheterocycles, carbamates, and ureas.

Regarding α-ketoheterocycles, these are reversible covalent inhibitors.[21] One molecule in this family, molecule **17**, has an oxazolpyridine as a heterocycle and exhibits an IC_{50} of 4.7 nM (**Table 3**, entry 1).[64] This low value is thought to be due to the ability of the pyridine to deplete electrons from the carbonyl of the ligand, thus facilitating the attack by Ser_{241}.[65] Additionally, this molecule appears to be highly selective for FAAH and produces analgesic effects in vivo. Another molecule in the family (**18**), patented by Janssens Pharmaceuticals, has a particularly interesting IC_{50} of 0.4 nM (entry 2).[51]

Table 3: Examples of α-ketoheterocycle-based inhibitors.

Entry	Structure	IC_{50}
1[64]	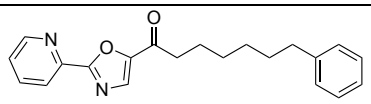 **17**, OL-135	4.7 nM
2[51]	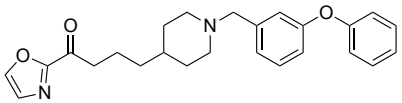 **18**	0.4 nM

Some carbamates, such as compound **19**, are also good inhibitors. The molecule was initially tested as an acetylcholinesterase inhibitor but was

found to be a FAAH inhibitor with an IC_{50} above 30 μM (**Table 4**, entry 1).[66] Other carbamates were then developed to lower the IC_{50} values. These carbamates are irreversible (or slowly reversible) inhibitors of FAAH.[67-68] URB-597 (**20**) is the lead compound of this family and has an IC_{50} of 4.6 nM (entry 2).[69]

Table 4: Examples of carbamate-based inhibitors.

Entry	Structure	IC_{50}
1[66]	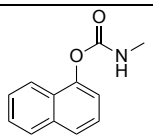 **19**	> 30 μM
2[69]	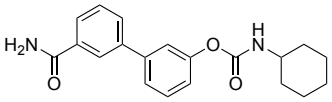 **20**, URB-597	4.6 nM

Some ureas also have the ability to inhibit FAAH. This family of irreversible inhibitors uses the urea carbonyl as an electrophile during the attack by Ser_{241}.[56] One of the first active compounds in this family, developed by Lilly Laboratories (**21**), showed analgesic properties in vivo, although it lacked selectivity (**Table 5**, entry 1).[20, 70] Other examples include compounds developed by Janssen-Takeda (**22**)[71] and Pfizer (**23**)[72] (entries 2 and 3).

Table 5: Examples of urea-based inhibitors.

Entry	Structure	IC_{50}
1[20]	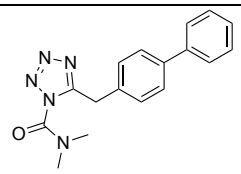 **21**, LY-2183240	12.4 nM
2[71]	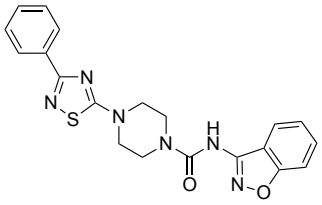 **22**	1 μM
3[72]	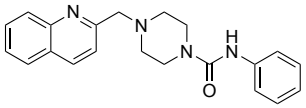 **23**, PF-622	33 nM

Other structural classes show good activity against FAAH occasionally. For example, some boronic acid derivatives, such as **24**, which has an IC_{50} of 9.1 nM and appears to be reversible inhibitor (**Table 6**, entry 1).[73] Additionally, arylheterocycles such as **25** (IC_{50} of 11 nM) are selective non-covalent inhibitors.[74] Benzothiazole derivatives like **26** (IC_{50} of 18 nM), discovered by HTS are selective for FAAH.[75] Pyrimidine derivatives like **27** (IC_{50} of 1 nM) are non-covalent inhibitor.[76-77] This list is not exhaustive but demonstrates the wide variety of chemical functions that can inhibit FAAH.

Table 6: Other examples of inhibitors.

Entry	Structure	IC_{50}
1[73]	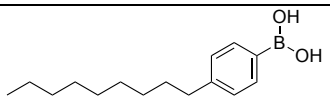 **24**	9.1 nM
2[74]	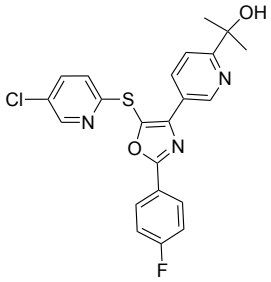 **25**, MK-4409	11 nM
3[75]	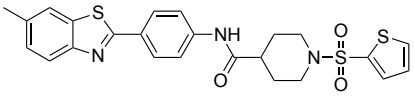 **26**	18 nM
4[77]	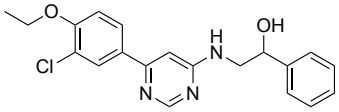 **27**	1 nM

Despite the myriad of molecules capable of inhibiting FAAH, it is pertinent to continue discovering new inhibitors and understanding their mechanisms, as no FAAH inhibitor is yet commercially available as a drug. An example illustrating the need for continued research is the 2016 incident when phase I trials were conducted by BIAL laboratories on the molecule BIA10-2474 (**28**) (**Figure 11**).[78] Developed to treat neuropathic pain, this molecule caused hospitalisation of patients receiving the highest dose (50 mg), with one patient in a state of brain death and others suffering from irreversible brain damage (headaches, consciousness disorders, memory disorders…). One of the hypotheses explaining this failure is the potentially poor selectivity of the molecule for FAAH in humans, binding to other serine

hydrolases in the brain. Another hypothesis is linked to the pharmacokinetics of **28**, causing *in situ* toxicity to cells involved in blood-brain barrier exchanges. It is important to note that the issues associated with the molecule BIA10-2474 are not directly related to FAAH inhibition.

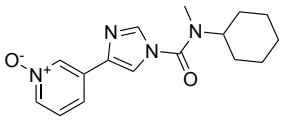

*Figure 11: BIA10-2474 (**28**).*

It is worth noting, however, that the case of BIAL10-2474 remains an isolated incident, unlike other clinical trials that did not lead to such dramatic outcomes. For instance, the molecule PF-0445785, tested in a phase I study in Singapore in 2009, showed promise for treating cannabis withdrawal and dependence in men.[79] Similarly, the molecule JNJ-42165279, whose phase I trials took place in Merksem (Belgium) in 2011, was investigated for treating autism-related symptoms, though its efficacy proved limited.[80]

Chapter 2: Previous results of the laboratory

2.1 Introduction

Our laboratory focuses on β-lactams as FAAH inhibitors. These studies began in 2006 in the group of Professor J. Marchand-Brynaert, in collaboration with Professors D. Lambert and G. Muccioli. A. Urbach, as part of his thesis, discovered that some β-lactam derivatives exhibited an inhibitory activity towards FAAH (**Figure 12**).[81] Originally, these molecules were investigated in the context of serine protease inhibition. However, it was found that they also possessed moderate activity against FAAH. Among the tested compounds, several drew particular attention, notably molecules **29** (IC_{50} = 21.9 µM), **30** (IC_{50} = 4.5 µM), and **31** (IC_{50} = 98 nM). Indeed, in addition to their good activity, it was also demonstrated that these molecules exhibited good selectivity for FAAH compared to MAGL, with respective IC_{50} values for **29**, **30**, and **31** of 817 µM, 657 µM, and 23.3 µM. In 2009, following this discovery, M. Feledziak began exploring this family of β-lactams as FAAH inhibitors as part of her thesis.[1]

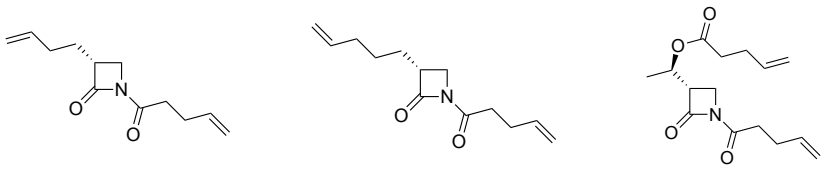

29 **30** **31**

*Figure 12 : **29**: IC_{50}(FAAH) = 21.9 µM; IC_{50}(MAGL) = 817 µM, **30**: IC_{50}(FAAH) = 4.5 µM; IC_{50}(MAGL) = 657 µM and **31**: IC_{50}(FAAH) = 98 nM; IC_{50}(MAGL) = 23.3 µM.*

2.2 Synthesis and structure – activity relationship

A series of 30 derivatives was prepared from commercially available acetoxy-azetidinone **32** (**Figure 13**).[82] The IC_{50} was determined for each of these molecules and the most active compounds were used for a docking study (see section 2.4). Pharmacological tests were conducted on recombinant *h*FAAH.

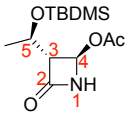

*Figure 13 :Commercially available acetoxy-azetidinone **32** used for the synthesis of the azetidinone derivatives.*

Analysis of the results indicates that inhibition of enzymatic activity is improved when positions C5-O and N1 are acylated by groups featuring a lipophilic chain (**Table 7**). Additionally, the absence of an acetate in position 4, replaced by a hydrogen, also promotes increased inhibition activity. This study led to the identification of a lead compound (**35**) with an IC_{50} value around 5 nM, which is 900 times lower than that of the initial hit discovered (**30**). It is also pertinent to note that this lead compound **35** demonstrates good selectivity for FAAH compared to MAGL, with a variation by a factor of 800.

Table 7 : IC_{50} hFAAH for synthesized azetidinone derivatives. From [82] , only derivatives with data are shown in this table.

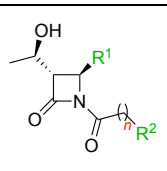

33

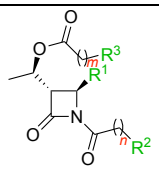

34

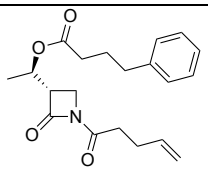

35

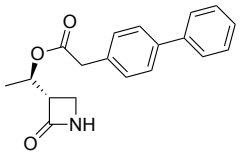

36

Compound	R^1	n	R^2	m	R^3	IC_{50} *h*FAAH[a]	% inhibition (MAGL)[b]	IC_{50} *h*MAGL[a]
33a	OAc	2	Ph			223.6	48	
33b	OAc	3	Ph			182.8	61	
33c	OAc	2	$CH=CH_2$			537.0	16	
33d	H	2	Ph			408.7	8	
33e	H	2	$CH=CH_2$			7.9	89 (8)	
34a	OAc	2	Ph	2	Ph	2.02	100 (0)	
34b	OAc	2	Ph	3	Ph	0.96	100 (0)	
34c	OAc	2	Ph	1	biPh	0.826	66	
34d	OAc	3	Ph	2	Ph	5.12	100 (0)	
34e	OAc	3	Ph	3	Ph	3.12	100 (0)	
34f	OAc	3	Ph	1	biPh	0.708	100 (0)	
34g	OAc	2	$CH=CH_2$	2	$CH=CH_2$	1.9	99 (33)	133
34h	H	2	Ph	2	Ph	0.157	100 (0)	
34i	H	2	Ph	3	Ph	0.049	100 (0)	
34j	H	2	Ph	4	Ph	0.091	100 (0)	
34k	H	2	Ph	1	biPh	0.050	31	
34l	H	3	Ph	2	Ph	0.057	54	
34m	H	3	Ph	3	Ph	0.030	100 (0)	
34n	H	3	Ph	4	Ph	0.045	59	
34o	H	3	Ph	1	biPh	0.032	0	
34p	H	4	Ph	3	Ph	0.449	39	
34q	H	4	Ph	1	biPh	0.236	25	
35	**H**	**2**	**$CH=CH_2$**	**3**	**Ph**	**0.005**	**89**	**4.06**
34r	H	2	$CH=CH_2$	1	biPh	0.012	91	1.84
34s	H	2	$CH=CH_2$	2	$CH=CH_2$	0.098	99	23.3
34t	H	2	$CH=CH_2$	3	$CH=CH_2$	0.032	8	4.72
34u	H	3	$CH=CH_2$	3	Ph	0.010	85	8.51
34v	H	3	$CH=CH_2$	1	biPh	0.014	67	15.6
36	H			1	biPh	6.5	16	

[a] IC_{50} in µM. [b] Percentage of inhibition at 10^{-4}M, in brackets: percentage of inhibition at 10^{-6}M.

The lead compound **35** identified from this β-lactam family exhibits an IC_{50} of 5.2 nM. It shows a median inhibitory capacity similar to the most well-known FAAH inhibitors: boronic acids (**24**),[73] carbamates (**20**),[83] ureas (**37**, **38**, **39**),[83] and pyrimidines (**40**)[83] (**Figure 14**). Following the

identification of this lead compound, pharmacological studies were conducted.

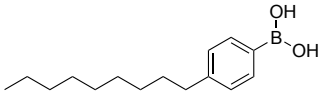

24, IC_{50} = 9.1 nM

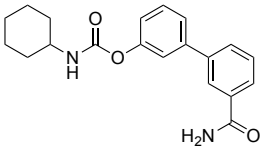

20, *URB-597*, IC_{50} = 4.6 nM

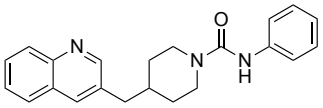

37, *PF-750*, IC_{50} = 33 nM

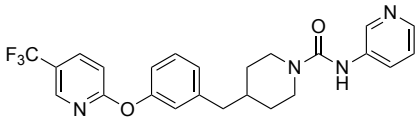

38, *PF-3845*, IC_{50} = 230 nM

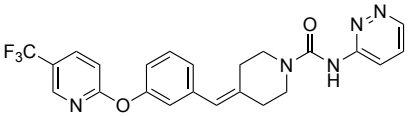

39, *PF-04457845*, IC_{50} = 7.2 nM

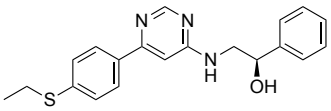

40, IC_{50} = 1.3 nM

*Figure 14 : Examples of FAAH inhibitors exhibiting a similar IC_{50} of the lead **35**.*

From a synthetic perspective, the lead compound which was identified, **35**, can be prepared in five steps from commercially available acetoxy-azetidinone **32** (**Scheme 2**).[82] Initially, the acetate group of **32** is substituted with a thiophenolate to yield **41**. Subsequently, the thiophenolate group is abstracted to obtain **42**, thus allowing a two-step reduction from **32**. Compound **42** is then N-acylated with pent-4-enoyl chloride, leading to **43**, from which the oxygen is subsequently deprotected to form alcohol **44**. Finally, this alcohol can be esterified with 4-phenylbutanoyl chloride to produce the lead compound **35** in 5 steps, with an overall yield of 54%.

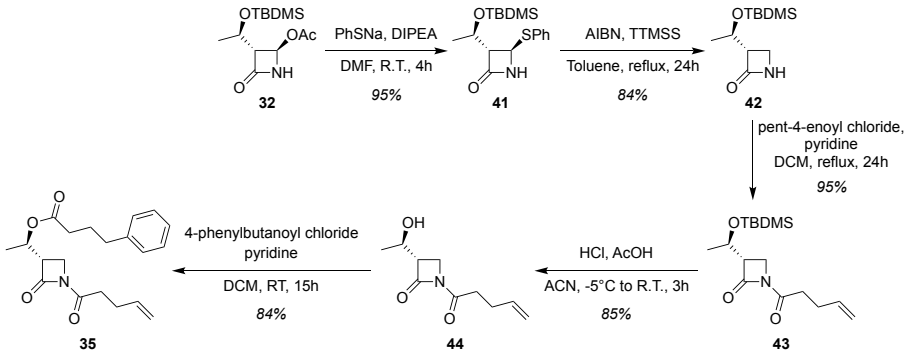

Scheme 2 : Synthesis pathway of lead compound 35r[82].

A structure-activity relationship (SAR) study was undertaken to identify the pharmacophore. Since the lead (**35**) contains multiple carbonyl moieties, the importance of these groups in the activity was evaluated.[3] To do this, analogues of the lead (**35**) were synthesised and their IC_{50} measured after removal of one or more carbonyl functions (**Figure 15**). Obtained results reveal firstly that the lead compound (**35**) remains the most active molecule. Moreover, compound **45** shows similar activity, suggesting that the carbonyl of the ester function does not influence inhibition and likely does not participate in the nucleophilic attack of Ser_{241}. However, when one of the other two carbonyls is absent (imide carbonyls), the IC_{50} increases considerably, suggesting their involvement in the interaction with FAAH. Additionally, the comparison between molecules **46** and **47** shows greater inhibition when the carbonyl is located on the ring (endocyclic carbonyl). It is also noted that the analogue with only the endocyclic carbonyl absent could not be synthesised or tested. However, studying the other structures still allows significant trends to be identified.

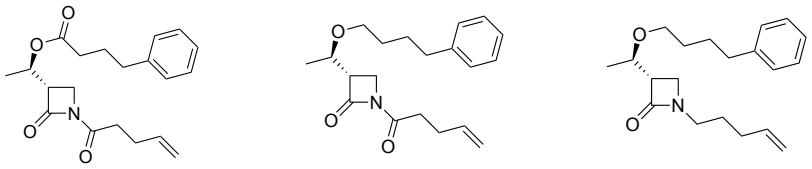

35, IC_{50} = 5.2 nM **45**, IC_{50} = 8.0 nM **46**, IC_{50} = 88.6 µM

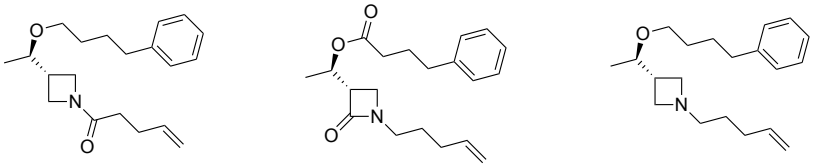

47, IC_{50} = 2.9 µM **48**, IC_{50} = 82.8 µM **49**, IC_{50} > 1000 µM

*Figure 15 : IC_{50} values for the lead and its derivatives: **35**, **45**, **46**, **47**, **48** and **49**.*[3]

2.3 Mode of inhibition

Studies were conducted to determine whether β-lactams **34** and **35** act as reversible or irreversible inhibitors. Several modes of action can indeed be envisaged for these β-lactam compounds. Firstly, the inhibitor may form a stable acyl-enzyme bond with FAAH, leading to irreversible inhibition. It is noteworthy that β-lactams are known as irreversible inhibitors of serine hydrolases such as β-lactamases[84] or DD-peptidases[85] *via* such interactions. Several other scenarios may, on the contrary, lead to a reversible inhibition. Indeed, the β-lactam could form an acyl-enzyme bond that would then be hydrolysed to regenerate the intact and functional enzyme. The β-lactam carbonyl could also react with FAAH to form a tetrahedral intermediate but not subsequent ring-opening of the β-lactam ring, thus allowing reversal and reformation of the β-lactam and enzyme. Finally, the inhibitor could not to form any covalent bond with FAAH and interact with the catalytic site *via* non-covalent interactions. These modes of action would also lead to reversible inhibition.[3]

To establish the mode of action of β-lactams **34** and **35**, M. Feledziak tried to determine whether inhibition is reversible or not. To do this, measurements of FAAH activity recovery after a large and dilution of the

inhibitor-enzyme solution were carried out.[82] This dilution operation enables to rapidly lower the inhibitor concentration. If inhibition is reversible, the enzyme activity will be almost completely recovered, whereas in the opposite case, FAAH activity will remain low. This experiment was carried out with references URB-597[67] (**20**) and methyl arachidonoyl fluorophosphonate[62] (MAFP, **15**), known to be irreversible inhibitors by forming a stable acyl-enzyme bond with FAAH, as well as with CAY-10402[86] (**50**), known to be a reversible inhibitor (**Figure 16**). This experiment was conducted with the β-lactams **35** and **34t**. The results show that enzyme activity is recovered a few minutes after dilution, suggesting reversible inhibition of FAAH (**Figure 17**).[82] To differentiate the three mechanisms leading to reversible inhibition, HPLC studies were then undertaken.

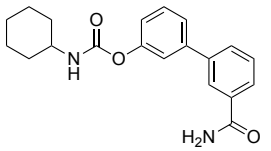

20, *URB-597*, IC_{50} = 4.6 nM

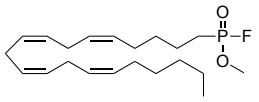

15, *MAFP*, IC_{50} = 1-3 nM[62]

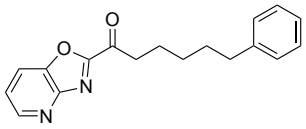

50, *CAY-10402*, IC_{50} = 1.1 nM[87]

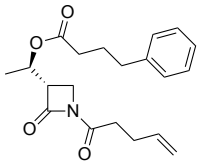

35, *lead*, IC_{50} = 5.2 nM

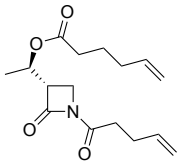

34t, IC_{50} = 32 nM

*Figure 16: molecules used for rapid dilution experiment. References: **20** (URB-597), **15** (*MAFP*), **50** (*CAY-10402*. β-lactams tested: **35** and **34t**.*

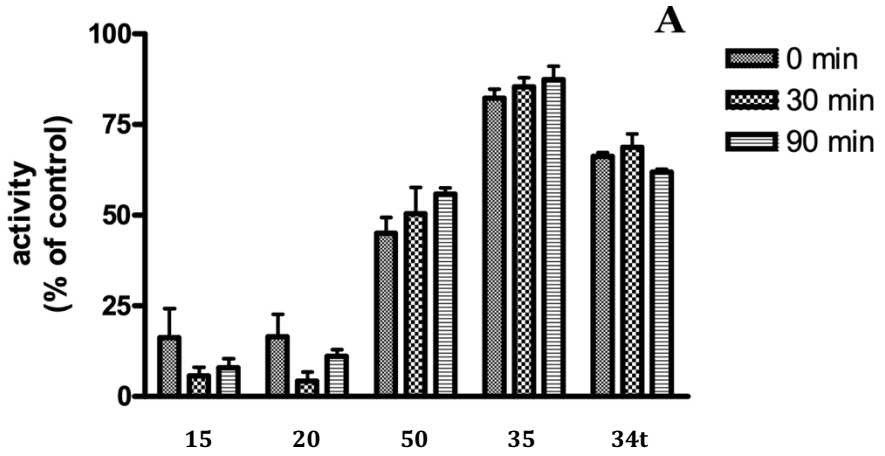

*Figure 17:Test of reversibility (influence of a rapid and large dilution on the recovery of hFAAH activity) for **15** (MAFP), **20** (URB-597), **50** (CAY-10402), **35**, **34t**. From [82].*

In order to deepen the understanding of the mechanism of action of β-lactams on FAAH, especially to determine if the β-lactam ring is opened by the enzyme, an HPLC-MS study was undertaken after an inhibition test.[3] Indeed, mass spectrometry could allow for the detection of a potential ring opening. A first experiment was conducted on a mixture composed of anandamide, liver homogenate (as source of FAAH), and the β-lactam inhibitor **45**. The results indicate that the β-lactam ring was indeed opened (**Figure 18**). This suggests that the ring opening could be due to FAAH or other hydrolases present in the homogenate. The experiment was repeated by adding URB-597 (**20**), a non-selective irreversible reference inhibitor, to the medium. It was observed that in the presence of URB-597, the β-lactam ring was not opened. Finally, a last experiment involved replacing URB-597 with PF-750 (**37**), a highly selective irreversible inhibitor of FAAH. In this case, the β-lactam was predominantly observed in its open form, suggesting that it is other hydrolases that cleave the β-lactam ring. These experiments, combined with reversibility tests (by rapid dilution),[82] lead to the conclusion that β-lactams are degraded by hydrolases but not by FAAH. To confirm these results, the same set of three experiments (without another inhibitor, in the presence of URB-597, and in the presence of PF-750) was

performed using recombinant *h*FAAH. In all three cases, β-lactam **45** was not degraded. This suggests that the mode of action of these inhibitors on FAAH does not rely on the opening of the β-lactam core, unlike the mechanism involved in the inhibition of penicillin binding proteins (PBPs) by β-lactams. This result is interesting as it is consistent with the reversible mode of action suggested by rapid dilution tests.

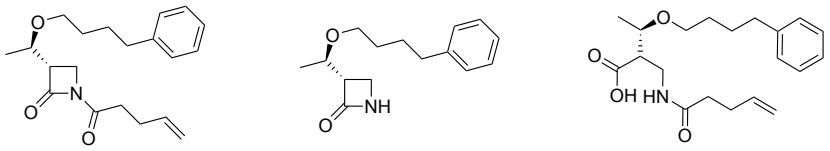

45 **51** **52**

*Figure 18: Structures of the compounds detected by HPLC/MS analysis of **45** and native (or denatured) hFAAH or liver homogenate. From [3].*

2.4 Docking studies

To better understand the mechanism of FAAH inhibition by β-lactams **34** and **35** and their interactions with the enzyme cavity, a molecular modelling (docking) study was undertaken in collaboration with the team of Prof. C. Michaux (UNamur). As the 3D structure of *h*FAAH has not yet been determined by X-ray diffraction analysis, the structure published for a "humanised" rat FAAH (*h/r*FAAH) was used.[88] Initial studies revealed the importance of having one or two water molecules near the catalytic triad in the inhibitor/enzyme complex.[89] The developed models helped to identify new binding modes of the inhibitors. In particular, it was observed that the phenyl group of the lead **35** fits into a pocket composed of three phenylalanine residues (Phe_{338}, Phe_{381}, Phe_{192}), called the "phenyl pocket" (**Figure 19**). The methyl group was also observed to reside in a hydrophobic pocket of the enzyme cavity. As for the carbonyl functions of the imide, their conjugation with the free pair of nitrogen (which is planar) constrains them to be in the same plane, but two conformations are nevertheless possible: the two groups can be in *syn* or *anti*, Docking suggest that the *syn* conformation

is favoured in the catalytic pocket as it allows for stabilisation through hydrogen bonding between the two carbonyls and the serine and threonine residues of the catalytic triad.[88]

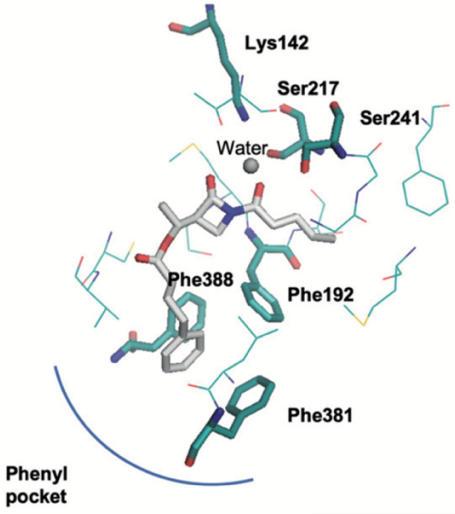

*Figure 19: Docking study conducted on the lead compound **35**. Hydrogens are not shown for clarity. Amino acids are depicted in turquoise, and the lead compound in white. From [49].*

Anti conformer is however inherently more stable than the *syn* form in solution, with a calculated ΔG of 2.5 kcal/mol for **35** (**Scheme 3**). It was thus reasoned that this equilibrium could have a negative impact on the inhibitors' activity.

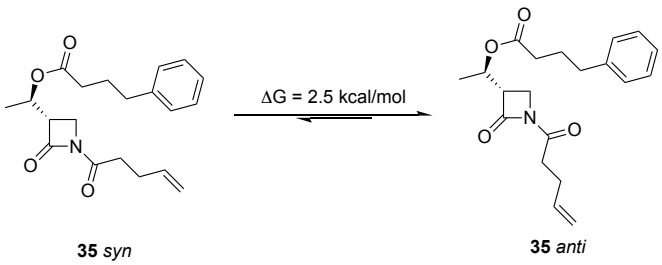

*Scheme 3: Calculated equilibrium between syn and anti conformations of the lead compound **35** (B3LYP-D3/6-31+G*(CH_2Cl_2)).*

2.5 Continuation of the structure-activity relationship study

Based on the promising results from docking and the experimental results obtained up to that point, Joséphine Caruano continued the study of the lead as an FAAH inhibitor in our laboratory (2012-2017).

Initially, considering the docking findings, the lead without the methyl group **53** was synthesised to assess the importance of the methyl and the asymmetric nature of the carbon bearing this methyl. Compound **53** was produced as a racemic mixture, and the two enantiomers were separated by chiral HPLC, although without being able to assign each fraction to a specific enantiomer.[2] The three compounds (the racemic mixture and each enantiomer) were subjected to pharmacological testing. As reported in **Table 8**, the racemic mixture and one of the enantiomers show practically identical activity, while the other compound is inactive. These results suggest that the activity of the racemic mixture is likely solely due to the active enantiomer (**Figure 20**).[2]

*Table 8: IC_{50} values of **53** (lead without the methyl) and its enantiomers.[2]*

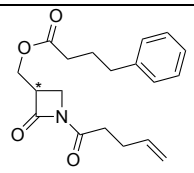

53

Compound	IC_{50}
Rac-**53**	10.3 µM
Enantiomer 1 (**53**)	12.7 µM
Enantiomer 2 (**53**)	> 100 µM
Lead (**35**)	4.2 nM

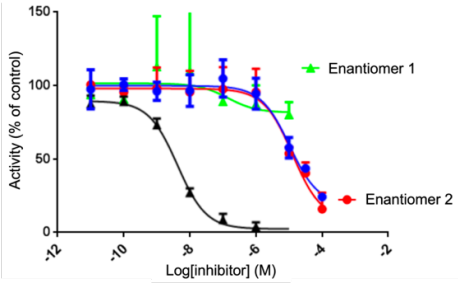

*Figure 20: Inhibition curves of lead **35** (black), racemic mixture of **53**(blue), enantiomer 1 of **53** (red), and enantiomer 2 of **53** (green).[2]*

Subsequently, the lead without the terminal double bond (**54**) was prepared to assess the impact of this unsaturation on the efficacy of inhibition. With an IC_{50} of 8.0 nM, it appears that this double bond is not essential (**Table 9**).[2]

*Table 9: IC_{50} values of **54** (Lead with the double bond reduced).[2]*

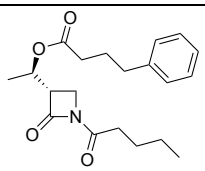	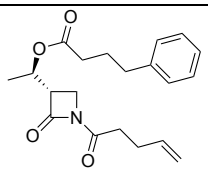
54	**35**
Compound	**IC_{50}**
54	8.0 nM
Lead (**35**)	4.2 nM

Taken together, the works briefly summarised above establish the foundation of this project, the objectives and strategies of which will be detailed in the following chapter.

Chapter 3: Objectives and strategies

In the previous chapter, we presented the results obtained earlier regarding the synthesis and pharmacological evaluation of β-lactams as FAAH inhibitors. This chapter aims to detail the objectives and strategies adopted within the scope of this thesis, arising from the research described in the previous chapter.

3.1 General objectives and methodology

The main goal of this project is to enhance our understanding of the interactions of lactam-type inhibitors with of the catalytic site of FAAH. Simultaneously, we aim to increase the activity and optimise the properties of these inhibitors. To this end, the IC_{50} values of the different molecules obtained will be determined. However, it is essential to note that the primary goal of this project is not to optimise IC_{50} values, which are already very good for our family of molecules (*e.g.* lead compound **35** with an IC_{50} of 4.9 nM). Our main objective is to better understand the mechanism of action of these lactam inhibitors. The IC_{50} values measured will primarily serve as indicators, allowing us to experimentally assess the impact of structural changes on the inhibitory capacity of our molecules, in order to rationalise these results with respect to their mode of action. Of course, although this is not our main goal, an improvement in IC_{50} values compared to the current benchmark would also be a favourable outcome.

To achieve these objectives, our approach relies on close collaborations among three distinct domains of medicinal chemistry: organic synthesis, pharmacological evaluation, and docking. These three domains form a virtuous cycle that enables an iterative approach. Firstly, organic synthesis will allow us to design new lactams that have not yet been synthesized. Once these new molecules are obtained, they will be pharmacologically evaluated, notably by determining their potency. Finally, knowing the activity of our new molecules, docking simulations will be

conducted to interpret the pharmacological results and better understand the interactions of our molecules with the enzymatic cavity responsible for their activity. This docking step will also open perspectives on promising new molecules, thus allowing us to continue this cycle of collaborations.

3.2 Design and synthesis of new lactams

3.2.1 Bicyclic compounds

In Chapter 2, it was emphasised that docking studies highlighted the importance of the interaction between the two carbonyls of the imide function with the Ser_{217} amino acid residue of the catalytic triad, thus necessitating a *syn* conformation of the two carbonyls of the imide function in the β-lactam inhibitor. Calculation indicated that there is an equilibrium between *syn* and *anti* conformations, with the latter being favoured. However, it is also disadvantageous for inhibition. To remedy this situation, we sought to block the molecule in the *syn* conformation, hypothesising that this would increase the activity of the inhibitors. For this purpose, bicyclic scaffold **55** was considered and specifically the bicyclic equivalent **56** of the lead compound (**Figure 21**).

55 **56**

*Figure 21: bicyclic scaffold analogue of the lead (**55**), [4.2.0] bicyclic analogue of the lead (**56**).*

To obtain the desired compound **56**, we chose to start from the acetoxy-azetidinone **32**, which is the closest commercially available compound to the structure of the target molecule. **Scheme 4** describes the retrosynthetic pathway envisaged to obtain the desired product. The ester

56 can be derived from the corresponding alcohol (**57**). Allylation can be accomplished from fragment **59** by deprotonation and addition of the allyl group. Furthermore, the bicyclic core can be obtained through ring-closing metathesis of **61**, which itself can be easily prepared from the commercially available azetidinone **32** (which was already the starting material for the lead synthesis[82]). It should be noted that within the scope of this project, we chose to first form the bicyclic core, then add the α side chain of the imide carbonyl before deprotecting the alcohol and forming the ester. Although the reverse order could have been considered, we deemed it more prudent to proceed with deprotection at the end to avoid any secondary reactions with the ester function, particularly during *N*-acylation.

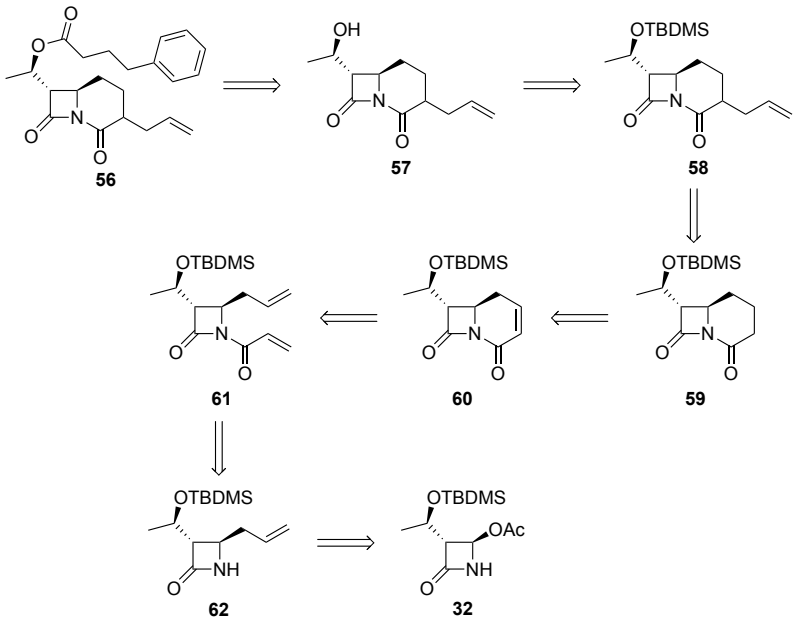

*Scheme 4: Retrosynthetic pathway to obtain **56**.*

3.2.2 Stereoisomers

A second part of this project involves the synthesis of the diastereomer (*S,S*) (**63**) of the lead compound **35** (**Figure 22**). This approach aims to investigate the impact of the stereocentre bearing the

phenylbutanolate group. Docking analyses indicate that the methyl associated with this carbon resides in a cavity where it establishes hydrophobic interactions. By reversing the stereocentre bearing the ester, the three-dimensional arrangement of this group within the cavity will be altered. This alteration could potentially affect the inhibitor's affinity for FAAH, thus providing an opportunity to study the importance of the stereocentres configuration on inhibitory capacity.

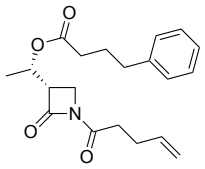

*Figure 22: Diastereomer of the lead (**63**)*

The synthesis of the diastereomer **63** of the lead also starts from acetoxy-azetidinone **32**. **Scheme 5** outlines the retrosynthetic pathway envisioned to obtain compound **63**. This compound can be synthesised through esterification from alcohol **64**, which can be obtained by reversing the absolute configuration of alcohol **44**. It is worth noting that this inversion had already been explored in various ways by J. Caruano, without yielding conclusive results.[2] Thus, we will have to investigate a more effective approach to obtain it. Alcohol **44** can be produced by deprotection of molecule **43**, which is formed by the abstraction of the acetate group from azetidinone **3**.

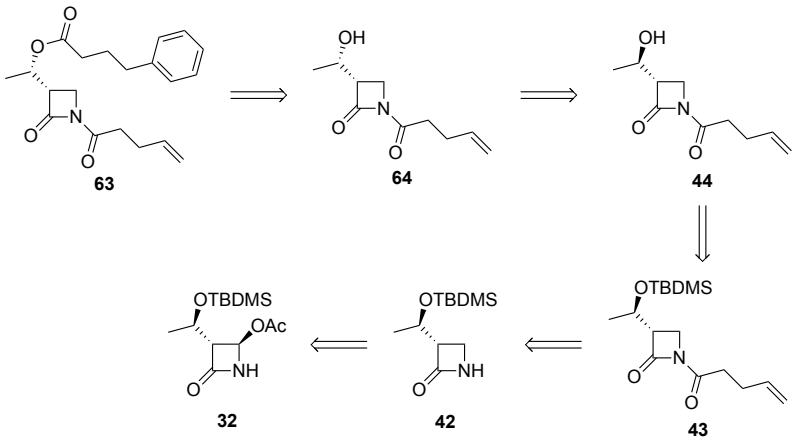

*Scheme 5 : Retrosynthetic pathway to obtain **63**.*

3.2.3 Other lactams

Another of our objectives is to examine the role of the β-lactam ring itself on FAAH inhibition. Until now, lactams have never been considered as FAAH inhibitors outside of our group's research. As pharmacological and docking studies showed that the specific reactivity of the β-lactam ring does not alter the activity, it is pertinent to inquire whether other lactams might exhibit promising activity. In particular, we found it interesting to vary the size of the lactam ring moiety. Accordingly, we are planning to synthesise γ-lactam **65** and δ-lactam **66** equivalents of the lead compound **35** (**Figure 23**). These modifications will influence not only the size of the ring itself but also the three-dimensional arrangement of the side chains. These compounds could also potentially offer greater physiological stability by being less rapidly hydrolysed by other enzymes. Therefore, we will be able to analyse these influences by comparing the activity of molecules **65** and **66** with that of the lead compound.

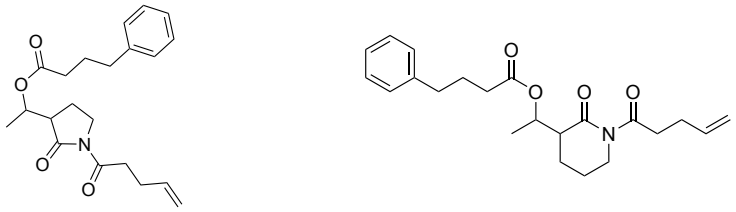

65 **66**

*Figure 23: γ-lactam equivalent of the lead (**65**) and δ-lactam equivalent of the lead (**66**).*

To obtain γ-lactam **65**, we envisage synthesising it through the *N*-acylation of **67**, which could be obtained by deprotection of the nitrogen of lactam **68** (**Scheme 6**). For this, an esterification with the alcohol derived from **69**, itself resulting from the reduction of the ketone of **70**, can be carried out. Regarding the latter, it can be obtained in two ways: either by protecting the nitrogen of lactam **71**, or by the α-acylation of the lactam **72** carbonyl.

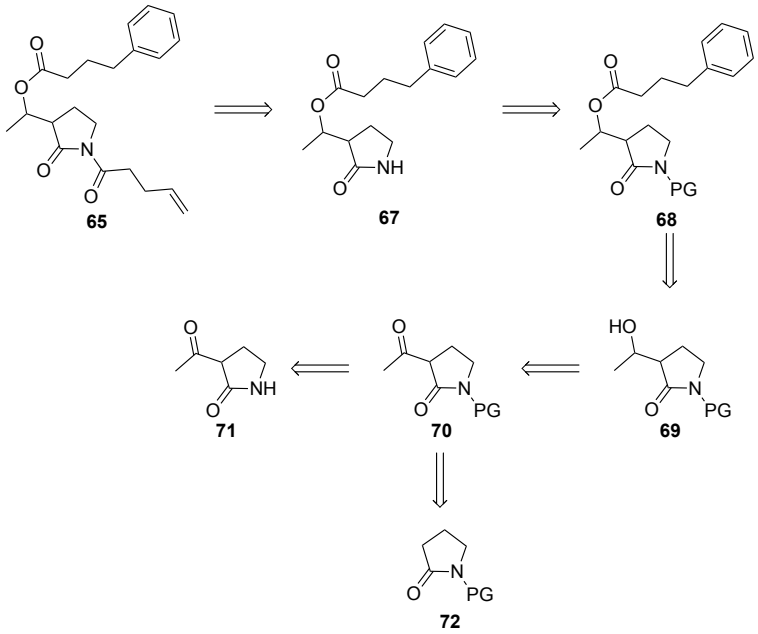

*Scheme 6 : Retrosynthetic pathway to obtain **65**.*

For the synthesis of δ-lactam **66**, we plan to use commercially available δ-valerolactam **78** (**Scheme 7**). For this, an esterification with the

alcohol of **73**, obtained by reduction of the ketone of **74**, can be carried out. The imide function could be generated by *N*-acylation of lactam **75**, derived from the deprotection of the nitrogen of **76**. The latter differs from δ-valerolactam **78** by the presence of a protecting group on the nitrogen and an acetyl group in α position of the carbonyl of δ-lactam.

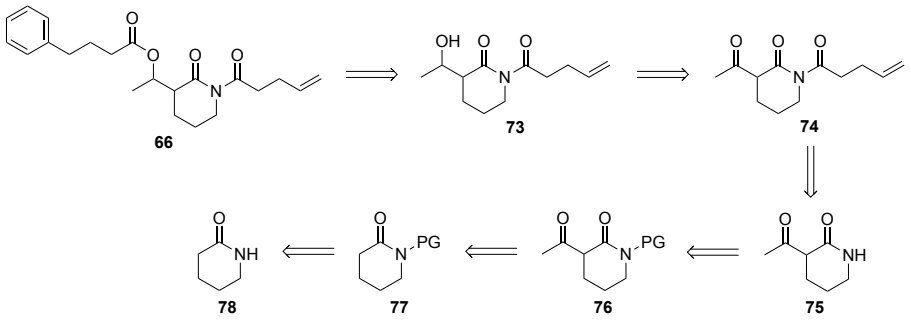

*Scheme 7 : Retrosynthetic pathway to obtain **66**.*

3.3 Pharmacological evaluation

After obtaining the target molecules, pharmacological studies will be conducted to deepen our understanding of the activity of our potential FAAH inhibitors.

3.3.1 *In vitro* studies

To evaluate the activity of our molecules as FAAH inhibitors, we will determine the potency of each of the target molecules. We will therefore determine the IC_{50} value of the molecules using a biochemical assay based on the high activity of FAAH in mouse brain. The IC_{50} value represents the concentration at which enzyme activity is reduced by half. As a precautionary measure, we will also determine the IC_{50} of all synthesis intermediates. We have chosen to work with mouse brain homogenate to obtain IC_{50} values for murine FAAH (*m*FAAH), whereas previous measurements had been conducted on human FAAH (*h*FAAH). Our decision to work with mice aligns

with the development of a drug. Indeed, in the process of developing a new drug, thorough studies on mice are conducted. Therefore, working with mice serves as a good starting point in this context. Additionally, in our laboratory, *m*FAAH is more readily available than *h*FAAH.

3.3.2 *In cellulo* studies

Once we have obtained the IC_{50} values, we will be able to identify the most promising molecules among the compound family under study. For these selected molecules, we will conduct *in cellulo* inhibition assays in J774, a mouse macrophage cell line.[90] The aim of these *in cellulo* tests is to determine whether our molecules are able to increase NAE levels, supporting *in cellulo* FAAH inhibition. Indeed, it is possible that the molecules may be degraded by other enzymes present in the cells, which could make our inhibitors ineffective for FAAH inhibition, even if they show promising IC_{50} values. To carry out these studies, we will perform dosing of NAEs, particularly AEA, to verify if the intra-cellular levels of these FAAH-substrates are increased following inhibitor incubation with the cells.

3.4 Docking studies

After completing the pharmacological studies, we will undertake docking studies. This phase of the project will be conducted in collaboration with Prof. C. Michaux from the Université de Namur. These docking analyses will allow us to deepen our understanding of the interactions between the inhibitors and the catalytic pocket of FAAH. They will provide us with an explanatory model of inhibitor activity, or lack thereof, and can serve as a predictive tool to identify promising molecules.

To date, docking studies have already been conducted on several molecules of the β-lactam family, including the lead compound **35**. Since pharmacological tests had previously been conducted on *h*FAAH, the

previous dockings were performed on the *h/r*FAAH, as the 3D structure of *h*FAAH had not yet been determined by X-ray diffraction analysis.[49] However, since we have chosen to determine the potency of the inhibitors for *m*FAAH, we will conduct the docking studies with *m*FAAH. For this purpose, the lead compound will be docked considering this new parameter, which could lead to different results. We will then compare these results with the docking on *h/r*FAAH to understand potential differences in the interaction of the inhibitor within the enzyme.

Once this step is completed, the new molecules we have obtained, and which show interesting results (satisfactory activity or conversely unexpected low activity), will be docked on *m*FAAH. Finally, these molecules will also be docked using the *h/r*FAAH to compare the docking results obtained with these two enzymes.

Chapter 4: Synthesis of bicyclic analogues of the lead compound

4.1 Introduction

As previously stated, for effective interaction with the catalytic triad, the imide function necessitates a *syn* conformation. However, there exists an equilibrium between the *syn* and the *anti* conformations, favouring the *anti* form with a computed ΔG of 2.5 kcal/mol. Hence, we hypothesised that this equilibrium might detrimentally affect the inhibitors' efficacy.[82]

Accordingly, our plan was to block the *syn* conformation of the imide function to assess its impact on inhibitor activity. To accomplish this goal, we proposed synthesising bicyclic compounds equivalents to the lead compound, which would prevent the two carbonyls from adopting an *anti* conformation. We have outlined the design of scaffold **55** to assess the pharmacological potential of bicyclic equivalents of the lead (**Figure 24**).

Lead **35**, IC_{50} = 4.2 nM **55**

*Figure 24: lead (**35**) and general scaffold of the bicyclic equivalents of the lead (**55**).*

When considering bicyclic β-lactams, several compounds can be envisioned. Among these, we chose to focus on [3.2.0] and [4.2.0] bicycles leading to the respective bicyclic analogues of our lead **79** and **56** (**Figure 25**). To determine which bicyclic system, [3.2.0] or [4.2.0], would be the best candidate as a FAAH inhibitor, we first prepared model compounds **80**[91] and **59**[2]. These precursors differ from the target compounds by replacing the ester chain with a TBDMS protecting group and by the absence of the α-side chain of the imide carbonyl. Once these two compounds obtained, their IC_{50} were determined to guide the next steps of our approach.

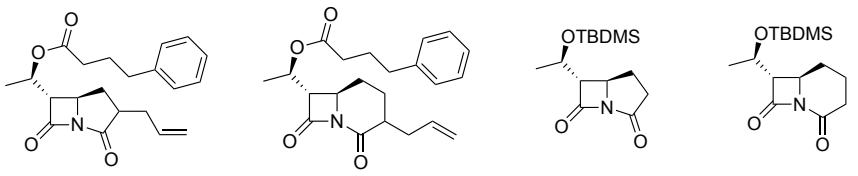

79 **56** **80** **59**

*Figure 25: [3.2.0] bicyclic analogue of the lead (**79**), [4.2.0] bicyclic analogue of the lead (**56**), [3.2.0] bicyclic precursor (**80**) and [4.2.0] bicyclic precursor (**59**).*

The synthesis of precursor **80** was carried out by Olivia Vander Auwera during her Master thesis in our laboratory (2014-2015).[91] **80** was obtained in 5 steps from commercially available acetoxy-azetidinone **32** (**Scheme 8**). The first step of the synthesis consists in the substitution of the acetate with phenylsulfonate. Subsequently, an alkylation was carried out at C3 of the lactam using an *in situ* generated Grignard reagent, yielding compound **82** with a retention of stereochemistry. Iodocyclisation was then performed, leading to the formation of the second cycle of **83**. A β-elimination was then executed, resulting in the formation of the double bond of **84**. Eventually, this latter was oxidised in the presence of ozone in order to generate the second carbonyl group of the imide function and hence obtain the [3.2.0] bicyclic precursor **80** with an overall yield of 11% over 5 steps.

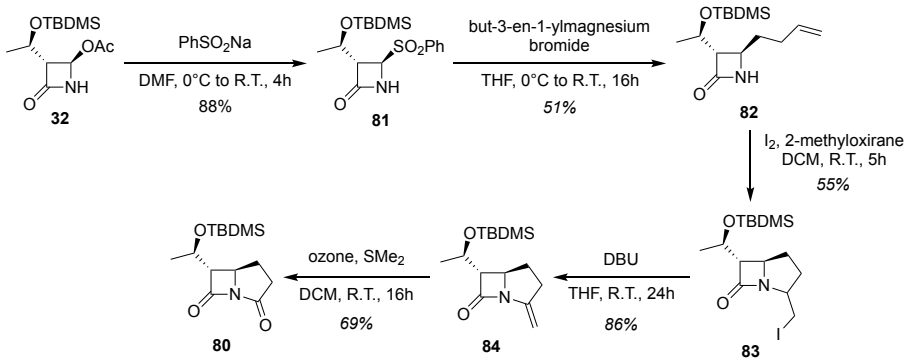

*Scheme 8: Synthesis pathway to obtain the model [3.2.0] bicycle **80**.*

The precursor **59**, on the other hand, was obtained by Joséphine Caruano (2012-2017).[2] **59** was obtained in 4 steps, also starting from the

commercially available acetoxy-azetidinone **32**. First, substitution of the acetate with an allyl group was carried out *via* the formation of an allylindium, resulting in the allylated compound **62** (**Scheme 9**). This compound was then *N*-acylated in the presence of acryloyl chloride, providing compound **61** with two terminal double bonds. Ring-closing metathesis using a second-generation Grubbs catalyst enabled the formation of the second cycle of **60**. This latter, having an α,β-unsaturation, was then hydrogenated, yielding the [4.2.0] bicyclic precursor **59** with an overall yield of 34% over 4 steps.

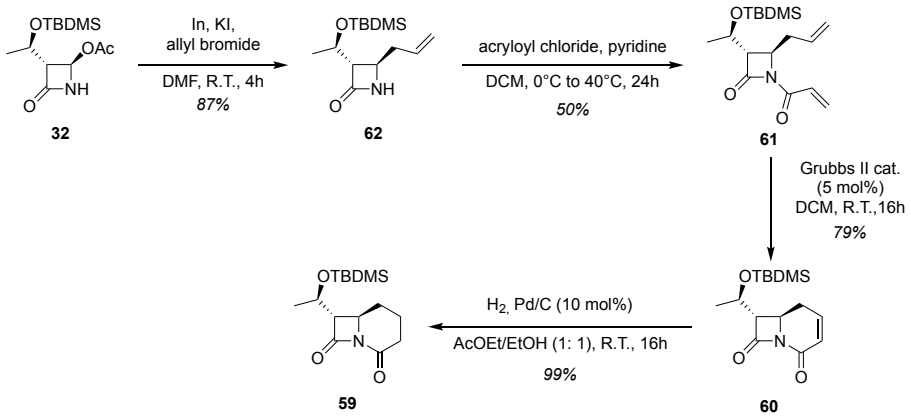

*Scheme 9: Synthesis pathway to obtain the model [4.2.0] bicycle **59**.*

The determination of IC_{50} on *m*FAAH was conducted on the two synthesised precursors. The [3.2.0] bicyclic compound **80** displays an IC_{50} of 288 nM,[91] while the [4.2.0] bicycle **59** exhibits an IC_{50} of 92 nM[2] (**Figure 26**). This suggests that bicyclic β-lactams featuring a second 6-membered cycle tend to be more effective in inhibiting FAAH compared to those with a second 5-membered cycle. These results prompted us to select the [4.2.0] bicyclic scaffold for the subsequent stages of our study.

80, IC_{50} = 288 nM **59**, IC_{50} = 92 nM

*Figure 26: [3.2.0] bicyclic precursor of the lead (**80**)[91] and [4.2.0] bicyclic precursor of the lead (**59**).[2]*

4.2 Synthesis of bicycle 56

This section aims to present and discuss the results as well as the strategies deployed to obtain the bicyclic β-lactam [4.2.0] **56**.

4.2.1 Allylation of azetidinone 32

The first reaction involves the substitution of the acetyl group of **32** with an allyl group (**Scheme 10**).[92] Allylindium is first generated by reacting metallic indium with transhalogenated allyl bromide using KI leading to allylindium sesquiiodide (**Scheme 11**). Once the organometallic complex is obtained, it adds onto the azetidinone *via* an S_N1-type mechanism, yielding compound **62** with an average yield of 87% and a total diastereoselectivity, without requiring purification. The reaction time (4 hours) is doubled compared to the initially published conditions.[92]

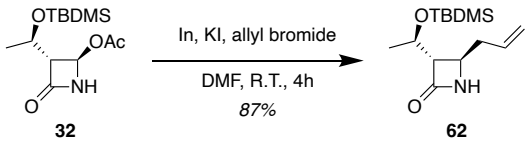

*Scheme 10: Allylation of azetidinone **32**.[92]*

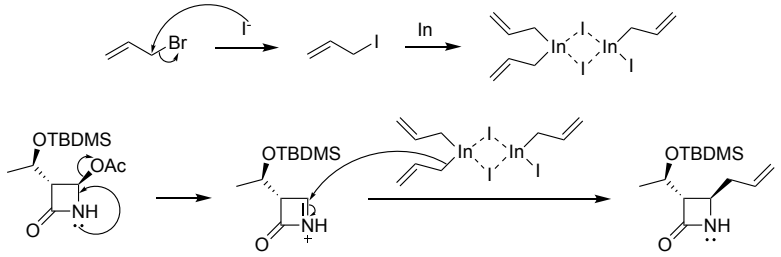

*Scheme 11: Allylation mechanism of azetidinone **32**.*

4.2.2 *N*-acylation of 62

Initially, compound **61** was obtained by treating compound **62** with acryloyl chloride in the presence of pyridine (**Scheme 12**).[82] However, the desired product was obtained with a low 12% yield after purification. One possible explanation for this low yield could be the lack of nucleophilicity of pyridine reacting with acryloyl chloride. An alternative would be to use a more nucleophilic base, such as triethylamine, or a strong base to directly deprotonate the lactam nitrogen. The latter approach was preferred.

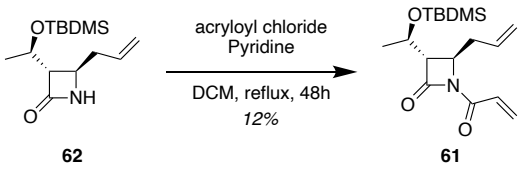

*Scheme 12: N-acylation of **62** using pyridine.[82]*

To improve the yield of the reaction leading to compound **61**, new conditions were developed. In this approach, compound **62** is deprotonated at 0°C with *n*BuLi, then acryloyl chloride is added (**Scheme 13**). The reaction mixture is then refluxed in DCM for 24 hours. The *N*-acylated product **61** is then obtained with a yield of 77% after purification on silica gel. Although it is known that carbenes can be formed when DCM is in the presence of *n*BuLi, we were mindful of this possibility but did not observe this phenomenon here.

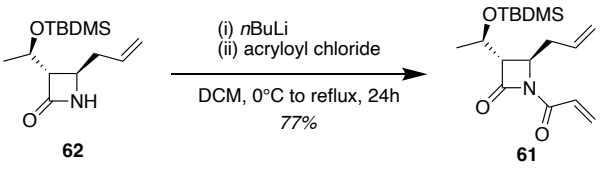

*Scheme 13: N-acylation of **62** using nBuLi.*

4.2.3 Ring-closing metathesis of 61

To obtain the desired bicyclic motif, a ring-closing metathesis is carried out (**Scheme 14**). The *N*-acyl compound **61** is treated with second-generation Grubbs catalyst overnight in DCM at room temperature. The bicyclic product **60** is isolated with a yield of 61% after a purification by silica gel chromatography.

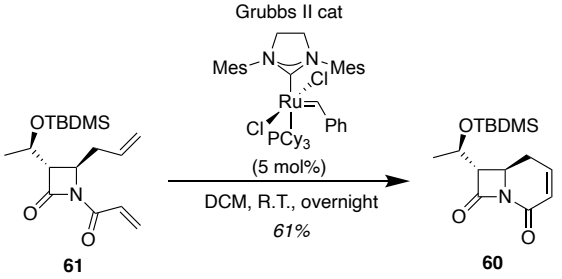

*Scheme 14: Ring-closing metathesis of **61**.*

4.2.4 Hydrogenation of 60

At this stage, the bicyclic β-lactam **60** is reduced under a hydrogen atmosphere in the presence of a Pd/C catalyst (10 mol%) (**Scheme 15**). Compound **59** is then obtained with a yield of 99% after filtration over a celite pad to remove the heterogeneous catalyst.

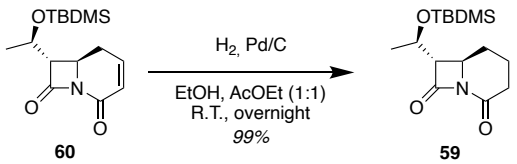

*Scheme 15: Hydrogenation of **60**.*

4.2.5 Alkylation of 59

In our laboratory, Joséphine Caruano had already conducted preliminary work on the allylation of the bicycle **59**. Various experimental conditions had been explored, varying the base used and the reaction temperature. **Table 10** summarises the different experimental conditions employed.

Table 10: Allylation conditions tested by J. Caruano.[2]

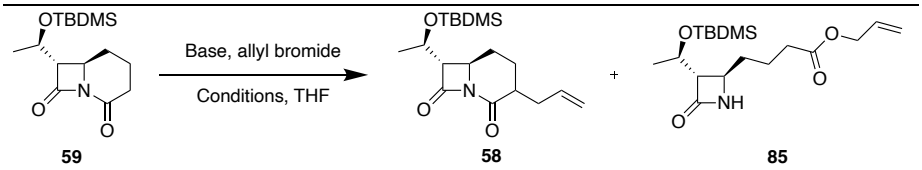

59 **58** **85**

Entry	Base	Temperature	Results
1	LDA	-78°C to R.T.	complex mixture[a]
2	LiHMDS	-78°C to R.T.	complex mixture[a]
3	DBU	R.T.	**59** and **85** (82/18)
4	DBU + KI	R.T.	**59** and **85** (69/31)
5	DBU + KI	R.T. to reflux	**59** and **85** (67/33)
6	LDA + TMSCl	-78°C to reflux	**59**

[a] The work-up was carried out without the addition of another organic solvent.

Regardless of the base, temperature, or additive used, the reaction primarily leads to the recovery of the starting material (**59**), potentially accompanied by the formation of the secondary product **85**. The latter likely results from direct *O*-allylation followed by a six-membered ring opening *via* attack by a water molecule during the work-up (**Scheme 16**).

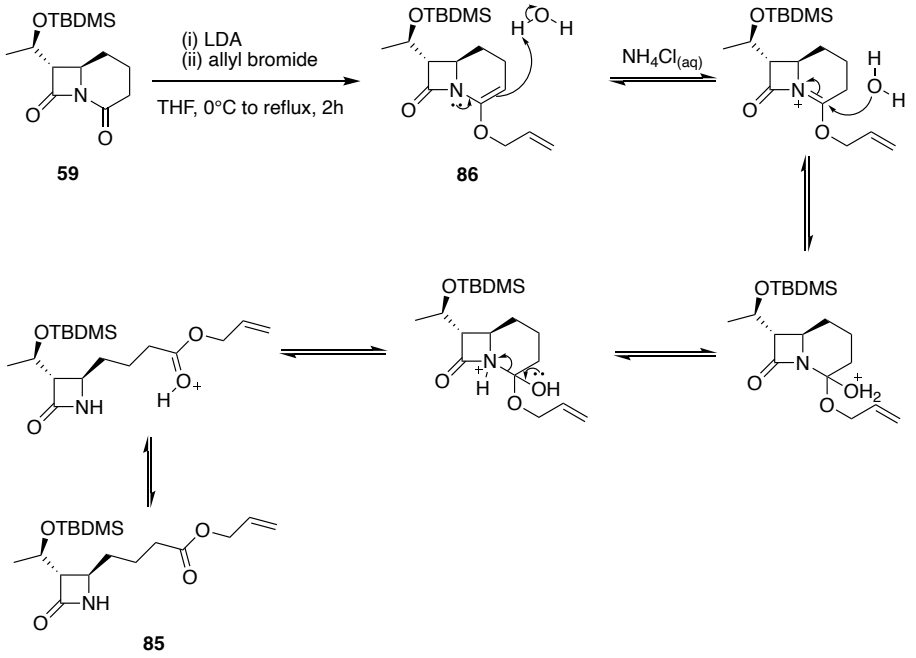

Scheme 16: Suggested mechanism to explain the ring opening of the O-allylated bicycle.

Based on the results obtained by Joséphine Caruano, we initiated our work by attempting to replicate an allylation using the same method. Compound **59** was treated with LDA at 0°C. Then, KI and allyl bromide were added, and the mixture was refluxed in THF for two hours. After aqueous work-up, mass spectrometry analysis was performed on the crude product obtained. This analysis confirmed the presence of the secondary product **85** and the absence of the desired product **58** (**Scheme 17**). These results are consistent with those obtained previously.

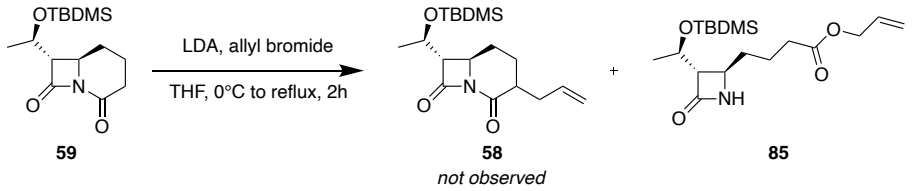

*Scheme 17: Allylation of **59** using LDA and allyl bromide. Compound **58** was not observed by HRMS.*

After confirming these results, we repeated the reaction without performing the work-up step, thus preventing the compound from reacting with water. The aim was to generate the *O*-allylated product **86** without opening it, in order to subject it to a Claisen rearrangement to obtain compound **58**. The previous reaction was therefore reproduced under the same reaction conditions, but after the two hours of reflux, we added the $Pd^{II}(CH_3CN)_2Cl_2$ complex in order to catalyse the Claisen rearrangement (**Scheme 18**).[93] Reflux was maintained for an additional 16 hours. Then, the solution was filtered over a silica pad to remove the palladium complex. Mass spectrometry analysis was performed directly, revealing the presence of product **87** but not of compound **58**. This suggests that the Claisen rearrangement did not occur. The difference in secondary product compared to the previous experiment is explained by the fact that no work-up was performed at the end of the reaction, and the crude product was directly analysed by mass spectrometry using methanol as the analysis solvent. This also seems to confirm that the use of a protic solvent can lead to the opening of the *O*-allylated product **86**.

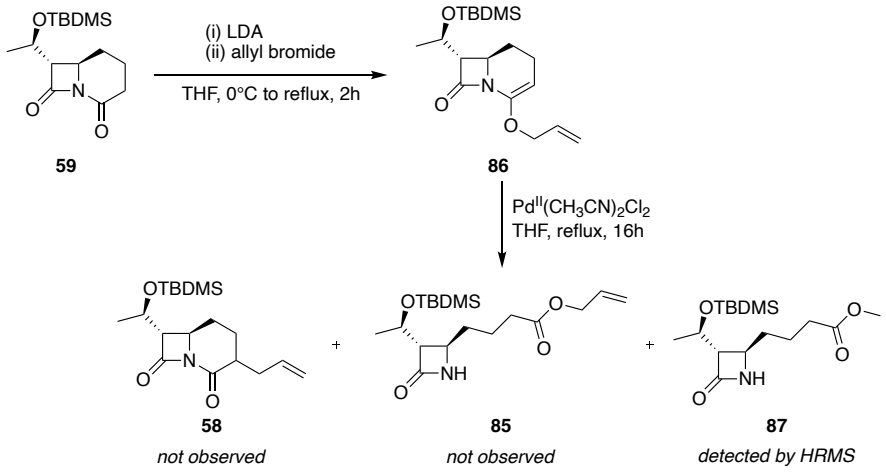

*Scheme 18: O-allylation of **59** followed by Claisen rearrangement catalysed by $Pd^{II}(CH_3CN)_2Cl_2$ on **86**.*

Facing these problems, we decided to explore another approach using an enone intermediate to form an *in situ* metal enolate. We chose to use enone **88**, readily available in stock. We investigated the formation of an aluminyl enol ether following the procedure described by Tsuda *et al.* in 1987.[94] The process involves the use of the MeCu catalyst (5 mol%, obtained by the reaction between CuI and MeLi), in the presence of 1.5 equivalents of HMPA, followed by 1.1 equivalents of DIBAL (**Scheme 19**). The mixture is then stirred for 30 minutes at -78°C. Subsequently, compound **88** is added, and the mixture is kept at -78°C for an additional hour to form the aluminium enol ether **89**, followed by the addition of 1.1 equivalent of MeLi to generate the enolate **90**. After 15 minutes, 3 equivalents of allyl bromide are added, and the reaction mixture is allowed to return to room temperature for 2 hours to obtain compound **56**. Unfortunately, at the end of this reaction, only starting material **88** could be observed. Two hypotheses can explain this lack of reactivity. On one hand, it is conceivable that the copper(I) catalyst fails to coordinate with the double bond, preventing sufficient activation for DIBAL hydride to add on 4 position. On the other hand, it is possible that copper(I) coordination proceeds correctly but DIBAL hydride fails to add to the double bond due to geometric reasons. In any case, it appears that the aluminium enol ether formation step is not successful.

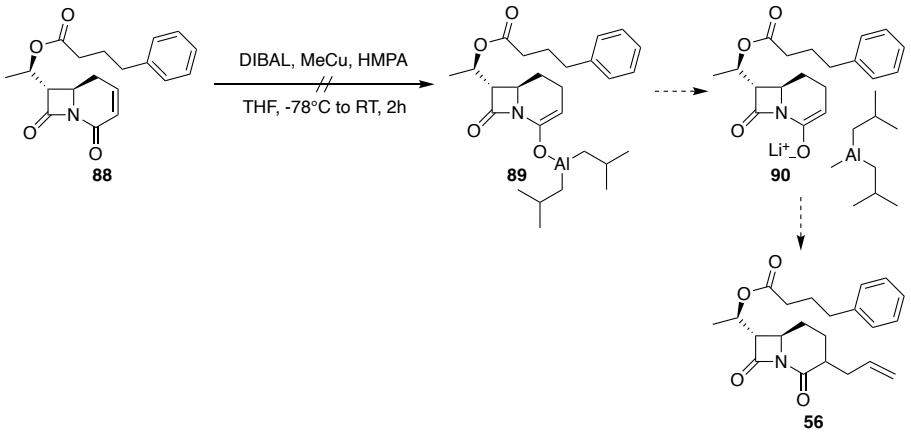

*Scheme 19: C-Allylation of **88** via generation of aluminium enol ether **89**.*

At this stage, several approaches have been considered to obtain bicycle **56**. Unfortunately, none of them yielded conclusive results, resulting in either ring opening, degradation, or the recovery of starting material. Thus, we have exhausted our options for introducing the allyl group on α position of the carbonyl. However, structure-activity relationship studies have revealed that the double bond of the pentenoyl group had little impact on the IC_{50}, with a value of 4.2 nM for the lead (**35**) and 8.0 nM for the lead without the double bond (**54**) (**Figure 27**).[2] Therefore, the hypothesis that the bicyclic equivalent of the lead with the reduced double bond (**91**) could have similar activity to that of bicyclic β-lactam **56** seems quite plausible. On the other hand, replacing the allyl group with a propyl group opens up a whole range of new synthesis strategies to explore.

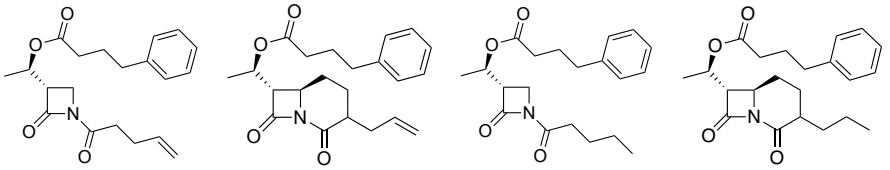

35 **56** **54** **91**

Figure 27: Equivalent of the lead and the bicycle with the reduced double bond.

4.3 Synthesis of the bicycle 91 *via* an alkylation reaction

The bicycle **59** is treated with LDA at 0°C in THF and stirred for 30 minutes before being allowed to warm up to room temperature (**Scheme 20**). Then, propyl bromide and 0.1 equivalent of KI are added, and the solution is refluxed in THF for 72 hours. Unfortunately, ^1H NMR after purification reveals a complex mixture that does not allow for the identification of the products obtained. However, the desired product **92** could not be detected in the crude reaction mixture by mass spectrometry. This observation is not surprising, as the reactivity is similar to that of

allylation, since the substrate and conditions are identical, only the nature of the alkyl halide is modified.

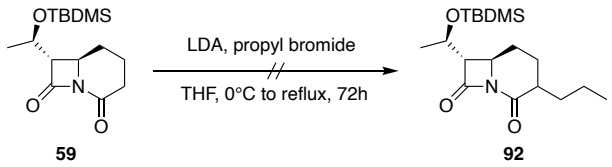

*Scheme 20: alkylation of **59** using LDA and propyl bromide.*

4.4 Synthesis of the bicycle 91 *via* an aldol condensation

An alternative to direct alkylation is to perform an aldol condensation followed by a crotonisation between the bicyclic β-lactam **59** and propionaldehyde. Subsequently, reduction of the double bond should yield a propyl group on the α position of the carbonyl. To do this, bicycle **59** is dissolved in THF at -78°C and deprotonated with LiHMDS (**Scheme 21**). After 1 hour of stirring, propionaldehyde is added to the solution, which is then left for 2 hours at -78°C. After work-up, the crude product is purified. However, purification did not separate products with very close Rf values. Despite this, this step helped eliminate certain products. Fractions potentially containing a product of interest were combined, yielding approximately 20 mg. Preparative TLC was then performed. Addition product **93** and a dehydrated product (**94** or **95**) were confirmed by ^{1}H NMR and mass spectrometry. However, only a few milligrams of each fraction could be obtained, and the products are not perfectly pure, making their identification difficult (NMR samples are too dilute). Nevertheless, NMR analyses seem to indicate that the elimination product obtained is not **94**, but rather compound **95**. This observation is surprising as this elimination does not follow Zaitsev's rule (**Scheme 21**).[95] However, this is not a problem for our objective, as the next step is to perform a reduction to obtain compound **92**.

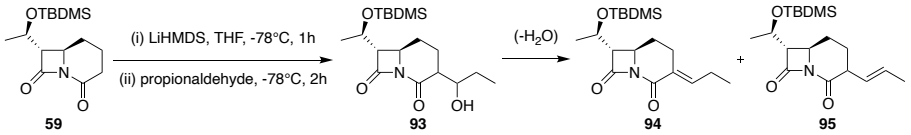

*Scheme 21: Aldol condensation of **59** followed by crotonisation of **93**.*

The different fractions were thus combined and subjected to elimination conditions in order to enrich the mixture in compound **94** and/or **95**. The mixture was dissolved in DCM in the presence of acetic anhydride, triethylamine, and a catalytic amount of DMAP (**Scheme 22**).[96] Unfortunately, these conditions did not lead to improved identification and separation of the compounds as similar results to the previous mixture were obtained.

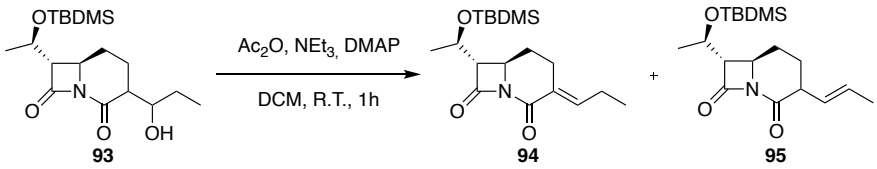

*Scheme 22:Deshydration of alcohol **93**.*

Despite our various attempts, we were unable to add an allyl or propyl chain at the α position of the carbonyl group in the bicyclic compound. As a result, we had to completely rethink our synthetic strategy to obtain compound **91**.

4.5 New strategy for the synthesis of the bicycle 91

So far, all the synthesis routes considered involved an allylation or alkylation once the bicycle was formed *via* an alkylation (or allylation) on the α position of the carbonyl, what did not work. So, we rethought the synthesis and considered introducing the side chain before cyclisation. This new synthetic strategy starts again from the commercially available azetidinone **32**. **Scheme 23** outlines the proposed retrosynthesis. Ester **91** can come from the corresponding alcohol **96**. The bicyclic core can be obtained by ring-

closing metathesis of **99**, which itself can be obtained from fragments **62** and **100**. Note that this strategy involves targeting compound **91** and not compound **56** since a reduction is required after ring-closing metathesis. The synthesis of **91** following this strategy was carried out by Juhans Dechenne as part of his Master thesis under our supervision (2019-2020).[97]

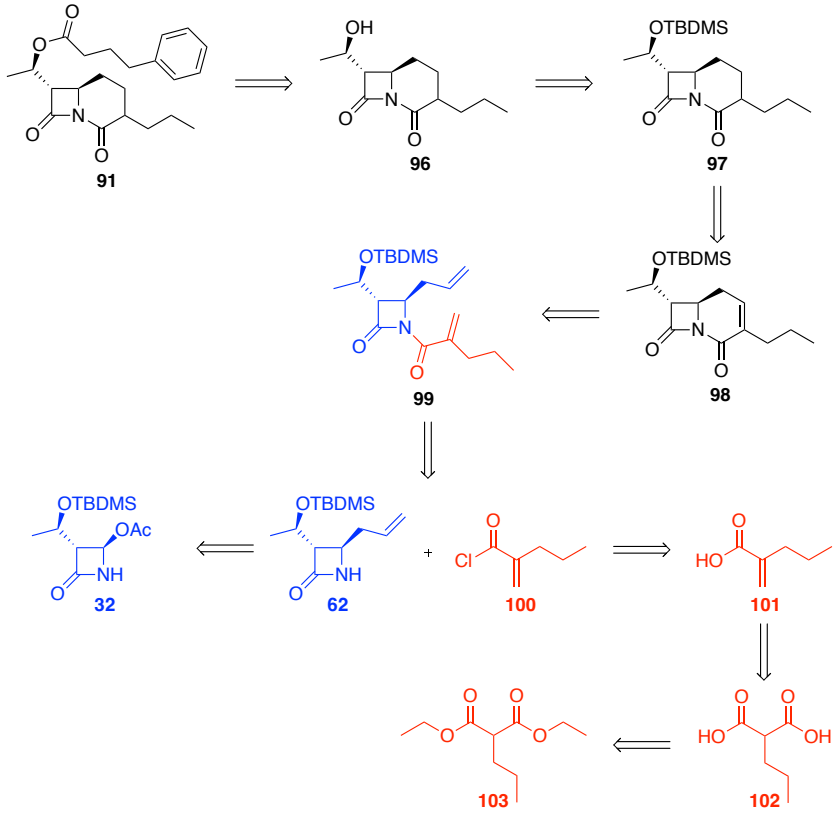

*Scheme 23: Retrosynthetic pathway to obtain **91**.*

4.5.1 Saponification of malonic ester 103

The objective of this reaction is to saponify diethyl *n*-propylmalonate **103** to obtain *n*-propylmalonic acid **102** (**Scheme 24**). For this, the ester is treated with KOH in a ethanol/water mixture (70/30) at 40°C for 24 hours, followed by acidification with HCl.[98] The diacid **102** is obtained pure with a yield of 97% without requiring any purification steps.

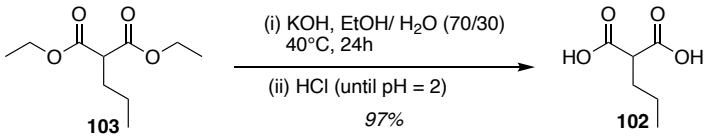

*Scheme 24: Saponification of diethyl n-propylmalonate **103**.*[98]

To perform this saponification, the initial reaction was carried out in ethanol for 3 hours without washing with hexane, and no product was observed (**Table 11**). A second attempt, with stirring for 24 hours followed by washing the crude product with hexane, yielded **102** in 52% yield. However, this yield seemed low compared to expectations for this type of reaction and the yields reported in the literature.[98] Therefore, the reaction was repeated using a mixture of ethanol and water (70/30), which allowed for better solubilisation of KOH. The reaction was stirred for 24 hours, followed by washing with hexane, resulting in a 97% yield

*Table 11: Conditions used to perform the saponification of **88**.*

Entry	Solvent used	Reaction duration	Washing with hexane	Yield
1	EtOH	3 h	No	0%
2	EtOH	24 h	Yes	52%
3	EtOH/H_2O (70/30)	24 h	Yes	97%

4.5.2 Synthesis of α,β-unsaturated acid 101

The objective of this step is to obtain α,β-unsaturated acid **101** *via* a Mannich reaction followed by a decarboxylation and elimination (**Scheme 25**). The first step, the Mannich reaction, is performed by reacting formaldehyde and diethylamine to form *N*-ethyl-*N*-methylenethanaminium, which is then attacked by the malonic carboxylate. The addition product then undergoes decarboxylation and elimination providing, after work-up, **101** with a 94% yield without the need for further purification.

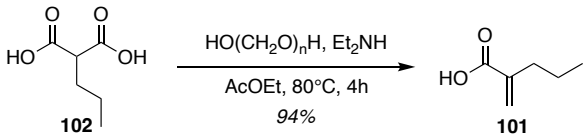

*Scheme 25:Decarboxylation of malonic acid **102**.*[99]

4.5.3 *N*-acylation of 62

Before proceeding to the *N*-acylation step of **62**, the synthesis of which is described in section 4.2.1, the carboxylic acid **101** undergoes chlorination to obtain the corresponding acyl chloride **100**. To achieve this, compound **62** is treated with oxalyl chloride and a catalytic amount of DMF, then stirred for 2 hours in DCM at room temperature. The solvent is evaporated before using the acyl chloride for the *N*-acylation step (**Scheme 26a**). For this step, the lactam is treated with *n*BuLi, followed by the addition of the previously prepared acyl chloride (**Scheme 26b**).[99] Unfortunately, the *N*-acylated product **99** could not be obtained, and the starting material **62** was recovered.

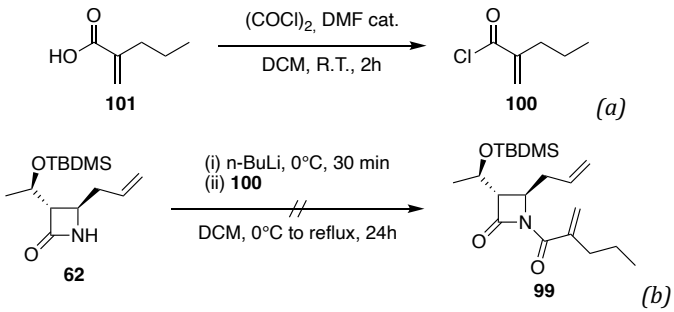

*Scheme 26: Chlorination of carboxylic acid **101** (a) followed by the N-acylation of **62** (b).*

Several reasons could explain this observation:

1) the synthesis of the acyl chloride fails;
2) the acyl chloride is formed but degrades during solvent evaporation;
3) the acyl chloride and the deprotonated lactam do not react.

To determine which of these hypotheses explains the lack of reactivity and thus address it, several tests were performed. First, we conducted a model

reaction using the substrate mentioned in the literature for this reaction.[99] The isolated acyl chloride was treated with aniline and triethylamine (**Table 12,** entry 2). No product was obtained. The reaction was repeated using pyridine instead of triethylamine, but again, no product was formed (entry 3). These results, which are consistent with our desired reaction results and contrary to the literature, suggest that the problem might be related to the formation of the acyl chloride or the post-reaction treatment. To verify this latter hypothesis, the reaction was repeated with compound **62** by adding the acyl chloride solution *in situ* directly after the reaction, without evaporating the solvent, using a cannulation system (entry 4). This time, the product was obtained, but with a low yield of 9%. The experimental conditions were then optimised (by fractionating the addition of the acyl chloride solution and using a larger chromatography column to facilitate product separation) (entry 5). After optimisation, the *N*-acylated product **100** was obtained with a yield of 67% after purification.

*Table 12: Tests conducted for the N-acylation reaction with acyl chloride **100**.*

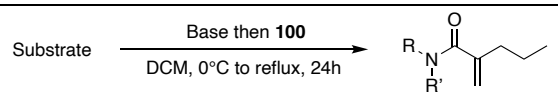

Entry	Substrate	Base	Yield
1	Lactam **62**	*n*BuLi	0%
2[99]	Aniline	Triethylamine	0%
3	Aniline	Pyridine	0%
4[a]	Lactam **62**	*n*BuLi	9%
5[a,b]	Lactam **62**	*n*BuLi	67%

*[a] acyl chloride **100** was added in situ, via a cannulation system. [b] after optimisation (fractionating the addition of the acyl chloride solution and using a larger chromatography column to facilitate product separation).*

4.5.4 Ring-closing metathesis of 99

The *N*-acylated product **99** undergoes ring-closing metathesis to generate bicycle **98**, following the procedure described in section 4.2.3. Compound **98** is obtained with a yield of 83% after purification (**Scheme 27**). It is notable that this yield is significantly higher than that of the ring-closing metatheses previously conducted in this project (see section 4.2.3 and [100]). Unlike the other metatheses, the propyl chain was already present, which may have facilitated better alignment of the double bonds to initiate the metathesis.

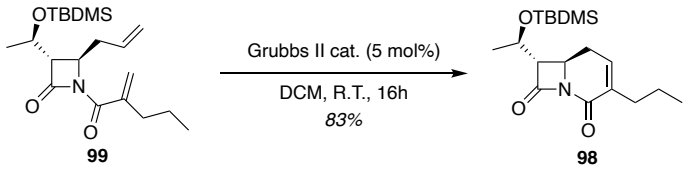

*Scheme 27: Ring-closing metathesis of **99**.*

4.5.5 Hydrogenation of 98

Compound **98** is reduced to **97** following the procedure described in section 4.2.4. The product is obtained with a yield of 99% after filtration through a celite pad to remove the heterogeneous support (**Scheme 28**). A mixture of diastereomers is obtained in a 51/49 ratio. This reduction is thus not diastereoselective, which is advantageous as it allows access to both diastereomers of the target molecule, providing the opportunity to test and compare the activity of the two diastereomers. However, the diastereomers are not separated and are used together in the next reaction.

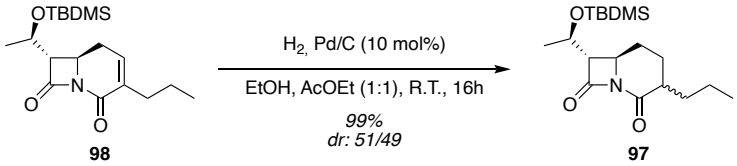

*Scheme 28: Hydrogenation of **98**.*

4.5.6 Deprotection of 97

The goal now is to deprotect the alcohol currently protected by a tert-butyldimethylsilyl group. For this, compound **97** is dissolved in a mixture of acetic acid and water (65% v/v) and heated to 90°C for 3 hours (**Scheme 29**). Compound **96** is obtained with a yield of 91%. The ratio of the two diastereomers determined by ^{1}H NMR is slightly modified to 61/39, suggesting that the deprotection conditions are slightly epimerising, probably due to the acidic medium and heating. The mixture of the two diastereomers is used as such in the next step.

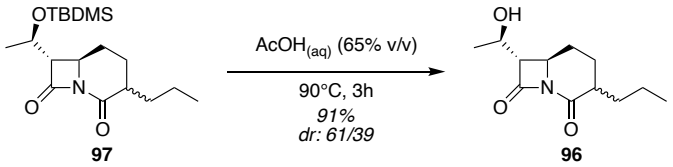

*Scheme 29: Deprotection of **97**.*

4.5.7 Esterification of 96

Finally, the last step involves esterifying **96** to obtain the target product **91**. A solution of **96** in DCM is treated with pyridine and 4-phenylbutanoyl chloride, and then stirred at room temperature for 24 hours (**Scheme 30**). The mixture of the two diastereomers is isolated with a yield of 42%, and the ratio of the two diastereomers, as determined by ^{1}H NMR, is 55/45. The two diastereomers were separated by flash column chromatography, yielding 72 mg of the first fraction and 45 mg of the second fraction, respectively.

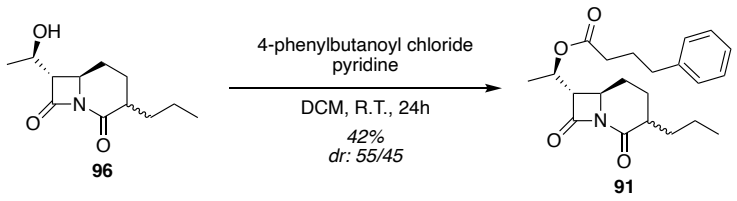

*Scheme 30: Esterification of **96**.*

For pharmacological testing, it is crucial to determine which fraction corresponds to which diastereomer in order to understand the influence of stereochemistry on the activity of the inhibitors. These two diastereomers differ by the absolute configuration of the carbon bearing the propyl chain. To achieve this identification, we first attempted to crystallise the products to determine their structure by X-ray diffraction analysis. Crystallisation tests were conducted in acetonitrile, ethyl acetate, dichloromethane, ethanol, and methanol. Unfortunately, none of these attempts succeeded in crystallising either of the two products.

Since it was not possible to determine the structure of the compounds by X-ray diffraction, NOESY analyses were conducted to try to differentiate them. We first assumed that these compounds adopt the azabicycle conformation shown in **Figure 28**.

Based on this hypothesis, the first fraction corresponds to the 3*R* stereochemistry because there is an NOE between protons "e" and "h," as well as another notable NOE between "h" and "g" (**Figure 28a**). The proton "h" also shows an NOE with "j" and "j'," which makes sense, although the correlation with the proton "g" is difficult to observe due to signal overlap.

The second fraction corresponds to the 3*S* isomer because the proton "h" shows an NOE with at least four protons, including "f" (or "g"), "j," "j'" (or "g'"), and "k" (**Figure 28b**). However, due to signal overlap, it is difficult to distinguish them clearly. Additionally, there is no correlation between "e" and "g." Although the absence of signals is not a conclusive evidence, it is

consistent with the fact that these two protons are far apart, as shown in the 3D structure.

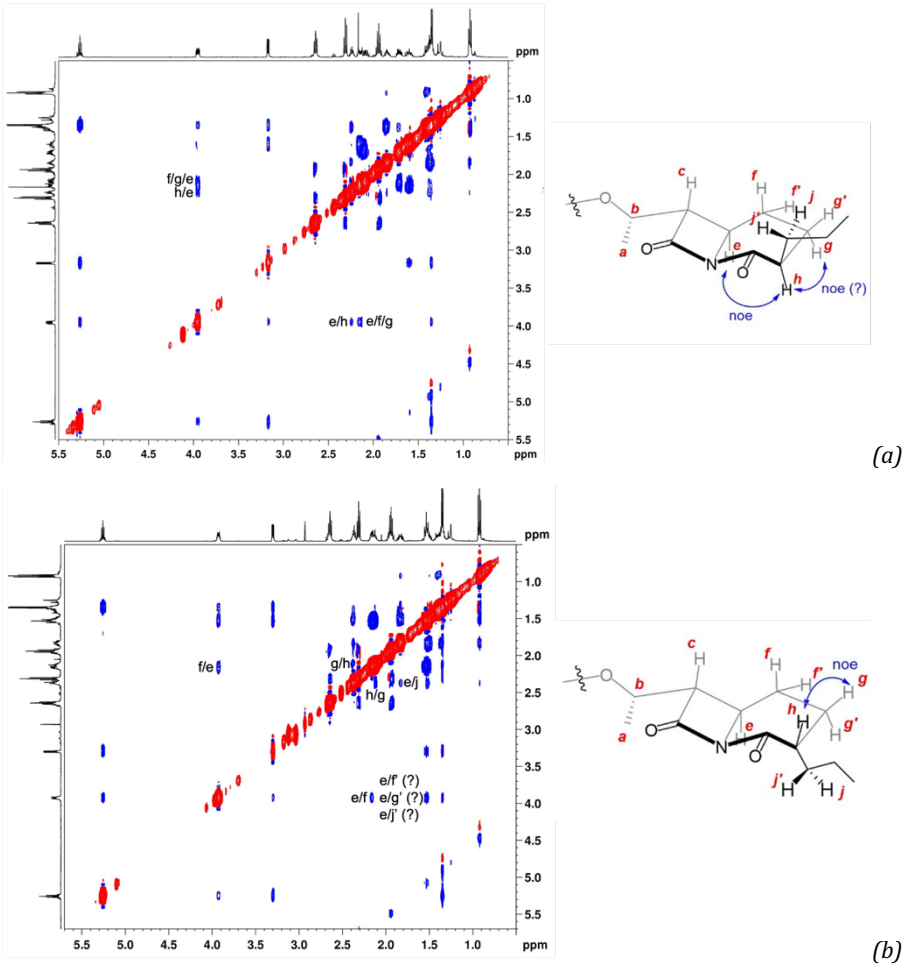

Figure 28: (a) $^{1}H,^{1}H$-NOESY NMR spectrum of fraction 1 in $CDCl_3$, zooming, absolute configuration 3R; (b) $^{1}H,^{1}H$-NOESY NMR spectrum of fraction 2 in $CDCl_3$, zooming, absolute configuration 3S.

The bicyclic equivalent of the lead compound with the reduced double bond, compound **91**, was obtained as a mixture of two diastereomers (55/45) in 6 steps starting from the commercially available azetidinone **32**, with an overall yield of 17%. The 2-propylacrylic acid **101** required for this synthesis was obtained in two steps with an overall yield of 91%.

4.6 Synthesis of other bicyclic compounds

After obtaining the bicycle **91**, the synthesis of easily accessible bicyclic analogues from intermediates of the previous syntheses was undertaken. Compound **104**, which preserves the bicyclic α,β-unsaturation, was first considered. Then, compound **105**, where the propyl group is replaced by another group positioned at the β-carbon of the imide carbonyl, was considered. The synthesis of compounds **104** and **105** was also part of Juhans Dechenne's Master thesis work carried out under our supervision (2019-2020) (**Figure 29**).[97]

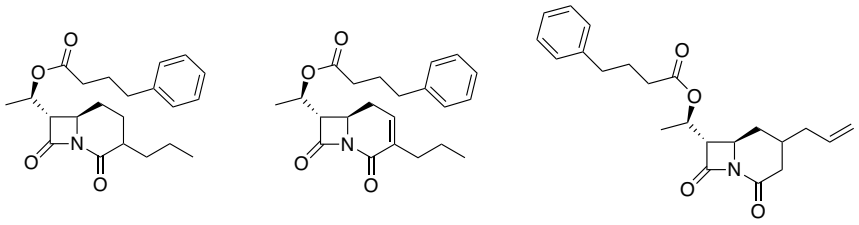

91 **104** **105**

*Figure 29: Structures of compounds **91**, **104** and **105**.*

4.6.1 Synthesis of bicyclic compound 104

Compound **104** can be easily obtained from compound **98**, an intermediate in the previous synthesis, as the starting material.

*4.6.1.1 Deprotection of **98***

Bicycle **98** is subjected to deprotection under the reaction conditions described in section 4.5.6 (**Scheme 31**). The alcohol **106** is obtained quantitatively, without the need of purification.

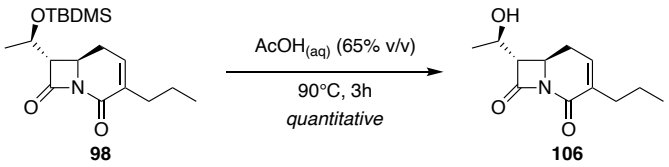

*Scheme 31: Deprotection of **98**.*

*4.6.1.2 Esterification of **106***

Next, alcohol **106** is esterified with 4-phenylbutanoyl chloride under the reaction conditions described in Section 4.5.7, resulting in the formation of compound **104** with a yield of 49% after purification (**Scheme 32**).

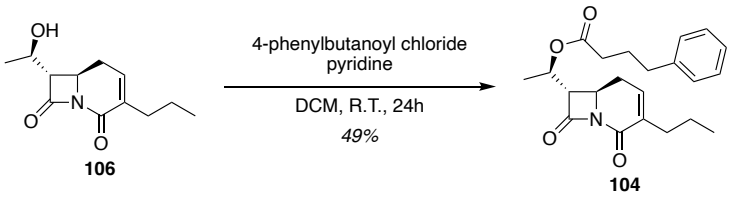

*Scheme 32: Esterification of **106**.*

Thus, compound **104** was synthesised in five steps from azetidinone **32**, with an overall yield of 23%.

4.6.2 Synthesis of bicyclic compound 105

The synthesis of compound **105** can be envisioned starting from the α,β-unsaturated bicycle **60**, the synthesis of which is described in section 4.2.3, through an 1,4-addition of an allyl cuprate *via* a Michael-type reaction.[101] To do this, CuI is first combined with TMEDA in THF, then cooled to -78°C (**Scheme 33**). Next, the allyl Grignard reagent is added, and the solution is stirred for 30 minutes. Finally, TMSCl is introduced, followed by addition of compound **60**. The reaction mixture is stirred at room temperature for 24 hours.

*Scheme 33: 1,4 allylation of **60**.*

Unfortunately, only the starting material was recovered after this procedure. Two hypotheses can be formulated. The first is that the allyl cuprate intermediate does not form, leaving the allyl Grignard reagent in solution. However, if this was the case, it would be expected that the allyl Grignard reagent would react directly with one of the carbonyl groups of the molecule, which was not observed since the starting material **60** was recovered intact. The second hypothesis is that the cuprate intermediate forms but is not reactive enough to interact with the α,β-unsaturated system. In this case, the starting material **60** would remain intact, and the cuprate intermediate would be removed during the aqueous work-up. This second hypothesis seems the most probable. Therefore, it would be relevant to repeat the experiment while varying the copper source to increase the reactivity of the cuprate intermediate, for example, by using CuCl. However, it was decided not to pursue this synthesis further due to the project's priorities.

4.7 Summary

At this stage of the project, two bicyclic compounds have been synthesised. Firstly, bicycle **91** was prepared in 6 steps from azetidinone **32**, with an overall yield of 17%. This compound was obtained as a mixture of two diastereomers, in a ratio of 55/45. These latter were separated and identified through NOESY analysis. Secondly, bicycle **104**, which is the α,β-unsaturated version of **91**, was synthesised in 5 steps from azetidinone **32**, with an overall yield of 24% (**Figure 30**).

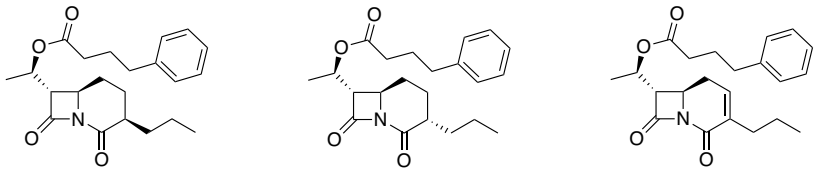

91a **91b** **104**

Figure 30: Bicyclic analogues of the lead compound obtained.

Chapter 5: Synthesis of stereoisomers of the lead compound

5.1 Introduction

The second part of this project involves synthesising and testing one of the diastereomers of the lead compound. Indeed, Docking studies have shown that the methyl group of the lead compound positions itself in a hydrophobic region of the enzyme cavity.[82] The objective is to prepare the (*S,S*) diastereomer **63** of the lead compound **35** by inverting the configuration of the carbon bearing the methyl group (**Figure 31**). This will allow us to study the importance of the stereochemistry of this stereocentre on the inhibitory capacity.

35 **63**

*Figure 31: Lead compound (**35**) and (S,S) diastereomer of the lead (**63**).*

5.2 First strategy

This first strategy follows the retrosynthetic pathway described in **scheme 34**. The compound **63** can be synthesised through esterification from alcohol **64**, which can be obtained by reversing the absolute configuration of alcohol **44**. Alcohol **44** can be produced by deprotection of molecule **43**, which is formed by the abstraction of the acetate group from azetidinone **32**.

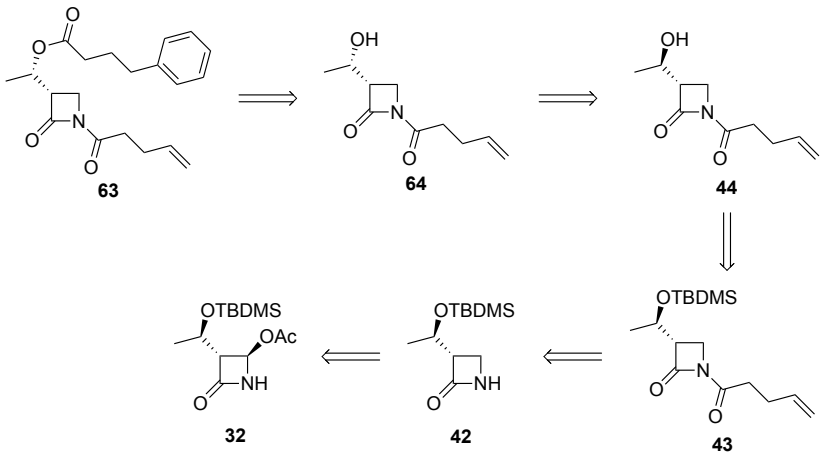

*Scheme 34: Retrosynthetic pathway to obtain **63**.*

5.2.1 Substitution of the acetate of 32 with thiophenolate

The objective of this step is to replace the acetate of azetidinone **32** with a thiophenolate group *via* an S_N1-type reaction, to create a better leaving group for forming compound **42**. To achieve this, compound **32** is treated with sodium thiophenolate and DIPEA in DMF for 4 hours at room temperature (**Scheme 35**). Compound **41** is obtained as a single diastereomer with a yield of 87% after purification.

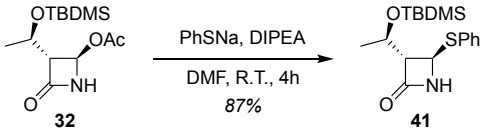

*Scheme 35: Substitution of the acetate of **32** with thiophenolate.*

5.2.2 Abstraction of thiophenolate of 41

Once compound **41** is obtained, the thiophenolate group is abstracted through a radical reaction. TTMSS and AIBN are added to **41** in toluene, and the reaction mixture is heated to 85°C for 24 hours (**Scheme 36**). Compound **42** is obtained with a 50% yield after purification.

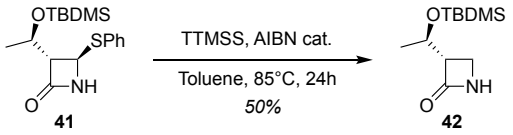

*Scheme 36: Abstraction of thiophenolate of **41**.*

5.2.3 Direct reduction of 32

Meanwhile, a method found in the literature allows the formation of compound **42** from azetidinone **32** in a single step *via* reduction.[102] To achieve this, the β-lactam is dissolved in ethanol cooled to 10°C, and 1.5 equivalents of $NaBH_4$ are added (**Scheme 37**). The reaction mixture is then allowed to rise to room temperature and stirred for 16 hours. Compound **42** is obtained in 60% yield after purification. This method has two advantages over the previous method: it offers a higher yield of 60% compared to 44% over the two steps of the previous method, and it is faster (shorter reaction time, only one reaction to perform, and a single purification).

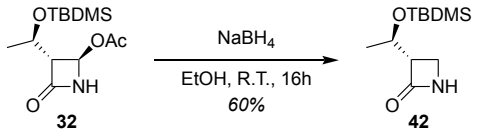

*Scheme 37: Direct reduction of **32**.*

5.2.4 *N*-acylation of 42

This reaction involves the *N*-acylation of compound **42** with the 4-pentenoyl group. It is carried out by mixing compound **42** with 4-pentenoyl chloride and pyridine, then refluxing the mixture in DCM for 24 hours (**Scheme 38**). Azetidinone **43** is obtained with a 75% yield after purification.

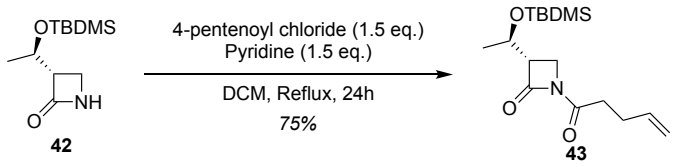

*Scheme 38: N-acylation of **42**.*

5.2.5 Deprotection of 43

The alcohol function of **43** can then be deprotected according to the procedure described in section 4.5.6 by stirring for 4 hours, yielding alcohol **44** quantitatively (**Scheme 39**).

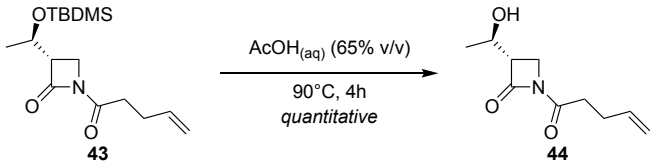

*Scheme 39: Deprotection of **43**.*

5.2.6 Inversion of the absolute configuration of the carbon bearing the alcohol 44

Previous work on inverting the stereochemistry of the alcohol of **44** was conducted by Joséphine Caruano (2012-2017).[2] Two approaches were considered. The first involved a Mitsunobu reaction using 4-phenylbutanoate as the nucleophile (**Table 13**). Unfortunately, this did not yield satisfactory results, as only the elimination product **107** was obtained in all cases, despite working at different temperatures. This suggests a competition between nucleophilic substitution and elimination, with the latter being favoured in our case, which is known to be a possible side reaction.[103-104]

Table 13: Mitsunobu conditions tested by J. Caruano.[2]

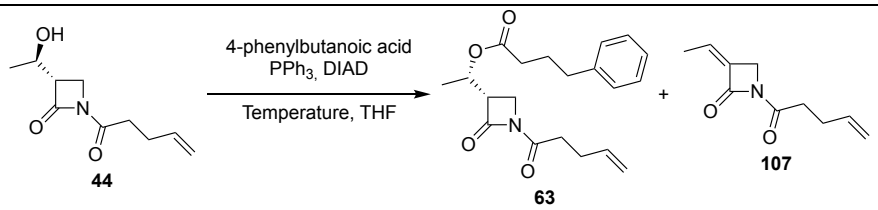

Entry	Temperature	Results
1	0°C to R.T.	**107**
2	0°C	**107**
3	-5°C to R.T.	**107**

The second approach explored by J. Caruano involved mesylating or tosylating compound **44** to create a good leaving group.[2] Once formed, this product could undergo an S_N2-type reaction with 4-phenylbutanoate, thus obtaining the ester with an inversion of stereochemistry. Several attempts were made for this first step, but none yielded satisfactory results (**Table 14**). Only very small amounts of product **108** were obtained, or the starting material was recovered.

Table 14: Mesylation / Tosylation conditions tested by J. Caruano during her thesis.[2]

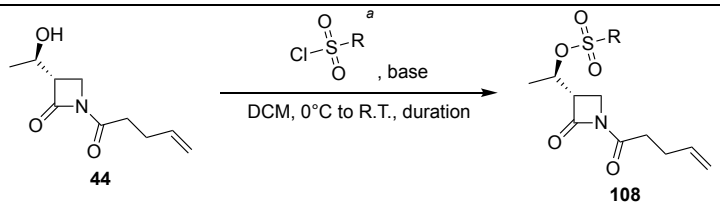

Entry	Reagent	Base	Reaction duration	Results
1	MsCl	Pyridine	16h	**108** (< 10%) + **44**
2	MsCl	Pyridine	24h	**108** (< 10%) + **44**
3	MsCl	Triethylamine	24h	**108** (< 10%) + **44**
4	TsCl	Triethylamine	36h	Traces of **108** + **44**
5	TsCl	Triethylamine	60h[b]	Traces of **108** + Degradation

[a] R = Me or pMe-C_6H_4, [b] 60h at room temperature followed by 4h at reflux.

Given the results obtained by J. Caruano, the mesylation was reproduced with a variation in the base. Specifically, alcohol **44** was combined with DBU at 0°C, followed by mesyl chloride, and the mixture was allowed to rise to room temperature for 24 hours (**Scheme 40**). After the work-up, an NMR analysis identified small amounts of **108**, starting material **44**, and elimination product **107** in respective proportions of 18%, 32%, and 50%. Although compound **108** was obtained in larger quantities than previously, the amounts were still too low to continue the synthesis using this method.

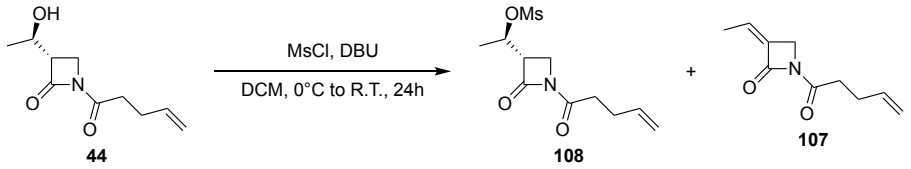

*Scheme 40: Mesylation conditions of **44** tested.*

In parallel, alternative Mitsunobu conditions were explored to invert the absolute configuration of the carbon bearing the alcohol of **44**. The literature, particularly the work of Herdewijn *et al.*, suggests modified conditions for the Mitsunobu reaction on substrates similar to ours.[102] Specifically, benzoic acid and tributylphosphine were added to a solution of alcohol **109** in toluene (**Scheme 41**), followed by the addition of TMAD. The mixture was maintained at 60°C for 24 hours, yielding **110** in 35% yield after purification. The substrates used differ from those commonly employed in the Mitsunobu reaction. The authors noted that these conditions resulted from an optimisation process aimed at improving initially very low yields, where the starting material and degradation products were primarily obtained. Although these new conditions increased the proportion of the desired product, the yield remains relatively low.

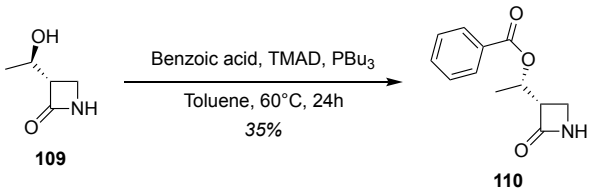

*Scheme 41: Mitsunobu conditions of **109** tested by Herdewijn et al.[102]*

Given these results, the decision was made to re-investigate the Mitsunobu reaction on alcohol **44**. **Table 15** summarises the various trials conducted. Initially, conditions similar to those of J. Caruano were repeated for comparison, using triphenylphosphine and diisopropyl azodicarboxylate.[2] Only the elimination product **107** was observed (entry 1). Next, the conditions developed by Herdewijn *et al.*, using tributylphosphine and tetramethylazodicarboxamide on alcohol **44**, were tested. Here too, only the elimination product was observed (entry 2). These results differ from those in the literature, probably due to the difference in the nature of the carboxylic acid and the starting substrate. The hypothesis is that the 4-phenylbutanoate might not be nucleophilic enough compared to benzoate. Therefore, the same conditions were repeated, but with benzoic acid replacing 4-phenylbutanoic acid (entry 3). Unfortunately, only the elimination product was observed here as well.

*Table 15: New conditions used for the Mitsunobu reaction on alcohol **44**.*

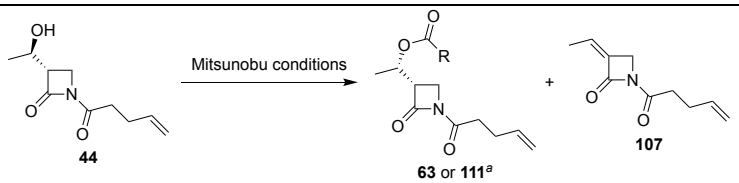

Entry	Solvent	Carboxylic acid	Phosphine	Reagent	Temperature	Results
1	THF	4-phenylbutanoic acid	PPh_3	DIAD	0°C to R.T.	**107**
2[b]	Toluene	4-phenylbutanoic acid	PBu_3	TMAD	0°C to 60°C	**107**
3[b]	Toluene	Benzoic acid	PBu_3	TMAD	0°C to 60°C	**107**

*[a] For **63** R = C_6H_5 and for **111** R = $(CH_2)_3C_6H_5$. [b] Conditions inspired by Herdewijn et al.[102]*

These results led us to closely examine the work published by Herdewijn *et al.*[102] First, it is notable that their yield is relatively low (*i.e.* 35%) and that degradation products were observed. We assumed these degradation products result from elimination, a hypothesis that aligns with our experimental observations, confirming the competition between substitution and elimination.

Next, we compared their results (see **scheme 41**) with those obtained by adapting their methodology (see **Table 15**, entry 3). The only difference is that their lactam is not protected, whereas ours is already *N*-acylated. This *N*-acyl group, having an electron-withdrawing effect, could drive the reaction towards elimination. Although this observation does not provide a direct solution to favour substitution with our substrate **44**, it opens up possibilities to perform the Mitsunobu reaction on substrate **109**, thereby considering a new synthetic route.

5.3 Second strategy

Considering the Mitsunobu reaction on substrate **109** leads us to reexamine the retrosynthetic pathway to obtain **63**. Overall, this new pathway is quite similar to the previous one in terms of fragmentation (see **Scheme 34**, section 5.2), but it differs in the order of addition of the fragments to the lactam core (**Scheme 42**). This retrosynthesis also allows starting from azetidinone **32**.

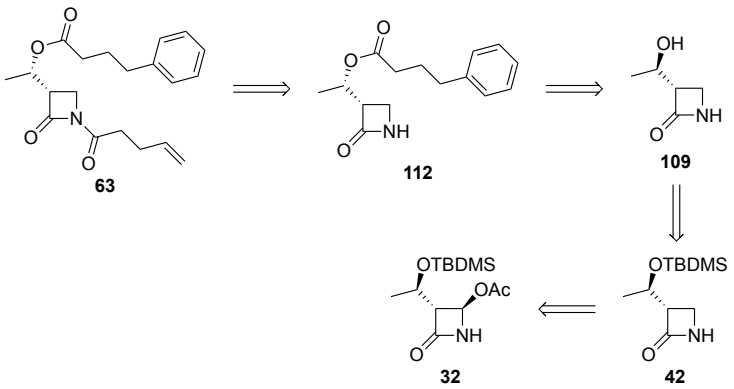

*Scheme 42: New retrosynthetic pathway to obtain **63**.*

5.3.1 Deprotection of 42

The alcohol **109** can be obtained from **42**, the synthesis of which is described in section 5.2.3 (**Scheme 43**). ^{1}H NMR spectrum confirms the formation of the desired product, accompanied by a byproduct **113**. This byproduct is the acetate ester formed through a Fischer esterification with the acetic acid used during deprotection. The product of interest and the byproduct are obtained in an NMR ratio of 36/64. Due to the high polarity of **109** and associated technical difficulties, the products could not be separated. Although **109** could theoretically be recovered from **113** by saponification, this manipulation did not significantly change the composition of the mixture.

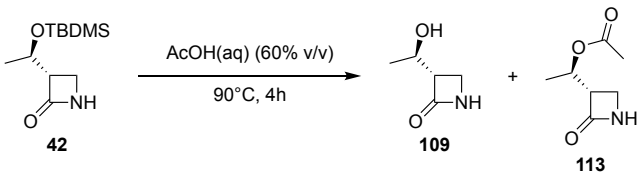

*Scheme 43: Deprotection of **42**.*

Since the usual method for deprotecting the alcohol **42** from its tert-butyldimethylsilyl group was ineffective, an alternative inspired by the conditions developed by Herdewijn et al. was employed.[102] Compound **42** is

dissolved in acetonitrile, followed by the addition of HCl. The reaction mixture is stirred at room temperature for two hours (**Scheme 44**). HCl is then neutralised with NaOH, and the product is purified by washing the NaCl with MeOH. The product **109** is obtained with a yield of 95% without requiring further purification.

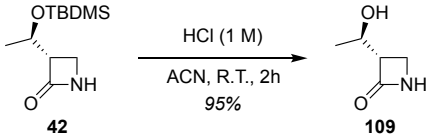

*Scheme 44: Deprotection of **42** using HCl conditions.[102]*

5.3.2 Esterification of 109 with inversion of configuration

The Mitsunobu reaction was undertaken according to the conditions described in section 5.2.6. to esterify alcohol **109** while inverting the configuration of the carbon bearing this functional group.[102] Alcohol **109** was dissolved in toluene, and then 4-phenylbutanoic acid, PBu_3, and TMAD were added at 0°C. The reaction mixture was stirred at 60°C for 24 hours before being purified by column chromatography (**Scheme 45**). Unfortunately, the purification did not allow isolation of the desired product, resulting in a mixture of three compounds: two apparent diastereomers **112** and an elimination product **114**. The presence of the substitution product (ester) and the elimination product was confirmed by HRMS. This reaction showed poor reproducibility and difficulties during scale-up. To increase the proportion of the substitution product relative to the elimination product, the reaction was repeated at room temperature, as heating might favour elimination. However, this attempt only produced the elimination product, which was surprising and unexplained. The initial conditions were therefore reused. Due to the mentioned difficulties, 141 mg of the mixture of the three products (**112** and **114**) was accumulated and used for the next N-acylation reaction, allowing for more optimal purification later.

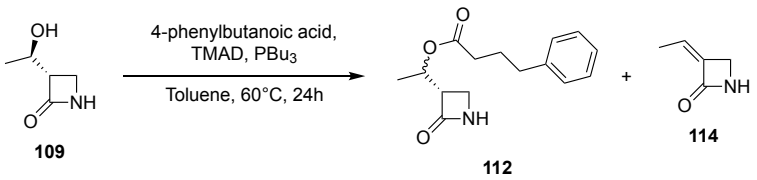

*Scheme 45: Mitsunobu reaction on alcohol **109**.*

5.3.3 N-acylation of 112 and 114

The mixture of the two diastereomers (**112**) and the elimination product (**114**) was then subjected to an N-acylation under the conditions described in section 5.2.4 (**Scheme 46**). After purification by column chromatography, two interesting fractions were obtained. The first fraction contained the two diastereomeric substitution products and the elimination product **107**. The second fraction corresponded to one of the two diastereomers.

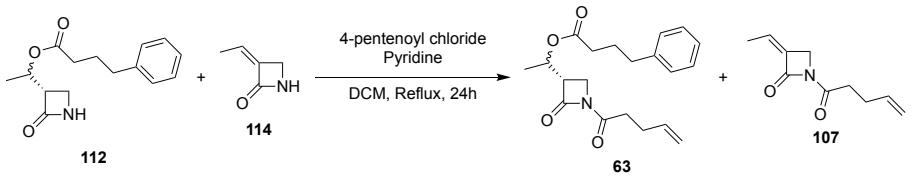

*Scheme 46: N-acylation of **112** and **114**.*

In order to identify and isolate the different products, studies were conducted on the two fractions independently. Before these studies, it is important to note that the Mitsunobu reaction partially succeeded, producing the desired compound as well as a diastereomer. As a reminder, the expected product has two asymmetric centres, allowing for the consideration of four possible stereoisomers (**Scheme 47**). Our initial hypothesis was that the reaction had produced the desired inversion stereoisomer **63**, but that an epimerisation of one of the asymmetric carbons had also occurred, thus forming **35** or **116**. With this hypothesis in mind, the studies were undertaken.

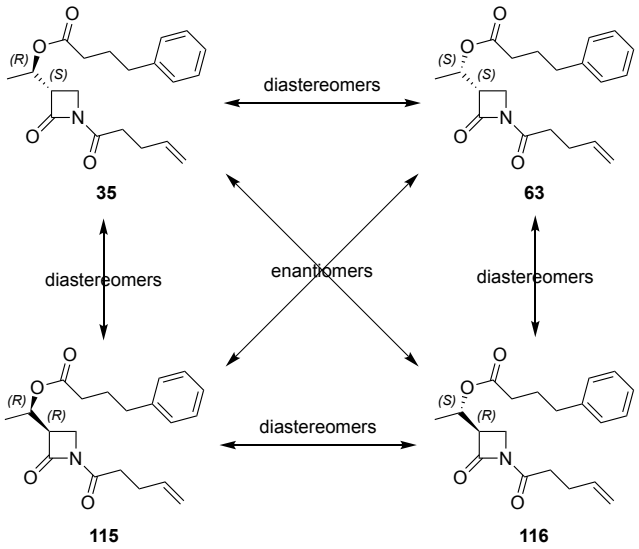

*Scheme 47: Stereoisomers of the lead compound. **35** corresponds to the lead, while **63** corresponds to the desired diastereomer.*

5.3.3.1 Fraction 1

Regarding the first fraction, an NMR analysis was conducted and identified three products. Two of these products correspond to the target compounds **63** and **116** (or **35**) as a mixture of diastereomers and the elimination product **107**, which was confirmed by HRMS. HPLC analyses, including chiral HPLC, revealed two signals. An HPLC-MS analysis helped us determining that one of the signals corresponded to **63** and **116** (or **35**) and the other to the elimination product, indicating that HPLC analyses did not separate the two diastereomers.

Since the products exhibit poor separation by column chromatography but good separation of the substitution products and the elimination product by HPLC, a semi-preparative HPLC was performed. This method successfully enabled isolating the mixture of diastereomers, as confirmed by NMR analysis, where two diastereomers were clearly visible (**Figure 32**). One of the NMR spectra perfectly matched that of the lead compound **35** that we had in stock.

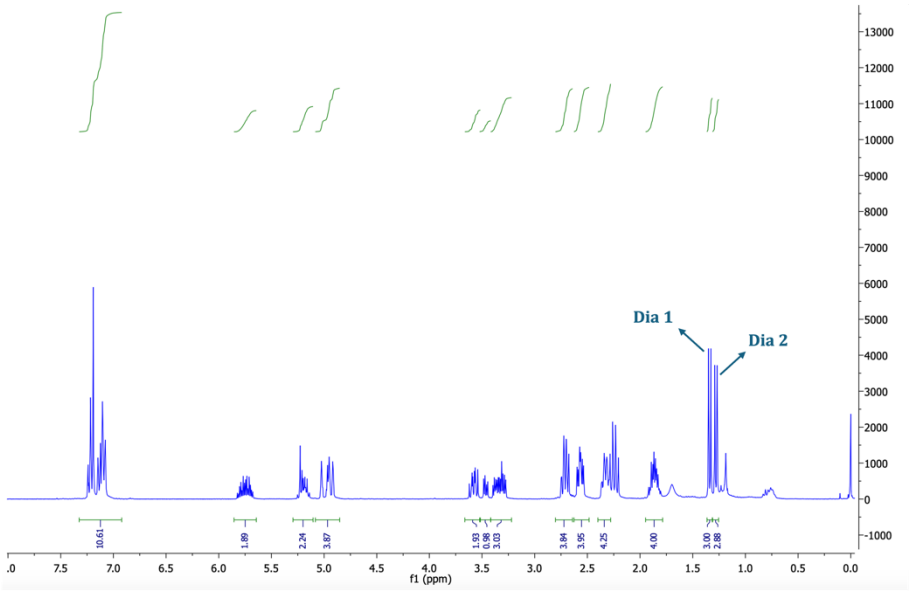

*Figure 32: ^{1}H NMR (300 MHz, $CDCl_3$) spectrum of Fraction 1 after purification by semi-preparative HPLC. Dia 1 corresponds to the lead **35** (or **116**). Dia 2 corresponds to the diastereomer **63** (or **115**).*

Given the mechanism of the Mitsunobu reaction, we hypothesised that the substitution product indeed underwent an inversion of configuration but also experienced an epimerisation of the asymmetric carbon on the lactam ring. This suggests the presence of a mixture of compounds **63** and **116** (see **Scheme 47**). If this hypothesis is correct, it could be advantageous as it would allow us to obtain the enantiomer of the lead compound **35**, which could be very interesting from a pharmacological perspective, provided we can separate the two diastereomers. To confirm our hypotheses and determine the next steps, a more detailed analysis was conducted on fraction 2.

5.3.3.2 Fraction 2

Regarding the second fraction, NMR analysis showed the presence of a single product whose spectrum perfectly matches that of the lead compound **35** (**Figure 33**). This indicates that a small fraction of one of the

diastereomers was isolated, although it is not the desired one. According to our hypothesis, we likely obtained and isolated the enantiomer **116** of the lead. Even though the mechanism of the Mitsunobu reaction suggests it is **116** and not **35**, experimental confirmation is necessary.

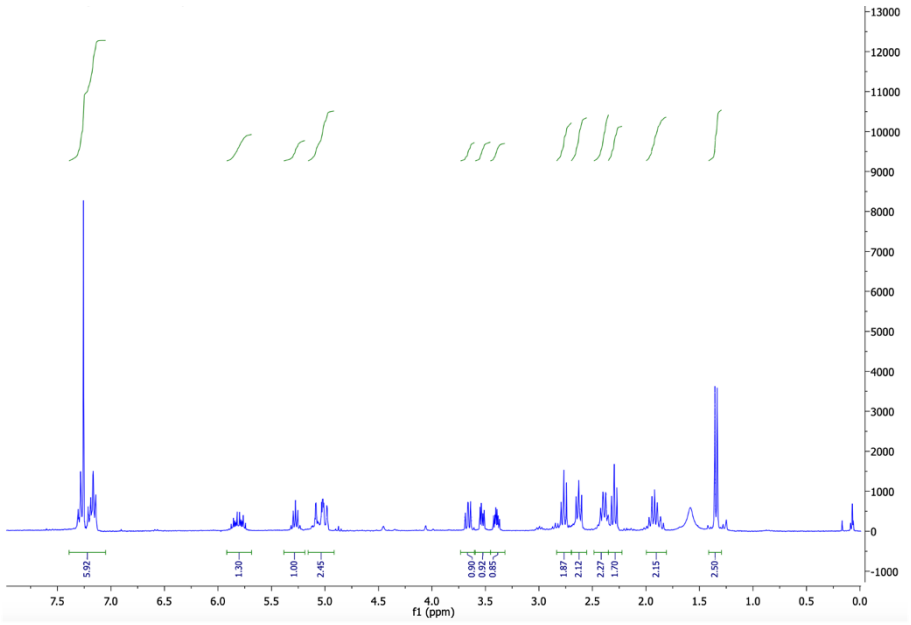

*Figure 33: ^{1}H NMR (300 MHz, $CDCl_3$) spectrum of Fraction 2. This spectrum corresponds to lead **35** or its enantiomer **116**.*

A chiral HPLC analysis was performed, but it failed to differentiate between the stereoisomers. The fact that chiral HPLC could not separate the two peaks is not conclusive, especially since we have already shown that the diastereomers could not be differentiated by HPLC using our conditions.

We then measured the specific optical rotation. The analyses, performed on solutions of compounds in DCM, showed a specific rotation of 3.7° for the lead **35** and -1.5° for fraction 2. This suggests that it could be the enantiomer **116**. However, this evidence is not sufficient. Given that the angle is close to 0°, it is difficult to determine whether it is the opposite angle,

considering the margin of error, or if it is indeed a mixture of enantiomers responsible for the different value from that of the lead's opposite.

To more precisely determine which enantiomer is present in fraction 2, a circular dichroism (CD) analysis was conducted in collaboration with Prof. C. Michaux and J. Mignon (UNamur). **Figure 34** shows the CD curves obtained for the lead compound (used as a reference for the pure enantiomer **35**) and fraction 2. The analyses were carried out within a wavelength range of 220 nm to 300 nm. The samples were dissolved in chloroform at identical concentrations. As it can be observed, the curve for fraction 2 exhibits a similar profile to that of the lead compound but with a lower intensity. If we had the pure enantiomer of the lead compound (**116**), we would expect a mirror-image curve of the lead compound. Moreover, Prof. Marc de Wergifosse and Robin Crits (UCLouvain) performed a CD spectrum simulation for lead **35** using DFT methods at 0 K, 50 K, 100 K, and 298.15 K (see section 10.3.2). Since the simulated spectrum for the lead **35** matches the experimentally obtained spectrum, this analysis confirms that lead **35** corresponds to the expected enantiomer and that fraction 2 predominantly contains this lead. These results therefore suggest that fraction 2 contains a mixture of the lead compound and its enantiomer, with the lead compound predominating.

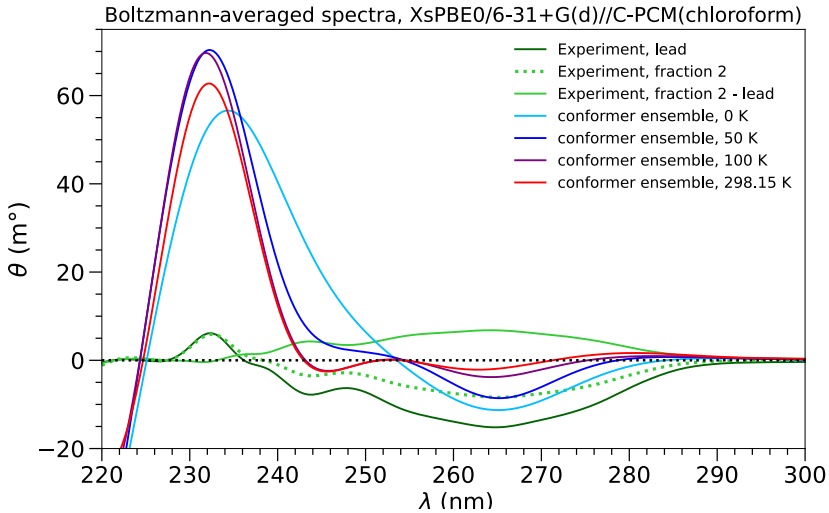

*Figure 34: Circular dichroism analysis of the lead compound **35** and Fraction 2; simulated CD spectrum for the lead **35** at 0 K, 50 K, 100 K and 298.15 K.*

By correlating the results obtained for the two fractions, we concluded that a mixture of at least three stereoisomers is present (**35**, **63**, and **116**). This could be explained in two ways. The first hypothesis is that the Mitsunobu reaction worked, but both asymmetric centres epimerised. The second hypothesis is that the Mitsunobu reaction followed an S_N1-type mechanism, followed by the epimerisation of the asymmetric centre on the ring. It is difficult to determine which of these hypotheses is correct, but it is unlikely that the Mitsunobu reaction follows an S_N1 mechanism, making the first hypothesis more coherent.

Given this explanation and the results obtained from circular dichroism, it is reasonable to think that stereoisomer **63** is present along with its enantiomer **115** in fraction 1. We hypothesise that fraction 1 is actually a mixture of all four stereoisomers, which is not ideal for pharmacological tests. Unfortunately, despite all the strategies explored, we have not been able to make further synthetic or separation progresses on this

project. Nevertheless, pharmacological tests will be conducted as an indication on the two fractions (see Section 7.2).

Chapter 6: Synthesis of other lactams

6.1 Introduction

This project also aims to extend our studies on lactams as FAAH inhibitors to γ- and δ-lactams. Our goal is to synthesise and pharmacologically test the γ-lactam **65** and the δ-lactam **66** analogues of the lead compound. In parallel, we also plan to synthesise and test the β-lactam **117**, which corresponds to the lead without the ester carbonyl and double bond. These two parameters had been tested individually and had not shown any influence on the inhibitor's activity. We wanted to evaluate the influence of the combination of these two parameters. This chapter presents the synthesis of molecules **65**, **66**, and **117** (**Figure 35**).

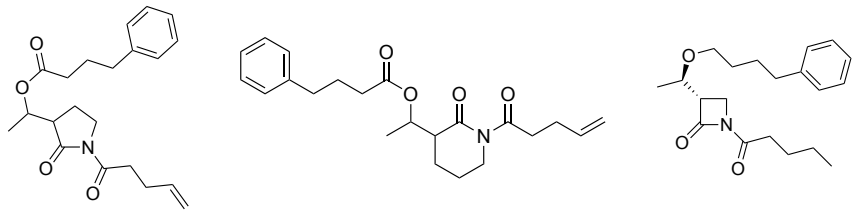

65 **66** **117**

*Figure 35: γ-Lactam **65** and δ-lactam **66**, analogues of the lead compound. Analogue of the lead without the ester carbonyl and double bond (**117**).*

6.2 Synthesis of γ-Lactam 65

As mentioned in section 3.4, the synthesis of γ-lactam **65** can be considered starting from **71** or **72** Initially, we chose **71** as the starting point for our synthesis.

6.2.1 Preparation of lactam 71

The β-lactam **71** can be synthesised from 4-acetylbutyric acid by reacting it with diphenyl azidophosphate and triethylamine (**Scheme 48**).[105] However, we only obtained a low isolated yield of 11%, which is not suitable as a starting point for the synthesis. These results are surprising, as

the publication from which the conditions are inspired reports a yield of 65%.[105] The low yield of the method has also been confirmed by other sources.[106]

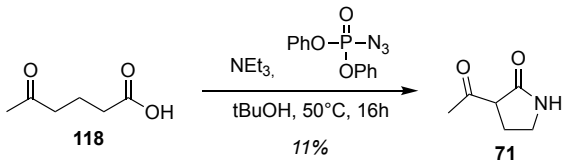

*Scheme 48: Formation of γ-lactam **71**.*

6.2.2 Acetylation of 119

Given the difficulty in obtaining compound **71**, we prioritised the synthesis of compound **120** from a protected 2-pyrrolidinone. Specifically, we used commercially available 1-benzyl-2-pyrrolidinone **119**. This was deprotonated with LDA and then reacted with methyl acetate to give compound **120** with a yield of 98% (**Scheme 49**).[106]

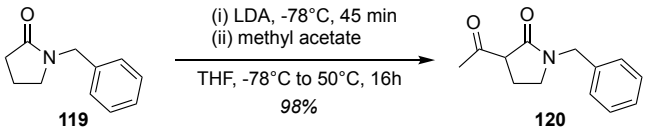

*Scheme 49: Acetylation of **119**.*

At this stage, the deprotection of the nitrogen in **120** to obtain compound **71** was tested to assess the ease of removing the benzyl group. **Table 16** summarises the various conditions tested. Unfortunately, the methods in entries 1 to 3 only led to the recovery of the starting material, while the conditions in entries 4 and 5 resulted in product degradation.

*Table 16: Conditions tested for the deprotection of **120**.*

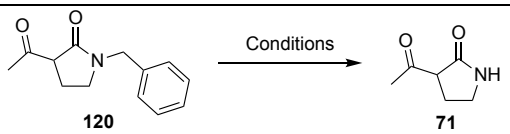

Entry	Conditions	Results
1	H_2, Pd/C, EtOH/AcOEt (1: 1), 16h	**120**
2	H_2, Pd/C, AcOH, 16h	**120**
3	HCOOH, 2h at R.T. then 2h at 60°C	**120**
4[107]	KBr, oxone, CH_3NO_2, 30°C, 24h	Degradation
5[108]	Triflic acid, toluene, µw, 180°C, 25 min	Degradation

6.2.3 Formation of 121

Given the difficulty in deprotecting the nitrogen of **120**, alternative protecting groups were considered, including 1-(4-methoxybenzyl)pyrrolidin-2-one **121**. For this, a PMB group was added to the lactam **122** (**Scheme 50**). First, PMB-Br (**123**) substrate was easily obtained from PMB-OH (**124**) with yield of 88%. Then, pyrrolidin-2-one **122** was *N*-alkylated using PMB-Br, leading to compound **121** with a yield of 81%. It should be noted that this alkylation was also attempted with PMB-OTs, but it did not yield lactam **121** due to difficulties in achieving good conversion during the synthesis of PMB-OTs.

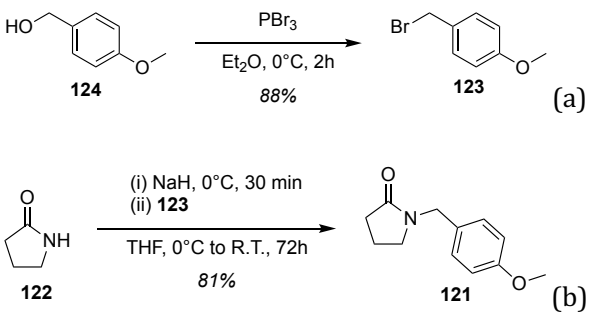

*Scheme 50: (a) Formation of 1-(bromomethyl)-4-methoxybenzene **123** and (b) N-acylation of **122** (b).*

After protecting the 2-pyrrolidinone with the PMB group, a deprotection test was performed using cerium ammonium nitrate (CAN). These conditions successfully deprotected **121**, confirming that the PMB group can be removed when needed.

6.2.4 Acetylation of 121

Compound **121** is acetylated following the method described in section 6.2.2, yielding compound **125** with a 39% yield (**Scheme 51**). It is noteworthy that the yield of this reaction is considerably lower than that of the benzyl equivalent (*i.e.* 98% yield for **120**).

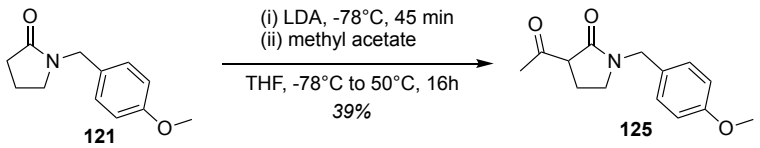

*Scheme 51: Acetylation of **121**.*

6.2.5 Reduction of 125

The ketone of γ-lactam **125** is then reduced to form alcohol **126** (**Scheme 52**). For this, compound **125** is treated with $NaBH_4$ in ethanol for 2 hours at room temperature, yielding **126** with a 97% yield after purification. It should also be noted that, at this stage, a mixture of diastereomers (and enantiomers) is present. It was decided to keep this mixture of stereoisomers and separate them once the target compound is obtained.

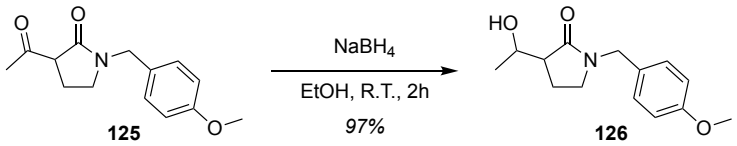

*Scheme 52: Reduction of ketone **125**.*

6.2.6 Esterification of 126

Alcohol **126** is then esterified following the procedure described in section 4.5.7, yielding ester **127** in 58% yield after purification (**Scheme 53**).

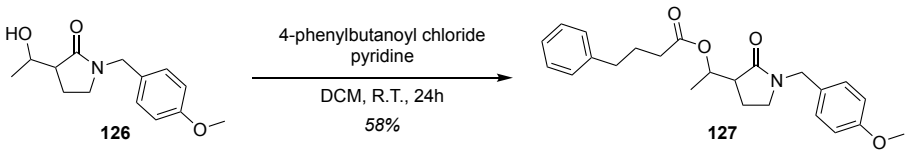

*Scheme 53: Esterification of **126**.*

6.2.7 Deprotection of 127

The objective of the reaction is to deprotect the nitrogen of the γ-lactam to obtain compound **67**, which can then be *N*-acylated to yield the target molecule **65**. The conditions tested for deprotecting lactam **121** were used initially (**Table 17**). To achieve this, lactam **127** was exposed to CAN in ethanol at room temperature for 2 hours (entry 1). Unfortunately, only trace amounts of **67** were observed. This is surprising, as preliminary tests on **121** had worked perfectly, suggesting that the presence of the side chain hindered CAN from accessing the nitrogen. However, determining the precise effects preventing this deprotection is challenging. The conditions were repeated, replacing ethanol with an ACN/H_2O (5:1) mixture and stirring for 16 hours (entry 2). Again, only a small amount of **67** was obtained (yield of 7%). Further exploration of solvent influence was conducted using an EtOH/H_2O (3:1) mixture at room temperature for 16 hours (entry 3), resulting in a slightly higher yield (20%). However, this is still insufficient, as the product needs to undergo an additional reaction followed by stereoisomer separation. Therefore, other deprotection conditions were explored. Specifically, γ-lactam **127** was exposed to trifluoroacetic acid at room temperature for either 16 hours or 96 hours, resulting in either recovery of the starting material or degradation (entries 4 and 5).

*Table 17: Conditions used for the deprotection of **127**.*

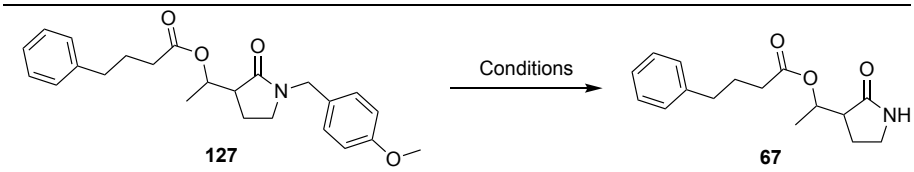

Entry	Conditions	Results
1	CAN, EtOH, R.T., 16h	**127** + traces of **67**
2	CAN, ACN/H_2O (5:1), R.T., 16h	**127** + **67** (7%)
3	CAN, EtOH/H_2O (3:1), R.T., 16h	**127** + **67** (20%)
4	TFA, R.T., 16h	**127**
5	TFA, R.T., 96h	Degradation

At this stage, we have not succeeded in finding satisfactory deprotection conditions. Due to the project's priorities, we did not pursue further deprotection tests. Nevertheless, an alternative would be to revisit the synthetic route using another protecting group that could be more easily removed later, such as the BOC group (**128**), CBZ group (**129**), or Alloc group (**130**) (**Table 18**).

Table 18: Protecting groups under consideration with their protection and deprotection conditions.

Protecting group	Compound	Protection conditions	Deprotection conditions
-BOC	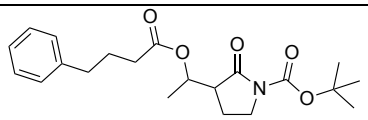 **128**	BOC_2O, DMAP, ACN	HCl
-CBZ	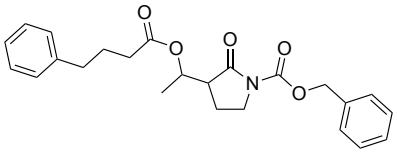 **129**	CBZ-Cl, NEt_3, THF	H_2, Pd/C, MeOH
-Alloc	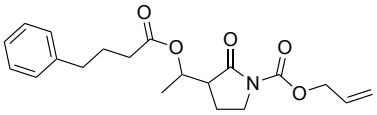 **130**	Alloc-Cl, NEt_3, THF	$Pd(PPh_3)_4$, THF

A test with the BOC protecting group was conducted (**Scheme 54**). The reaction yielded the protected lactam **128** with a 97% yield. However, the addition of the acetyl group resulted in the formation of the enol **131** rather than the ketone, along with numerous unidentified by-products.

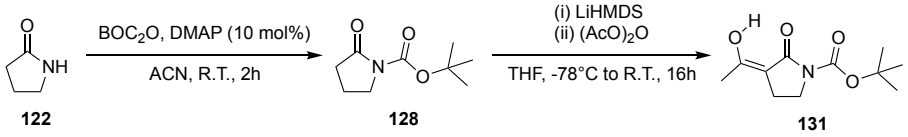

*Scheme 54: Protection of **122** with BOC protecting group followed by α-acetylation of **128**.*

6.3 Synthesis of δ-lactam 66

As mentioned in section 3.4, the synthesis of δ-lactam **66** can be considered starting from δ-valerolactam **78**. The synthesis of **66** was carried

out by Simon Degueldre as part of his Master thesis under our supervision (2020-2021).[109]

6.3.1 Protection of 78

The objective of this step is to protect δ-valerolactam **78** (**Table 19**) with a BOC group. Initially, the compound was treated with BOC_2O, DMAP, and NEt_3 for 2 hours at 0°C (entry 1).[110] DMAP was added as a catalyst to promote the nucleophilic attack on BOC_2O. However, this reaction yielded the protected lactam **77** with only a 2% yield, with almost complete recovery of the starting material. In a second attempt, compound **78** was deprotonated by LDA before carrying out a nucleophilic addition on BOC_2O (entry 2). This reaction performed slightly better but still resulted in a low yield of 21%. Finally, the use of DMAP (10 mol%) in the presence of BOC_2O in ACN (entry 3)[111] produced the protected lactam **77** with a yield of 60% after purification.

*Table 19: Conditions tested for the deprotection of **78**.*

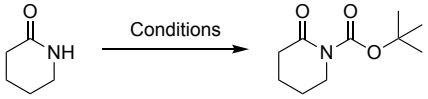

78 **77**

Entry	Conditions	Results
1[110]	BOC_2O (1.5 eq.), NEt_3 (1 eq.), DMAP (10 mol%), DCM, 0°C, 2h	**78** + **77** (2%)
2	(i) LDA (1.2 eq.), (ii) BOC_2O (1.2 eq.), THF, -78°C to R.T., 18h	**78** + **77** (21%)
3[111]	BOC_2O (1.2 eq.), DMAP (10 mol%), ACN, R.T., 2h	**77** (60%)

6.3.2 Acetylation of 77

The objective is then to acetylate the α position of the lactam carbonyl in **77** to obtain compound **76**. Initially, conditions inspired by section 6.2.2 were used. Lactam **77** was deprotonated with LDA, followed by the addition of methyl acetate (**Scheme 55**). However, the desired product was not observed; the starting material being recovered. It is possible that methyl acetate is not sufficiently electrophilic to be attacked by the deprotonated lactam.

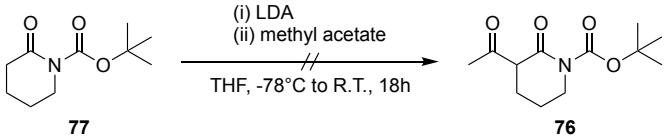

*Scheme 55: Acetylation of **77** using methyl acetate.*

Methyl acetate was therefore replaced by acetyl chloride. Given the previously encountered difficulties described in section 4.5.3, acetyl chloride was synthesised just before use and added *in situ* to the reaction mixture (**scheme 56**).

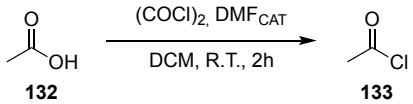

*Scheme 56: Formation of acetyl chloride **133**.*

Initially, lactam **77** was treated with acetyl chloride and pyridine, with or without DMAP catalysis (**Table 20**, entries 1 and 2). In both cases, only the starting material was recovered. A third attempt was made using DMAP alone instead of pyridine (entry 3), yielding the same results. The strategy was then modified by first deprotonating lactam **77** with LiHMDS before adding either acetyl chloride (entry 4) or acetic anhydride (entry 5), which resulted in the desired product with respective yields of 7% and 14% after purification. However, the desired product was obtained as a mixture of

the ketone and its enol tautomer **134** in a 2:1 ratio. These results and yields are consistent with those described in the literature by Kenny et al.[112] Moreover, calculation of ΔG using Density Functional Theory (DFT) methods predicts a value of 0.2 kcal/mol (**Scheme 57**). Given that this is a mixture of two forms in equilibrium, it was decided to use this mixture for the subsequent reaction.

*Table 20: Conditions tested to acetylate **77**.*

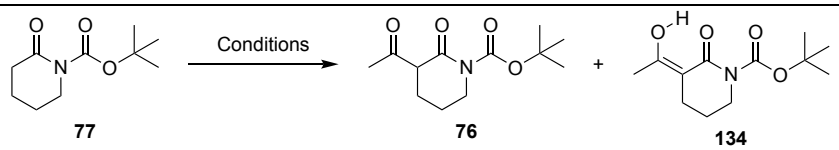

Entry	Conditions	Results
1	CH_3COCl, pyridine (2 eq), DCM, R.T., 18h	**77**
2	CH_3COCl, pyridine (2 eq), $DMAP_{CAT}$, DCM, reflux, 18h	**77**
3	CH_3COCl, $DMAP_{CAT}$, DCM, reflux, 18h	**77**
4	(i) LiHMDS, (ii) CH_3COCl, THF, 0°C to R.T., 18h	**134** + **76** (2: 1), 7%
5	(i) LiHMDS, (ii) $(CH_3CO)_2O$, THF, -78°C, 1h	**134** + **76** (2: 1), 14%

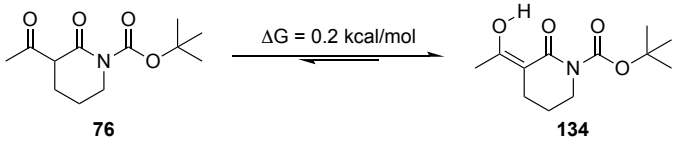

*Scheme 57: Calculated equilibrium between ketone **76** and enol **134** (M06-2X/6-311+G**($CHCl_3$)//M06-2X/6-31+G*($CHCl_3$).*

6.3.3 Deprotection of 76

The goal of the next step is to deprotect the nitrogen of the mixture of **134** and **76** from its BOC group. To achieve this, the mixture is treated with trifluoroacetic acid at room temperature for two hours (**Scheme 58**). The mixture of deprotected products **75** and **135** was obtained with a yield of 51%.

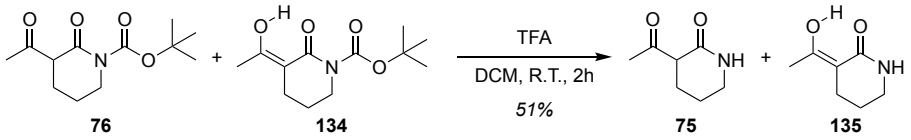

*Scheme 58: Deprotection of **76**.*

6.3.4 *N*-acylation of 75

The compound **75** is then *N*-acylated according to the procedure described in section 5.2.4 to obtain **74** (**Table 21**). Initially, 1 equivalent of lactam **75** was reacted with 1.5 equivalents of 4-pentenoyl chloride. The target product **74** was not obtained; instead, compound **136** was isolated with a yield of 45% (entry 1). This product results from both *N*-acylation and esterification occurring simultaneously. These results are understandable, given the ease with which compound **75** undergoes keto-enol tautomerism favouring the enol form. The formation of the ester corresponds to the nucleophilic attack of the oxygen of the enolate on 4-pentenoyl chloride. To investigate the preferential reaction (*N*-acylation or esterification), the reaction was repeated with varying equivalents of the two reactants, using an excess of lactam **75**. Using 1.5 equivalents of lactam and 1 equivalent of 4-pentenoyl chloride, only compound **136** was obtained with a yield of 54% (entry 2). Finally, with 3 equivalents of lactam and 1 equivalent of 4-pentenoyl chloride, only product **136** was observed in the crude mixture (entry 3). These results do not clearly determine which reaction is the most favoured, but it suggest that *N*-acylation occurs first, generating an electron-withdrawing group that favours the enol form, which then reacts *via* esterification faster than lactam **75**. At this stage of the project, lactam **136** was obtained. However, due to project priorities, the work was not pursued further beyond this point.

*Table 21: Conditions tested for N-acylation of **75**.*

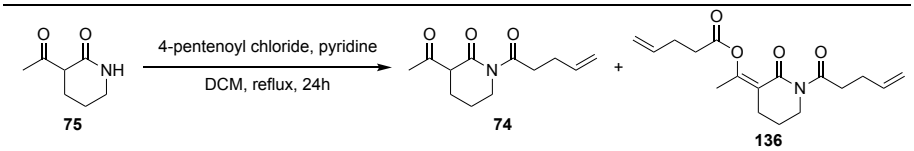

Entry	Eq. 75	Eq. 4-pentenoyl chloride	Results
1	1.00	1.50	**136** (45%)
2	1.25	1.00	**136** (54%)
3	3.00	1.00	**136**

6.4 Synthesis of β-lactam 117

The molecule **117** can be obtained from β-lactam **137**, which is already available in the laboratory. This lactam was synthesised by Marion Feledziak as part of her study on the pharmacophore and the influence of carbonyls on FAAH inhibition (see section 2.2).[3] She synthesised compound **137** in 7 steps starting from azetidinone **32** (**Scheme 59**). First, she substituted the acetate with thiophenolate to obtain **41**, and then abstracted it to get **42**. Next, she protected the lactam nitrogen by a PMB group (**138**), deprotected the alcohol to obtain **139**, and formed the ether **140** by reacting alcohol **139** with 4-phenylbutyl bromide. She then deprotected the nitrogen from its PMB group using CAN, obtaining **141**, on which she performed an *N*-acylation to obtain **137**. The overall yield of this synthesis is 7% over 7 steps.

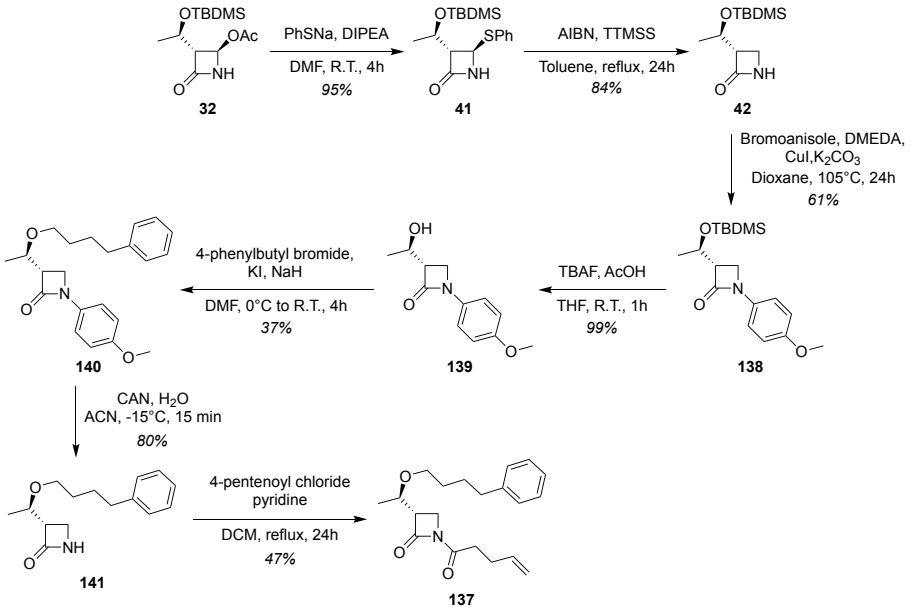

*Scheme 59: Synthesis pathway **137**.[3]*

On our side, compound **117** was obtained by hydrogenation of **137** (**Scheme 60**). The procedure described in section 4.2.4 was used, allowing us to obtain compound **117** quantitatively after filtration through a Celite pad to remove the palladium catalyst. Thus, the target compound was obtained in 8 steps with an overall yield of 7% from azetidinone **32**.

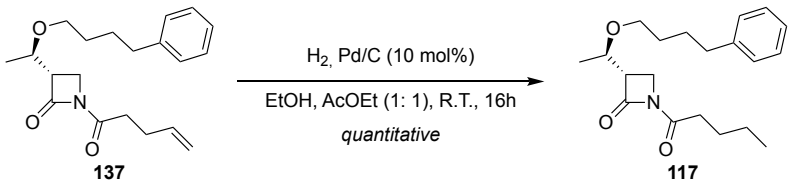

*Scheme 60: Hydrogenation of **137**.*

Chapter 7: Pharmacological evaluation

7.1 Introduction

This chapter presents the results of the pharmacological studies conducted during this project, which were divided into two main sections. First, *in vitro* tests were performed to determine the potency of the molecules obtained from the various syntheses for the inhibition of *m*FAAH. These tests aimed to evaluate the molecules' ability to inhibit FAAH and validate our working hypotheses. Second, cellular tests were conducted on a selection of molecules based on their potency. These cellular studies allowed us to examine the behaviour of the molecules within an intact cellular system and verify their ability to increase NAE levels.

7.2 Determination of the potency of the inhibitors

To determine the potency of the target molecules, we chose to work with *m*FAAH, as explained in section 3.5.1 dedicated to objectives and strategies. The principle involves measuring the inhibition of *m*FAAH as a function of the inhibitor concentration present in the medium, thereby determining an IC_{50} value.

To achieve this, solutions of the tested inhibitors at various concentrations are incubated in the presence of *m*FAAH (from a mouse brain preparation) and a constant concentration of anandamide **6** for all conditions. A small proportion of the anandamide used is tritiated on its ethanolamine part and serves as tracer for the reaction. Therefore, when FAAH hydrolyses AEA, tritiated ethanolamine is generated (**Scheme 61**). A chloroform and methanol mixture is then added to the reaction mixture to separate the lipophilic anandamide from the hydrophilic ethanolamine. The β^- emission from the tritium contained in the ethanolamine is then measured using liquid scintigraphy. In our working conditions, the higher the radioactivity measured in the aqueous fraction, the greater the concentration

of ethanolamine and therefore the larger anandamide hydrolysis. By comparing a control condition, where vehicle only is incubated with the enzyme preparation, and a "test" condition where a molecule of interest is present we can assess the relative level of enzyme activity and thus of inhibitor activity.

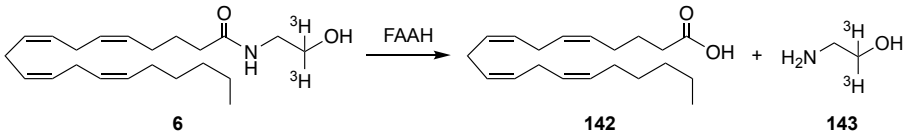

6 **142** **143**

*Scheme 61: Hydrolysis of tritiated anandamide **6** by FAAH.*

Given that all previously conducted and published IC_{50} tests were obtained for *h*FAAH, the first step was to confirm the transition from *h*FAAH to *m*FAAH and analyse the impact on the IC_{50} value.[82] To achieve this, we determined the IC_{50} value for lead **35** using *m*FAAH and compared it to the published value for *h*FAAH.[82] The referenced IC_{50} for *h*FAAH is 5.0 nM.[82] For *m*FAAH, we obtained an IC_{50} of 4.9 nM [3.8 – 6.4] (**Figure 36**). These similar values for both FAAH support the successful transition from human to murine FAAH.

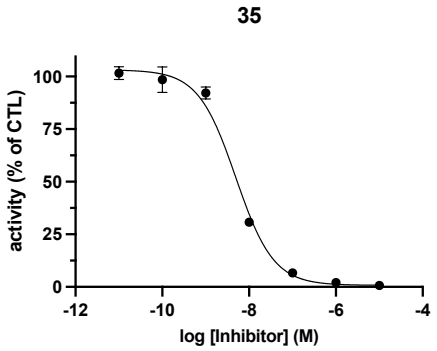

*Figure 36: Inhibition curve of lead **35** (IC_{50} = 4.9 nM [3.8 – 6.4]).*

To verify the transition from bicycle **56** to bicycle **91**, which are the bicyclic [4.2.0] equivalent of the lead **35** respectively with and without the terminal double bond (the latter being preferred for synthetic reasons), we

first needed to evaluate the impact of the double bond on inhibition (**Figure 37**). To achieve this, J. Caruano synthesised and tested the IC_{50} of **54**, on *m*FAAH. She obtained an IC_{50} of 8.0 nM.[2] We observed that this value is quite similar to that of lead **35**, allowing us to conclude that the presence of this double bond has no a major impact on the inhibition capacity of *m*FAAH. In doing so, we also validated the choice to transition from **56** to **91**.

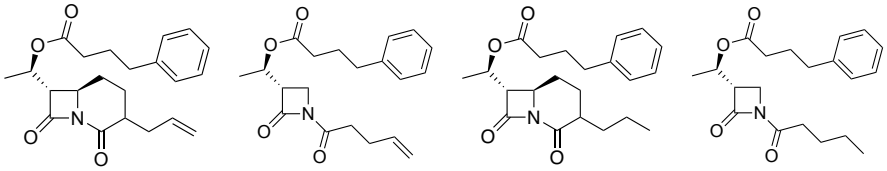

56 **35** **91** **54**

*Figure 37: Bicyclic equivalent of the lead (**56**), lead (**35**), reduced equivalent of bicycle **56** (**91**) and reduced equivalent of the lead (**54**).*

For bicycle **91**, two diastereomers are possible, **91a** and **91b**, which differ by the absolute configuration of the carbon in α to the carbonyl on the six-membered ring (**Figure 38**). The absolute configuration of this carbon is *(R)* for **91a** and *(S)* for **91b**. These two diastereomers were synthesised, isolated, and identified (see section 4.5.7). A modification of the synthesis of **91** also allowed us to obtain bicycle **104**, corresponding to the α,β-unsaturated equivalent of bicycle **91**. We then measured the IC_{50} of *m*FAAH for these three compounds. Compound **91a** has an IC_{50} of 55.0 nM [42.1 – 72.2], while the value is 197 nM [157 – 247] for **91b** and 171 nM [122 – 240] for **104** (**Figure 39**).

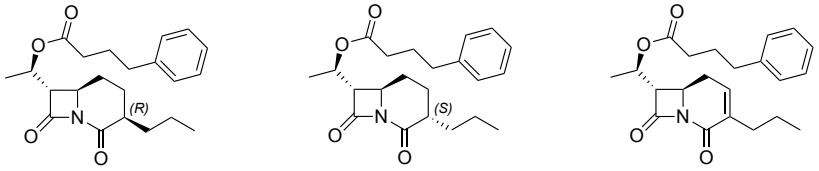

91a **91b** **104**

*Figure 38: Diastereomer (R) of **91** (**91a**), diastereomer (S) of **91** (**91b**) and α,β-unsaturated bicycle (**104**).*

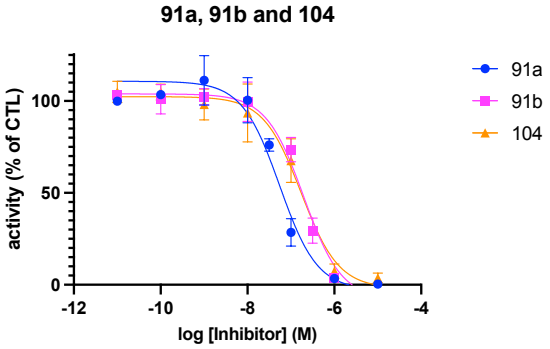

*Figure 39: Inhibition curves of **91a** (blue; IC_{50} = 55.0 nM [42.1 – 72.2]), **91b** (magenta; IC_{50} = 197.3 nM [157 – 247]) and **104** (orange; IC_{50} = 171.1 nM [122 -240]),*

Surprisingly, none of the three bicycles has a value comparable to that of lead **35** (4.9 nM [3.8 – 6.4]), showing significantly lower inhibition potency. This is unexpected because the bicycle structure forces the two carbonyls into a *syn* configuration unlike the lead where an equilibrium between the two conformations has been demonstrated, favouring the *anti* conformation. As discussed above, the docking studies have shown that this *syn* conformation is important, as the two carbonyls of the imide can interact with Ser_{241}. It is thus somewhat surprising that the IC_{50} values for each of the bicycles are higher. These results suggest that the intrinsic structure of the bicycle allows for less effective stabilisation of the molecule within the enzymatic cavity. To confirm this hypothesis and further explain it, it is necessary to turn to docking studies which could provide more detailed information (see section 8.3). Nevertheless, even if the tested bicycles are not as effective as the lead, they still have quite reasonable IC_{50} values, all being in the nanomolar range.

It is also interesting to compare the effectiveness of the three bicyclic compounds with each other. It is important to note that the configuration of the carbon bearing the propyl chain seems to have a significant impact on inhibition. Indeed, compound **91a** (configuration *(R)*) has an IC_{50} approximately 3.58 times smaller than **91b** (configuration *(S)*). Additionally,

compound **104**, possessing an α,β-unsaturation, and thus a planar propyl chain relative to the ring, shows an intermediate IC_{50} value. These results suggest that the propyl chain orients differently depending on the molecules and stabilises the molecule inside the enzymatic cavity with varying efficiency. It is also interesting to compare these values to that of molecule **144**, which is the equivalent of bicycle **91** without the propyl chain (**Figure 40**). This molecule is an intermediate from a synthetic strategy considered to obtain **56** in a previous project that was not conclusive.[100] The IC_{50} of **144** was measured, yielding a value of 44.7 nM. It is very surprising to note that this IC_{50} is lower than all the bicycles considered in this project. These results seem to indicate that the presence of the alkyl chain on the bicycle tends to decrease the potency of the molecules, whereas it had been previously demonstrated that the alkyl chain on the monocyclic β-lactam had a positive influence on the stabilisation of the molecule in the enzymatic cavity.[82] Considering all these results, it seems reasonable to think that the bicyclic compounds do not behave in the same way within the enzyme as the monocyclic compounds like lead **35**. Moreover, these results indicate that the bicycles do not position themselves in the enzymatic cavity as stably as the lead. Docking studies could thus provide valuable information to understand these differences (see section 8.3).

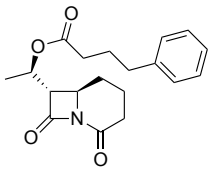

144

Figure 40: Bicycle without the propyl side chain.

Regarding the stereoisomers of the lead compound, as previously discussed we were not able to obtain the pure stereoisomers (see section 5.3.3). However, we reasoned that it would still bring interesting insights to test the mixtures that we obtained as those had different proportion of

stereoisomers. The first mixture consists of the lead **35** and its enantiomer **116** (fraction 1, see section 5.3.3.1), while the second mixture contains at least three of the four stereoisomers (**35**, **116**, and **63**), although we suspect the presence of all four (fraction 2, see section 5.3.3.2) (**Figure 41**). Given that these are mixtures of products, the obtained IC_{50} must be interpreted with caution. Indeed, each stereoisomer may have a different inhibition efficiency or even be inactive. Nonetheless, the evaluation of the median inhibitory capacity was carried out as an indicative measure to obtain a preliminary idea of the effectiveness of the lead stereoisomers. For fraction 1, an IC_{50} of 10.5 nM [8.6 – 12.9] was measured, while fraction 2 has an IC_{50} of 14.2 nM [12.1 – 16.2] (**Figure 42**). These values, although higher than that of the lead (4.9 nM [3.8 – 6.4]), initially suggest that the stereochemistry of the two present centres does not have a major influence. This seems particularly true for the mixture of the two enantiomers, but, as mentioned, these results should be interpreted with caution. Future investigations allowing to obtain the pure stereoisomers will help to validate our hypothesis.

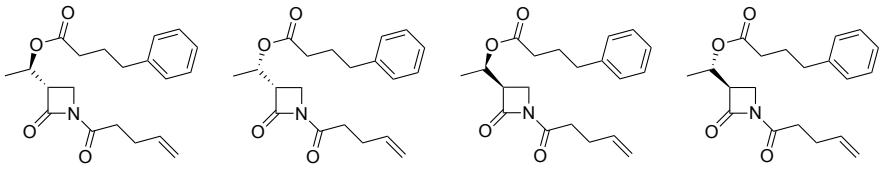

35 **63** **115** **116**

*Figure 41: Stereoisomers of the lead: **35** (lead), **63**, **115** and **116**.*

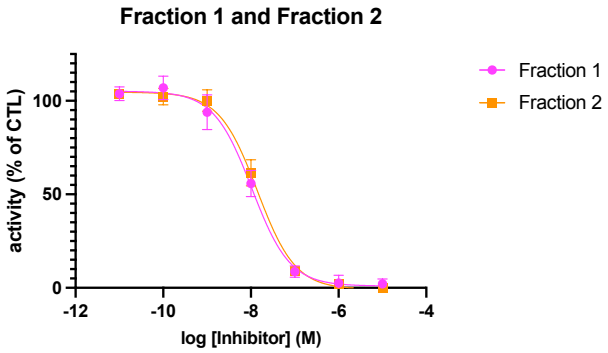

*Figure 42: Inhibition curves of Fraction 1 (magenta; containing **35** and **63**, IC_{50} = 10.5 nM [8.6 – 12.9]) and Fraction 2 (orange; containing **35**, **63**, **116** and probably **115**, 14.0 nM [12.1 – 16.2]).*

We are also planning to determine the potency of molecule **117**. As explained earlier (see section 6.1), it has been demonstrated that the carbonyl group of the ester function has virtually no influence on the inhibition efficiency, and its ether equivalent showed an IC_{50} similar to that of the lead (8.0 nM) (**Figure 43**).[3] Furthermore, it has been shown that the double bond is not essential for inhibition, with the reduced molecule having an IC_{50} of 8.0 nM.[2] This led us to consider the lead compound by combining the modifications that did not influence inhibition. This compound is of particular interest, as it is likely to offer greater stability under physiological conditions. Indeed, replacing the ester with an ether should prevent potential hydrolysis of the compound in these conditions. Unfortunately, the IC_{50} of molecule **117** has not yet been determined due to technical issues.

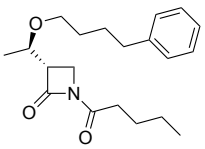

117

*Figure 43: Equivalent of the lead without the double bond and the carbonyl of the ester function (**117**).*

7.3 *In cellulo* studies

After determining the potency of the molecules in a biochemical assay, we conducted a study to verify whether the tested molecules could increase NAE levels in intact cells. The principle involves exposing cells to the studied inhibitor. If the molecule is effective (and is cell permeant), it will inhibit FAAH, allowing for an increase in NAE levels.

For this study, we used a murine macrophage cell line, namely the J774 cells. These cells were chosen as previous studies showed that they express FAAH and that well known FAAH inhibitors (*e.g.* PF-3845) are able to increase NAE levels .[113] J774 cells cultures were prepared with 10^7 cells per dishes (see section 10.2.2). The cells were incubated with the inhibitors (10 μM) or vehicle (DMSO) for 5h. Following the incubation, the cell lipid was extracted and the cellular NAE and endocannabinoids analysed by HPLC-MS/MS as routinely performed in the lab. Of note, the LC-MS/MS method used allows for the detection of several NAEs allowing to assess in a single experiment the effect of the molecules of interest on several NAEs. Here for the sake of clarity we will discuss the data obtained for the NAE most often reported in these types of assay, namely AEA **6**, PEA **10**, OEA **11**, and SEA **12** (**Figure 44**). While the former is an endocannabinoid, PEA, OEA and SEA do not bind the cannabinoid receptors and are thus not considered as endocannabinoids, but are "associated" to the endocannabinoid system as their biochemistry (synthesis, release, and degradation) is similar.

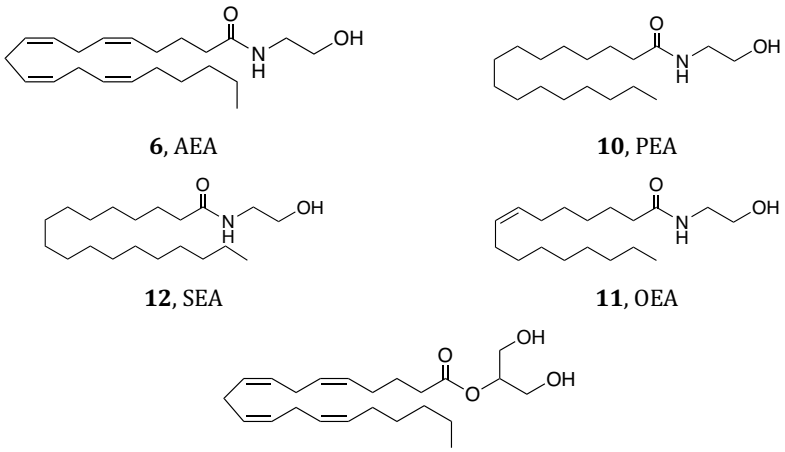

6, AEA **10**, PEA

12, SEA **11**, OEA

7, 2-AG

Figure 44: N-arachidonoylethanolamine (anandamide, AEA) ***6,*** *N-palmitoylethanolamine (PEA)* ***10****, N-stearoylethanolamine (SEA)* ***12****, N-oleoylethanolamine (OEA)* ***11*** *and 2-arachidonoylglycerol (2-AG)* ***7****.*

Five inhibitors were studied here. First, we focused on lead **35**, which had never been studied in cells before (**Figure 45**). Among the three bicyclic compounds obtained in this project, bicycle **91a** showed the best *in vitro* efficacy was also studied. The equivalent of the lead without the double bond, **54**, was also studied. It was demonstrated that the absence of the double bond does not affect the IC_{50}, so it is interesting to see if this trend is confirmed in cells. The fourth molecule is the lead equivalent with an ether function instead of the ester and without the double bond (**117**), allowing us to study the influence of the ester function in cells. It is known that ester functions can easily be hydrolysed in biological settings, thus reducing the concentration of the molecule. This comparison will help determining if this is the case for our molecules. Finally, molecule PF-3845 **38** was used as a reference. It is known to be a good inhibitor (IC_{50} = 230 nM), irreversible and highly selective for FAAH, and very effective *in vivo*.[83] The levels of NAE in inhibitor-treated cells were compared to those found in vehicle-treated cells following 5h of incubation in the presence of the treatment.

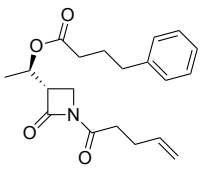

35, IC_{50} = 4.9 nM [3.8 -6.4]

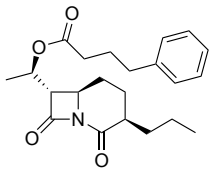

91a, IC_{50} = 55.0 nM [42.1 – 72.2]

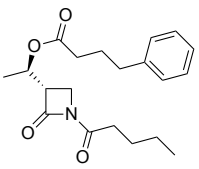

54, IC_{50} = 8.0 nM

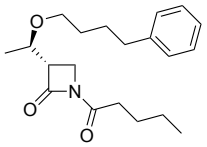

117, IC_{50} not determined

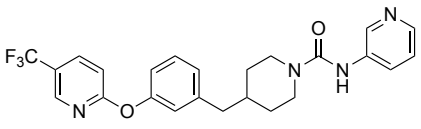

38, IC_{50} = 230 nM

*Figure 45: Lead (**35**), Diastereomer (R) of **91** (**91a**), reduced equivalent of the lead (**54**), Equivalent of the lead without the double bond and the carbonyl of the ester function (**117**) and PF-3845 (**38**).*

Regarding anandamide **6**, molecule PF-3845 increases its levels compared to the vehicle (**Figure 46**), as previously reported, confirming that incubating J774 cells with a FAAH inhibitor leads to increased AEA levels. Molecules **35** and **91a**, also increased AEA levels while molecule **54** showed a trend to increase AEA levels. In contrast, molecule **117** shows very good efficacy, similar to that of the reference PF-3845, which is encouraging. This suggests that all our β-lactam compounds can increase anandamide levels in cells and potentially be effective in acting on the endocannabinoid system. The molecule with an ether function also stands out, which could confirm our hypothesis of ester function hydrolysis.

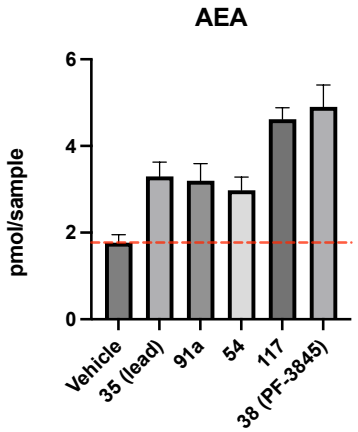

*Figure 46: AEA levels (in pmol/sample) measured for vehicle, **35**, **91a**, **54**, **117** and PF-3845 (**38**).*

Similar effects were observed for OEA **11** and PEA **10** levels (**Figure 47**). Molecules **35**, **91a**, and **54** do not significantly increase NAE levels. However, molecule **117** increases them significantly, although less effectively than PF-3845.

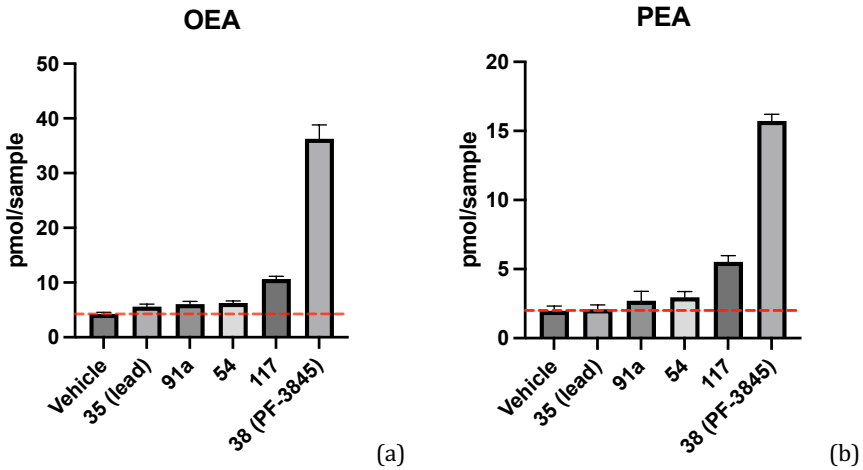

(a) (b)

*Figure 47: (a) OEA levels (in pmol/sample) measured for vehicle, **35**, **91a**, **54**, **117** and PF-3845 (**38**) and (b) PEA levels (in pmol/sample) measured for vehicle, **35**, **91a**, **54**, **117** and PF-3845 (**38**).*

Regarding SEA **12**, the lead **35** and its reduced version **54** showed a tendency to increase SEA levels in J774 cells while the bicycle **91a** did not alter SEA levels (**Figure 48**). As for the other NAE measured, molecule **117**, increased SEA levels almost to the same extent than the reference PF-3845.

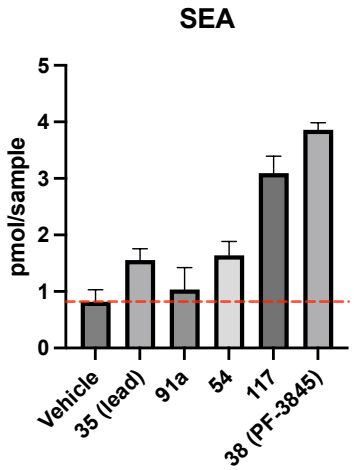

*Figure 48: SEA levels (in pmol/sample) measured for vehicle, **35**, **91a**, **54**, **117** and PF-3845 (**38**).*

Although 2-AG **7** levels are dependent on the activity of esterases (*i.e.* MAGL and ABHD6), it is interesting to assess its levels as 2-AG is the other major endocannabinoid. A small increase in 2-AG levels was observed with the reference FAAH inhibitor **38** and with the molecules **35** (our lead) and **54** (**Figure 49**). As a reminder, in vitro, both **38** (PF-3845) and the lead **35** are highly selective for FAAH vs MAGL suggesting that the increased 2-AG levels are not due to MAGL inhibition but rather to intracellular consequences of FAAH inhibition.

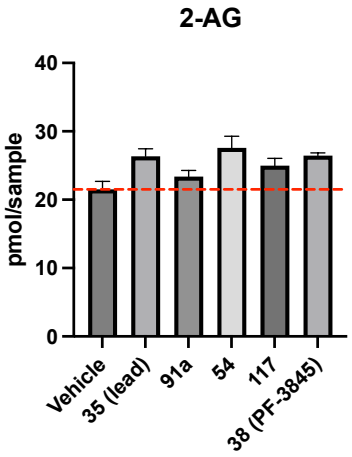

*Figure 49: 2-AG levels (in pmol/sample) measured for vehicle, **35**, **91a**, **54**, **117** and PF-3845 (**38**).*

In summary, although all the tested β-lactam increased AEA levels, molecule **117** stands out as increasing the levels of all the NAE measured.

Chapter 8: Docking studies

8.1 Introduction

Docking studies were conducted in collaboration with Professor Catherine Michaux (UNamur). They aimed at three main objectives: first, as mentioned in section 3.6, the pharmacological studies were performed on *m*FAAH whereas previous studies had been conducted on *h/r*FAAH. The docking studies probed the impact of this change in FAAH. Next, the modelling studies were applied to different molecules obtained in this project (bicyclic compounds **91a**, **91b**, **104**, and monolactams **54** and **117**; **Figure 50**) in order to understand how they are fitting inside and interacting with the enzyme. Finally, the study served as a predictive tool to propose new molecules that could enhance our understanding of β-lactam inhibitors.

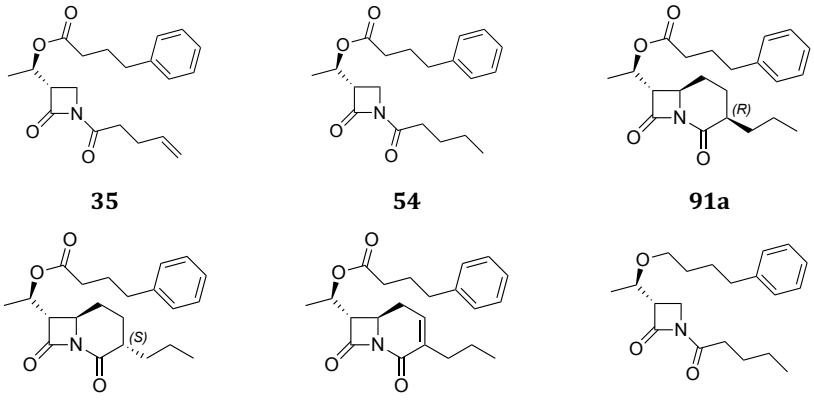

*Figure 50: lead (**35**), reduced equivalent of the lead (**54**), diastereomer (R) of **91** (**91a**), diastereomer (S) of **91** (**91b**), α,β-unsaturated bicycle (**104**) and equivalent of the lead without the double bond and the carbonyl of the ester function (**117**).*

8.2 Transition from *h*FAAH to *m*FAAH

The pharmacological studies in this project used *m*FAAH. However, until now, all published studies on our inhibitors had been conducted on *h*FAAH (see section 3.6.).[82] To assess whether the inhibitors are similarly potent for *h*FAAH and *m*FAAH, the IC_{50} of lead **35** was determined for *m*FAAH

(IC_{50} = 4.9 nM [3.8 – 6.4]). Comparing this result to the published data on *h*FAAH (IC_{50} = 5.0 nM), we found that lead **35** produced similar results for both FAAH.[82]

To validate this change, we conducted docking studies comparing *m*FAAH to *h/r*FAAH, as the 3D structure of *h*FAAH has not yet been determined by X-ray diffraction.[82, 88-89] Previous studies on the lead **35** for *h/r*FAAH had shown that the molecule adopted an interaction mode (called mode 1) with both carbonyls of the imide function ("CO_{lactam}" and "CO_{exo}") adopting a *syn* conformation in the enzymatic cavity (Ser_{217}-Ser_{241}-Lys_{142}), with the two carbonyls interacting with Ser_{241} and Ser_{217} *via* H-bonds (**Figure 51**) The phenyl group of the ester chain is located in a "phenyl pocket" formed by three phenylalanine residues (Phe_{388}, Phe_{381}, and Phe_{192}).

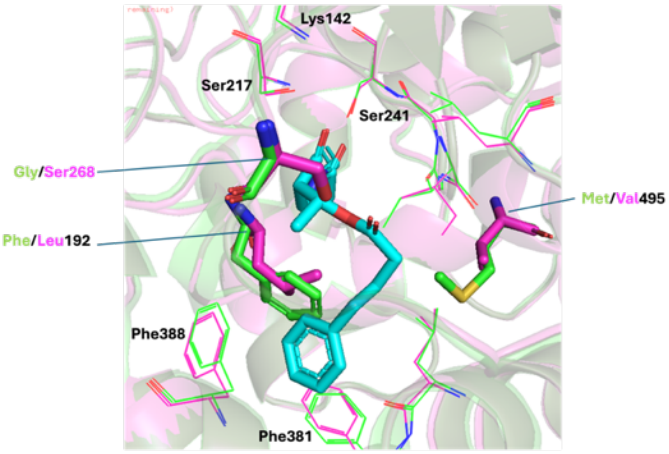

(a)

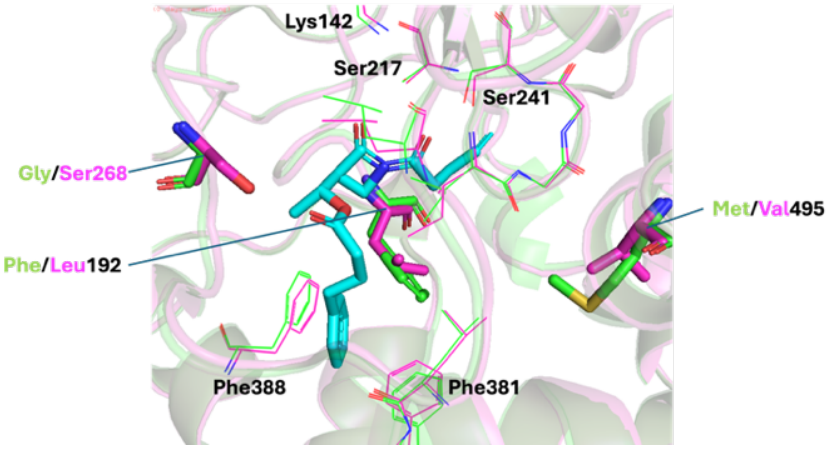

(b)

*Figure 51: Active site (a) in view A and (b) in view B of the human (green) and mouse (magenta) FAAH with **35** (turquoise) in the binding mode 1.*

Comparing *m*FAAH to *h/r*FAAH, we observed a high similarity between the sequences, with 84% identical sequence. In the binding site, only three amino acid residues differ:

- at position 192, phenylalanine in *h/r*FAAH is replaced by leucine in *m*FAAH;
- at position 268, glycine is replaced by serine;
- at position 495, methionine is replaced by valine (see **Figure 51**).

These differences do not affect the efficacy of lead **35**, which appears to bind similarly in the enzymatic cavity. These results support the similarity between *m*FAAH and *h*FAAH and underpin the relevance of working with *m*FAAH.

8.3 Results

Regarding the bicyclic β-lactams (**56** and **91**), intended to lock the *syn* configuration, we chose to prepare the reduced versions of the lead for synthetic reasons (see section 4.2.5). This choice was validated since the lead **35** and its reduced version **54** showed similar IC_{50} values (4.9 nM [3.8 - 6.4] and 8.0 nM, respectively). The docking studies support these results, showing

that the allyl group does not make particular interactions in this mode of interaction (mode 1) (**Table 22**).

*Table 22: Non-covalent interactions between mFAAH and the compounds **35**, **54**, **91a**, **117**, **145**, **146** and **147**.*

Entry	Compound	Non-covalent interactions[a] [Å]	Binding score function[b]	IC_{50} [nM]
1	**35**	***Mode 1*** $Ser_{217}(O)...O(CO_{lactam})$: 3.4 $Ser_{217}(O)...O(CO_{exo})$: 2.8 $Ser_{241}(O)...O(CO_{exo})$: 2.1 $Ser_{268}...O(CO_{ester})$: 3.8 Phe_{381}-Phe: 4.4 $Val_{270}(CH)...Phe$: 3.3	63.7	4.9
2	**54**	***Mode 1*** $Ser_{217}(O)...O(CO_{lactam})$: 3.8 $Ser_{217}(O)...O(CO_{exo})$: 2.7 $Ser_{241}(O)...O(CO_{exo})$: 2.4 $Ser_{268}...O(CO_{ester})$: 2.2 Phe_{381}-Phe: 4.8 $Val_{270}(CH)...Phe$: 3.0	66.5	8.0
3	**91a**	***Mode 2*** $Ser_{217}(O)...O(CO_{ester})$: 2.6 $Ser_{241}(O)...O(CO_{ester})$: 2.7 $Phe_{381}...CH$: 3.6 $Leu_{192}(CH)...Phe$: 2.9	52.10	55.0
4	**117**	***Mode 1*** $Ser_{217}(O)...O(CO_{lactam})$: 3.6 $Ser_{217}(O)...O(CO_{exo})$: 2.7 $Ser_{241}(O)...O(CO_{exo})$: 2.4 Phe_{381}-Phe: 4.8 $Val_{270}(CH)...Phe$: 3.0	62.40	n.d.

Entry	Compound	Non-covalent interactions[a] [Å]	Binding score function[b]	IC_{50} [nM]
5	**145**	***Other mode*** *(with the phenyl pointing towards the enzyme surface)* $Ser_{268}(O)...O(CO_{lactam})$: 2.1 $Val_{270}(N_{backbone})...O(CO_{lactam})$: 2.7	47.40	n.d.
6	**146**	***Mode 2*** *(8th solution)* No H-bonds $Leu_{192}(CH)...Phe$: 2.7 $Phe_{381}...CH$: 4.5	39.39	n.d.
7	**147**	***Mode 2*** $Ser_{217}(O)...O(CO_{ester})$: 2.7 $Ser_{241}(O)...O(CO_{ester})$: 2.9 $Leu_{192}(CH)...Phe$: 2.9 $Phe_{381}...CH$: 3.5	53.78	n.d.
		Mode 2 $Ser_{217}(O)...O(CO_{ester})$: 2.6 $Ser\ 241(O)...O(CO_{ester})$: 2.5 Phe_{381}-Phe: 5.1 $Val_{270}(CH)...Phe$: 2.9	63.67	n.d.

[a]Non-covalent interactions are given for H-bonds (in blue), π-π interactions (measured as the distance between aromatic centroids, in purple) and CH-π interactions (measured as the distance between a H and an aromatic centroid, in green). [b]The binding score function is a mathematical function that provides a numerical value (score) representing the affinity of the inhibitor (ligand) for each of its conformations with the target protein. The higher the value of the binding score function, the greater the affinity between the ligand and the target.

Bicycles **91a**, **91b**, and **104** were docked and compared to the results of **54**. The pharmacological results were surprising because the bicycles were less effective inhibitors despite the locked *syn* configuration. In fact, the docking studies revealed that the bicycles did not interact in the same

binding mode as the monocyclic compounds (mode 1). In the most favourable binding mode of the bicycles, the ester interacts with the catalytic triad, and the alkyl chain is located in the phenyl pocket. The phenyl group, meanwhile, is at the beginning of the ACB chain (**Figure 52**). In this new binding mode (mode 2), the molecule reverses in the enzymatic cavity compared to mode 1. It is important to emphasise that for bicyclic compounds, mode 1 exhibits fewer stabilising interactions than mode 2, which explains why the molecules preferentially adopt this second mode of interaction. The problem with this new binding mode is that it results in the loss of several molecular interactions with the enzyme (see **Table 22**). First, it is the ester, not the imide, that is oriented towards the serines of the triad. This limits the hydrogen bonds to one carbonyl ("CO_{ester}") with Ser_{241} and Ser_{217}, whereas in mode 1, the monolactams could form three H-bonds thanks to the two carbonyls of the imide (CO_{lactam} and CO_{exo}). Furthermore, in mode 2, the imide can no longer interact at all, unlike in mode 1 where the CO_{ester} could form an H-bond with Ser_{268}. Finally, in mode 2, the loss of the double bond could reduce interaction efficiency, as the allyl group could establish π-π interactions with the phenyl pocket.

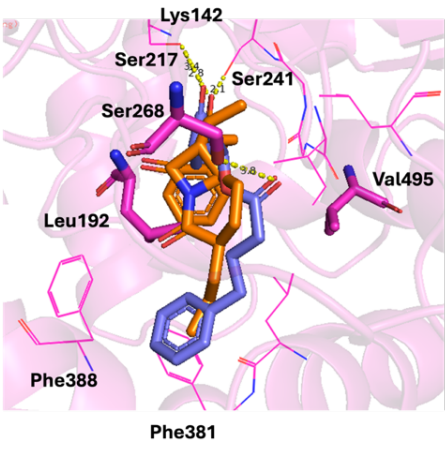

(a)

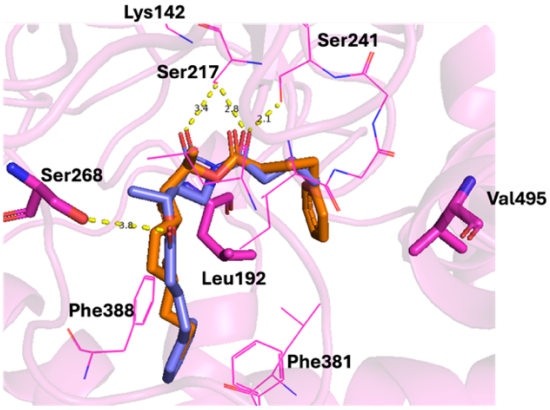

(b)

*Figure 52: Active site (a) in view A and (b) in view B of the mouse (magenta) FAAH with **54** (purple) and **91a** (orange).*

The docking studies also allowed us to compare the three bicycles **91a**, **91b**, and **104** among themselves (**Figure 53**). The three compounds position themselves similarly, with only differences in the alkyl chain, which, in the case of **91b** and **104**, is closer to Leu_{380} than **91a**, possibly leading to steric clash. These observations are consistent with the measured IC_{50} values (55.0 nM [42.1 – 72.2] for **91a**, 197 nM [157 – 247] for **91b**, and 171 nM [122 – 240] for **104**).

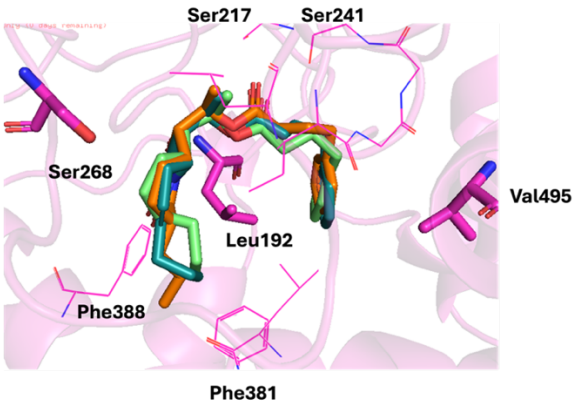

*Figure 53: Active site of the mFAAH (magenta) with **91a** (orange), **91b** (light green) and **104** (dark green).*

Having conducted these docking studies on *m*FAAH, we then performed them on *h/r*FAAH. For **91a** and **91b**, identical results were obtained with only mode 2 observed. However, for compound **104**, both modes are possible (with a predominance of mode 1) for *h/r*FAAH, while only mode 2 is observed for *m*FAAH. These unexpected results are difficult to rationalise in a simple way and must be due to the subtle differences between the two enzymes.

For β-lactam **117**, the docking studies showed that it interacts in the same mode as the lead (mode 1), but with a slightly lower function score than compound **54**, likely due to the loss of the H-bond of CO_{ester} with Ser_{268}, as the ester is replaced by an ether in the case of molecule **117**. In *h/r*FAAH, the same conclusions can be drawn.

8.4 Perspectives

We envisaged the docking of three new bicyclic molecules in order to investigate the importance of the different interactions and try to find a bicyclic β-lactam with improved FAAH inhibition activity.

First, two molecules, **145** and **146**, with modifications compared to **91a**, allow us to validate our hypotheses about the interaction mode of bicyclic compounds (**Figure 54**). For molecule **145**, the ester function is replaced by an ether function, depriving the molecule of CO_{ester}, which interacts with the serines of the triad (**Figure 55**). Studies show that this bicycle **145** does not stabilise well in the enzymatic cavity, so we expect it to have a poor IC_{50}. Bicycle **146** retains the ester function, but the CO_{lactam} and CO_{exo} carbonyls on the cycle have been removed, transforming the imide function into an amine function. Our results show that this compound continues to interact with the enzymatic cavity (**Figure 56**). We expect it to have an IC_{50} similar to **91a**. Once synthesised and their IC_{50} values determined, these molecules should reinforce the explanation of the

interaction mode and explain the lower efficacy of bicyclic compounds compared to the lead.

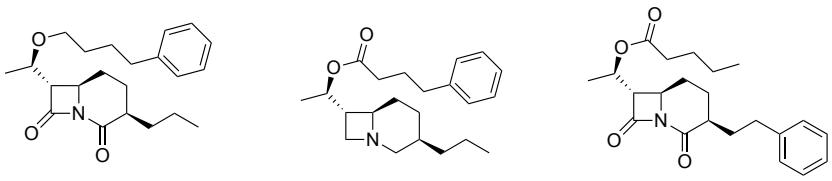

145 **146** **147**

*Figure 54:Equivalents of the bicycle **91a** with the ester replaced by ether (**145**), the imide replaced by amine (**146**), the alkyl and phenyl chains are reversed (**147**).*

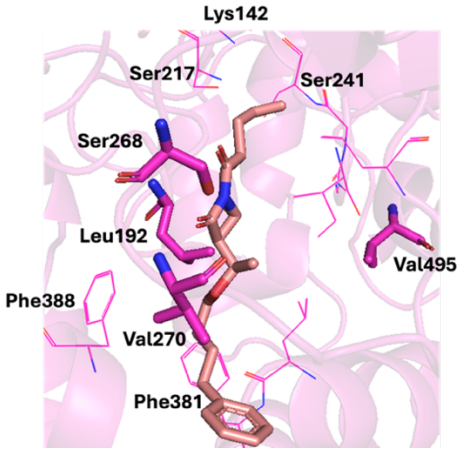

(a)

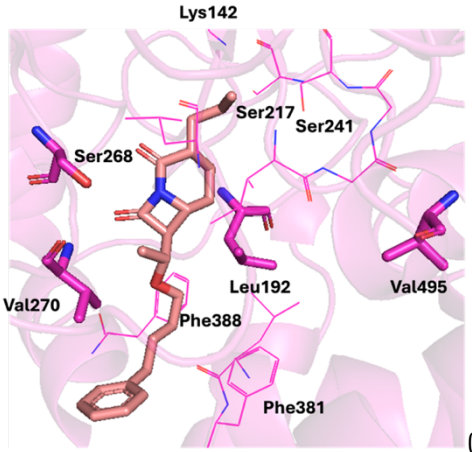

(b)

*Figure 55: Active site (a) in view A and (b) in view B of the mouse (magenta) FAAH with **145** (light pink). Binding score function of 39.39 for mode 2 and 47.40 for the other mode.*

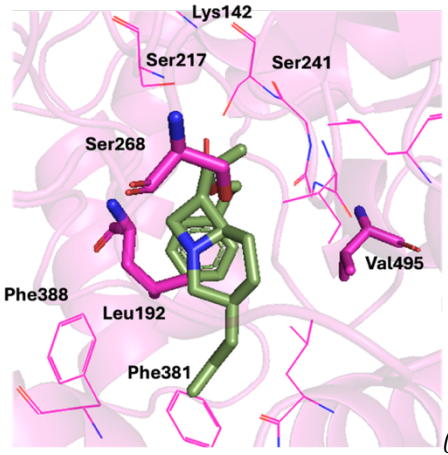

(a)

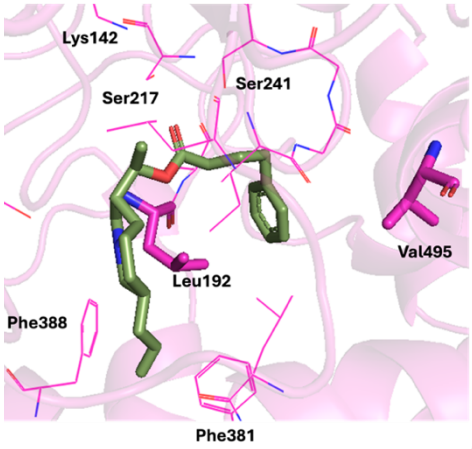

(b)

*Figure 56: Active site (a) in view A and (b) in view B of the mouse (magenta) FAAH with **146** (dark green). Binding score function of 53.78 for mode 2*

The third molecule, **147**, reverses the two side chains of the bicyclic compound, placing the phenyl chain on the nitrogen and the alkyl chain on the ester (see **Figure 54**). Docking studies show that this molecule also adopts mode 2, but the phenyl group now ends up in the phenyl pocket, allowing additional interactions and a higher function score (**Figure 57**). Testing this molecule would not only support our hypotheses about the

interaction mode but also use our new knowledge to improve the efficacy of β-lactam compounds as FAAH inhibitors.

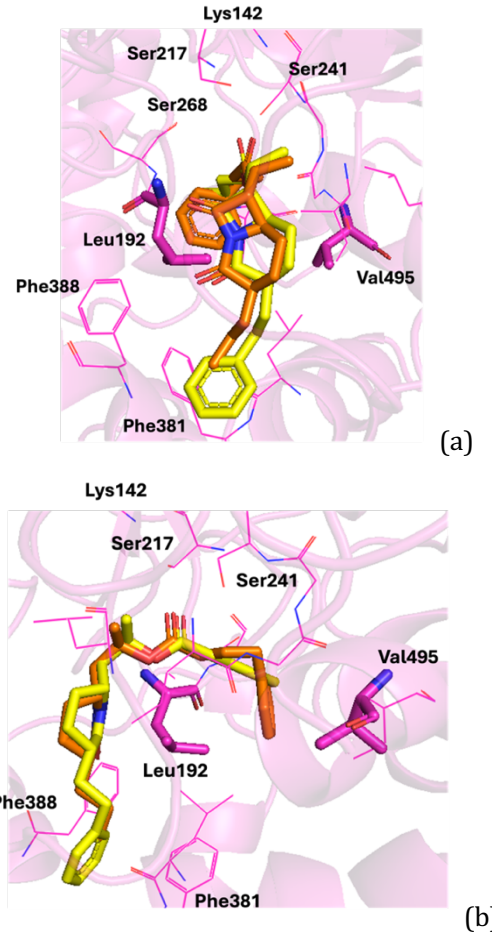

Figure 57: Active site (a) in view A and (b) in view B of the mouse (magenta) FAAH with ***91a*** *(orange) and* ***147*** *(yellow). Binding score function of 63.67 for mode 2*

Chapter 9: Conclusions and perspectives

The synthesis of different compounds, pharmacological results, and docking studies have been addressed separately for clarity in this manuscript. However, it is crucial to emphasise that these areas are closely linked and interdependent. This concluding chapter aims to summarise the progress of the investigation cycle for each studied target: synthesis, pharmacology, docking, and so on. As mentioned in section 3.1 on the general objectives and methodology of this project, there is a virtuous circle between these three research areas. They are highly dependent on each other and mutually reinforcing. This manuscript also aims to demonstrate the highly interdisciplinary nature of this project.

9.1 Transition from *h*FAAH to *m*FAAH

To determine the potency of the synthesised molecules, we chose to work with mouse brain homogenate, which allowed us to obtain the IC_{50} values for *m*FAAH. Our choice to work with mice aligns with the development of a drug. Indeed, in the process of developing a new drug, thorough studies on mice are conducted. Therefore, working with mice serves as a good starting point in this context. Additionally, in our laboratory, *m*FAAH is more readily available than *h*FAAH.

To validate this transition, we determined the IC_{50} of the lead compound **35** for *m*FAAH and obtained a value of 4.9 nM [3.8 – 6.4], very close to the published value for *h*FAAH (5.0 nM).[82] These similar values allowed us to validate this change. Additionally, this validation was corroborated by docking studies, which revealed only three amino acid residue changes in the enzymatic cavity, without a significant impact on the interactions of the lead compound with the enzyme.

9.2 Bicyclic Compounds

The project involving bicyclic β-lactam compounds began following docking studies that demonstrated that the two carbonyls of the imide function in our compounds adopt a *syn* conformation to interact optimally with the serines in the catalytic triad.[82] However, for monolactams, there is an equilibrium between *syn* and *anti* conformations, favouring the *anti* conformation. Considering bicyclic compounds allowed us to lock the *syn* configuration for these compounds.

The bicyclic equivalent **56** of the lead compound **35** was thus considered but, despite all our attempts, we were unable to synthesise it (**Figure 58**). The main difficulty was the inability to insert the allyl chain in the α position of the carbonyl, leading to the opening of the bicycles at the six-membered ring. However, after confirming that the double bond does not affect the potency of our inhibitors, we considered **91**, the reduced version of **56**. Bicyclic **91** was synthesised in six steps from commercially available azetidinone **32**, with an overall yield of 17%. The success of this synthetic route, compared to the one attempted for **56**, is attributed to the direct insertion of the propyl chain during N-acylation before the ring-closing metathesis. Compound **91** was obtained as a mixture of two diastereomers, **91a** and **91b**, in a 55/45 ratio. The two diastereomers were isolated and identified *via* NOESY analysis.

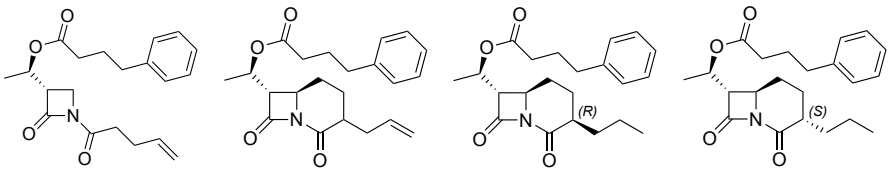

35 **56** **91a** **91b**

*Figure 58: Lead (**35**), [4.2.0] bicyclic analogue of the lead (**56**), diastereomer (R) of **91** (**91a**) and diastereomer (S) of **91** (**91b**).*

By modifying the synthetic route to obtain **91**, we also produced its α,β-unsaturated equivalent **104** in five steps, with an overall yield of 24% (**Figure 59**).

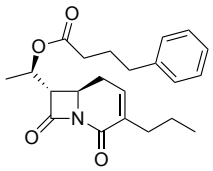

104

*Figure 59: α,β-unsaturated bicycle (**104**).*

Pharmacological studies were conducted on these bicyclic compounds. The median inhibitory concentration was determined for *m*FAAH for the three bicycles **91a**, **91b**, and **104**. Surprisingly, the inhibitors were not as effective as expected, with IC_{50} values of 55.0 nM [42.1 – 72.2], 197 nM [157 – 247], and 171 nM [122 – 240], respectively, even though the *syn* configuration of the two imide carbonyls was locked. These results suggested that another factor was influencing the difference. Subsequent cell tests (murine macrophages J774) on bicyclic **91a** showed that the inhibitor moderately increased AEA (**6**) and SEA (**12**) levels in cells, without increasing 2-AG (**7**) levels, demonstrating its selectivity towards the FAAH over MAGL.

Docking studies provided answers regarding the lack of efficacy of the bicyclic compounds. These studies showed that the bicyclic compounds did not interact in the enzymatic cavity in the same way as the monolactams (mode 1). In contrast, bicyclic compounds have a different interaction mode (mode 2) where the ester carbonyl interacted with the serines in the catalytic triad, the phenyl group was at the beginning of the ACB channel, and the alkyl chain was in the phenyl pocket. The imide function did not make significant interactions. Essentially, the bicyclic compounds were reversed in the enzymatic cavity compared to the monolactams. Making fewer stabilising

interactions could explain their lower inhibitory efficacy as seen in the IC_{50} evaluations.

Docking studies also opened interesting perspectives for further research on bicyclic compounds, justifying the consideration of three new molecules (**Figure 60**). Firstly, it would be interesting to prepare molecules **145** and **146**. Molecule **145** is the bicyclic **91a** with the ester function replaced by an ether function. We expect this molecule to have a worse IC_{50} than **91a** because the single carbonyl interacting with the serines in the catalytic triad is now absent. We also considered molecule **146**, where the carbonyls of the imide function were removed, which should not significantly alter the IC_{50} since these two carbonyls do not make significant interactions. These two molecules will strengthen our hypotheses regarding the lack of efficacy of the bicyclic compounds. To use our new knowledge to improve the efficacy of bicyclic compounds, we also considered molecule **147**, where the phenyl-containing chain and the alkyl chain were reversed compared to **91a**, allowing the phenyl group to interact with the phenyl pocket again.

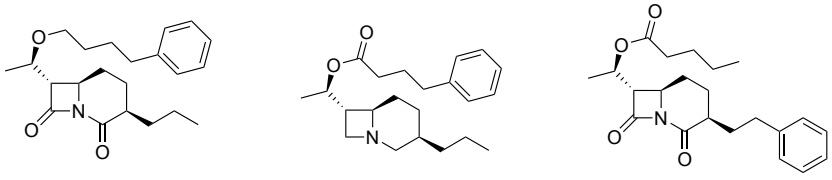

145 **146** **147**

*Figure 60: Equivalents of the bicycle **76a** with the ester replaced by ether (**145**), the imide replaced by amine (**146**) and the alkyl and phenyl chains are reversed (**147**).*

For the synthesis of **145**, we could follow the method for **91a**, replacing the esterification step with a reaction forming an ether (**Scheme 62**). For example, 4-phenylbutyryl bromide in the presence of KI and NaH, conditions previously published for the synthesis of **137**, could be used.[3]

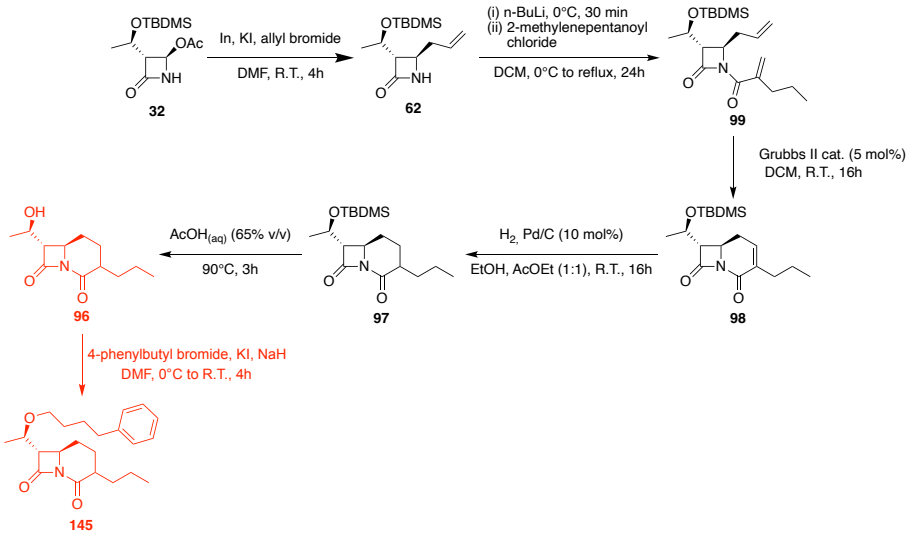

*Scheme 62:Proposed synthesis of **145**.*

For the synthesis of **146**, we could also follow the method for **91a**, inserting a reduction step with $LiAlH_4$ between hydrogenation and alcohol deprotection to transform the imide into an amine (**Scheme 63**).[114]

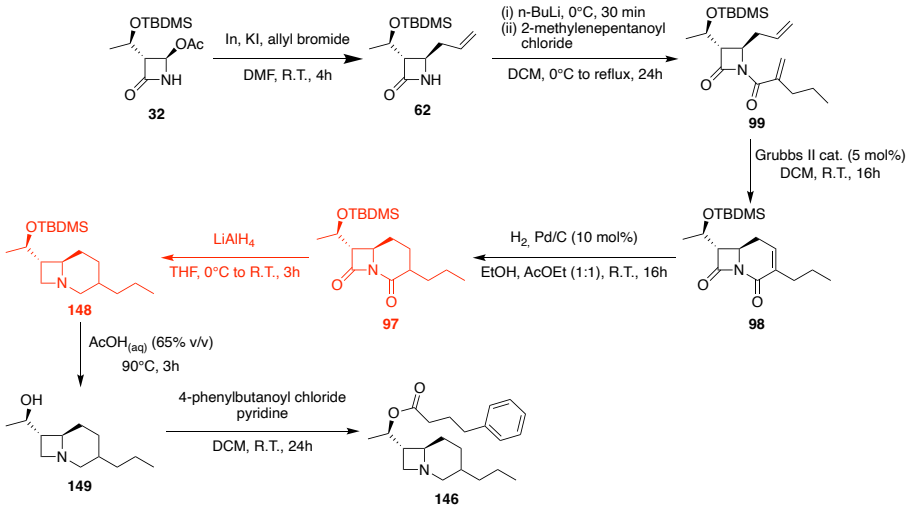

*Scheme 63: Proposed synthesis of **154**.*

For the synthesis of **147**, we could replace the diethyl n-propylmalonate used for **91a** with commercially available diethyl 2-

phenethylmalonate and 4-phenylbutanoyl chloride with pentanoyl chloride (**Scheme 64**).

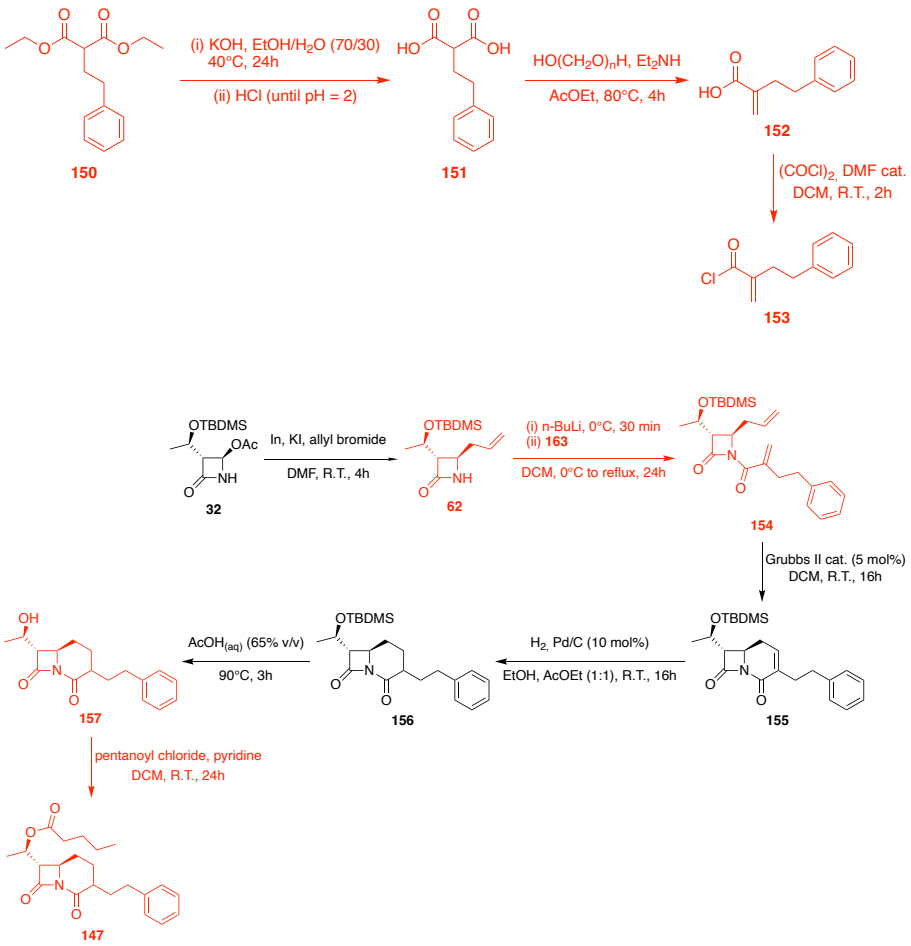

*Scheme 64: Proposed synthesis of **147**.*

In conclusion, this project involving bicyclic β-lactam compounds is an excellent example of the project's philosophy, where multiple bridges were made between organic synthesis, pharmacology, and docking to improve our understanding of these compounds.

Moreover, although these bicyclic compounds have a slightly higher IC_{50} than lead compound **35**, it is noteworthy that they still exhibit quite respectable potency compared to values reported in the literature. Indeed,

our best bicyclic compound, **91a**, with an IC_{50} of 55.0 nM [42.1 – 72.2], is slightly less effective than some well-known inhibitors, such as URB-597 (**20**, 4.6 nM)[69] or OL-135 (**17**, 4.7 nM)[64], but demonstrates comparable potency to others, such as PF-750 (**37**, 33 nM).[72]

9.3 Diastereomer 63 of the lead

In a previous project, molecule **53** was synthesised to study the influence of the methyl group on inhibitor activity (**Figure 61**).[2] In this context, two enantiomers were obtained, separated, and tested independently. One enantiomer showed a moderate IC_{50} of 12.7 µM, while the other was completely inactive. This prompted us to investigate the influence of the lead compound's asymmetric centres on its efficacy against FAAH. To do so, we explored the diastereomer **63**, where the absolute configuration of the carbon bearing the ester is reversed, to study its effect.

53 **63**

*Figure 61: Equivalent of the lead without the methyl (**53**) and diastereomer (**63**) of the lead.*

To synthesise diastereomer **63**, we initially adopted a synthetic route involving *N*-acylation followed by inversion of the alcohol-bearing carbon's configuration. Various methods were considered, but all attempts resulted in the formation of the elimination product **107**, demonstrating a competition between elimination and nucleophilic substitution, exclusively favouring elimination (**Figure 62**).[2] In this project, we focused particularly on the Mitsunobu reaction, also previously considered, which led us to the same conclusions. However, research by Herdewijn *et al.* showed a Mitsunobu

reaction on β-lactam **109** with benzoic acid.[102] Using their conditions with lactam **44** and 4-phenylbutanoic acid, we again observed only the elimination product. Similar conclusions were drawn using benzoic acid for comparison with Herdewijn *et al.*'s work. These various tests and result comparisons led us to understand that *N*-acylation, and thus imide formation, likely caused a strong electron-withdrawing effect, favouring elimination over substitution.

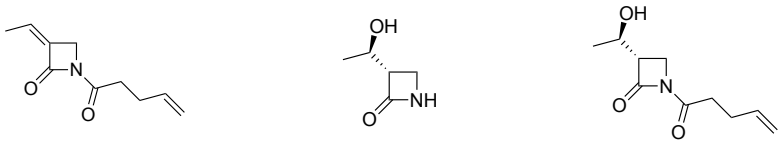

107 **109** **44**

*Figure 62: Elimination side product **107**, alcohol **109** and alcohol **44**.*

These results led us to revise our synthetic route and perform the esterification first, inverting the absolute configuration of the functional group's carbon, before conducting *N*-acylation. To achieve this, we repeated a Mitsunobu reaction using alcohol **109** and the published conditions, but this time with 4-phenylbutanoic acid.[102] Although this new strategy still largely produced the elimination product, the substitution product was also obtained. Following this synthetic route, compound **63** was obtained. Unfortunately, only two product mixtures were obtained. Analysis showed that the first mixture contained lead compound **35** and its enantiomer **116** (**Figure 63**). The second mixture contained a combination of at least three of the four stereoisomers (**35**, **116**, and **63**). Our hypotheses suggest the serious consideration of **115** formation, as the presence of **35** and **116** in the first mixture can only be explained by epimerisations during the Mitsunobu reaction, which cannot proceed *via* an S_N1 mechanism.

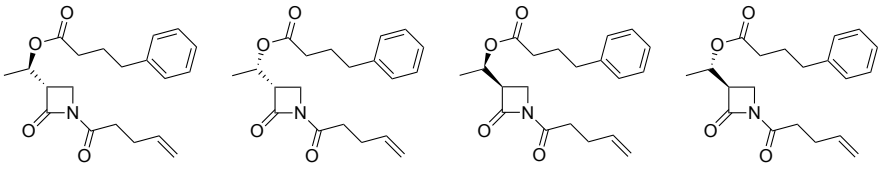

35 **63** **115** **116**

*Figure 63: Stereoisomers of the lead: **35** (lead), **63**, **115** and **116**.*

The determination of the IC_{50} of these two mixtures was conducted for indicative purposes. The first fraction (containing **35** and **116**) presented an IC_{50} of 10.5 nM [8.6 – 12.9], while the second fraction (containing **35**, **116**, **63**, and likely **115**) showed an IC_{50} of 14.0 nM [12.1 – 16.2]. These results suggest that the two stereogenic centres do not significantly influence inhibition, which is interesting, given that the absence of the methyl group significantly impacts inhibition depending on the configuration. It is very interesting to observe that these stereoisomeric mixtures have IC_{50} values quite comparable to well-known FAAH inhibitors, such as LY-2183240 (**21**, 12.4 nM)[20] or MK-4409 (**25**, 11 nM).[74] However, these IC_{50} values should be interpreted cautiously, as they were measured on mixtures. This provides a preliminary indication, but it would be more accurate to conduct tests on pure stereoisomers. Therefore, it is essential to either find a way to separate the different stereoisomers in the existing mixtures or develop a new method to obtain pure **63**. This method should allow for the inversion of the carbon configuration without causing elimination, producing diastereomerically pure **63** while preventing any epimerisation.

9.4 γ-Lactam 65 and δ-Lactam 66

Until now, only β-lactams have been investigated by our laboratory as FAAH inhibitors. We then questioned the influence of lactam ring size on the quality of inhibition. This led us to consider molecules **65** and **66**, which are the γ-lactam and δ-lactam equivalents of lead compound **35**, respectively (**Figure 64**). These compounds should potentially allow for greater

physiological stability. Unfortunately, these syntheses could not be completed due to the prioritisation of other aspects of this project.

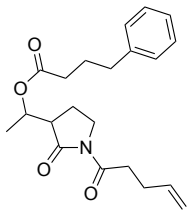

65

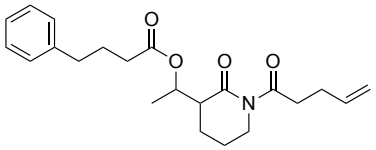

66

*Figure 64: γ-lactam equivalent **65** and δ-lactam equivalent **66** of the lead compound.*

Regarding γ-lactam **65**, we managed to obtain lactam **127**, where the ester is present, but the nitrogen remains protected (**Figure 65**). The main challenge encountered during this project was the deprotection of amide function. So far, no deprotection method has been successfully implemented. Two protecting groups were considered: the PMB group, where the deprotection was unsuccessful on **127**, and the benzyl group, where the deprotection was also unsuccessful on **120**. It would be useful to investigate new deprotection conditions for either benzyl or PMB. If no successful solution can be found, another protecting group, such as CBZ or Alloc, should be considered.

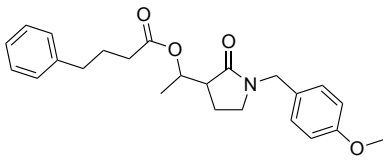

127

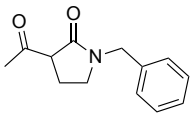

120

*Figure 65: Products used for the deprotection step for the paramethoxybenzyl protecting group (**127**) and benzyl protecting group (**120**).*

For δ-lactam **66**, the main difficulty was the presence of a keto-enol equilibrium for **76** and **75**, favouring the enol form (**Scheme 65**). During *N*-acylation, this led to a double reaction: *N*-acylation on one hand and esterification with the enol on the other. Our various tests did not allow us to

favour one reaction over the other to exploit any potential difference in reactivity. To successfully complete this project, it is important to continue the search of a preferential reaction either on the enol or on the lactam. If this is not possible, a method to block the enol's reactivity should be found to allow only the desired reaction to occur.

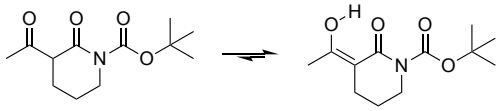

76 **134**

*Scheme 65: Equilibrium between ketone **76** and enol **134**.*

Both considered lactams have their substitution at the α-position of the lactam carbonyl. However, we could also consider inserting this group on other positions of these rings (**Figure 66**). This opens the door to a whole series of γ-lactams and δ-lactams worth investigating if **65** and **66** prove to be promising, in order to deepen our understanding of these lactams as FAAH inhibitors.

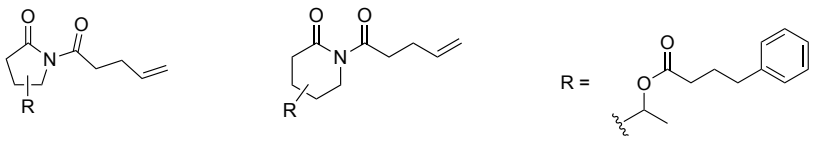

158 **159**

*Figure 66: Other γ-lactams (**158**) and δ-lactams (**159**) envisaged.*

9.5 β-Lactam 117

It had been previously demonstrated that the carbonyl group of the ester function had almost no influence on the inhibitory efficacy of monolactams (IC_{50} of 4.9 nM [3.8 – 6.4] for lead **35** and 8.0 nM for its ether equivalent **45**) (**Figure 67**).[3] Moreover, it was also shown that the double bond was not essential for inhibition, as the reduced molecule **54** exhibited an IC_{50} of 8.0 nM.[2] This led us to consider molecule **117**, which combines these modifications that did not affect inhibition.

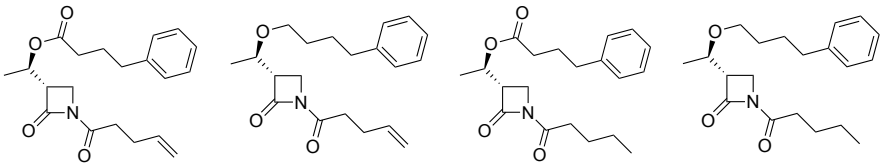

35 **45** **54** **117**

*Figure 67: Lead compound (**35**) and its equivalents with an ether in place of the ester (**45**), with a single bond instead of a double bond (**54**) and with both modifications combined (**117**).*

Molecule **117** was obtained from compound **45**, which was previously prepared and used in the pharmacophore study.[3] A reduction was then performed, directly yielding **117**. At this stage, the potency of compound **117** has not yet been evaluated due to technical issues.

As with the bicyclic compounds, cellular studies were conducted for lactam **117**. The results were very positive, as it proved to be the best molecule for increasing NAE levels in cells. It moderately increased the levels of OEA (**11**) and PEA (**10**), but significantly boosted the levels of AEA (**6**) and SEA (**12**), almost as much as the reference PF-3845, known to be *in cellulo* a very good FAAH inhibitor.[83] Additionally, similar to the bicyclic compounds, molecule **117** did not increase the levels of 2-AG (**7**), supporting its selectivity for FAAH over MAGL. Docking studies were also conducted for this compound, showing that the molecule interacts very well within the enzyme cavity, with a slightly lower docking score than the lead, likely due to the absence of the carbonyl group that interacts with Ser_{268} in the case of the lead.

9.6 General Conclusions

This thesis, through its various investigations, highlights the importance of an interdisciplinary approach in medicinal chemistry research. By integrating the fields of organic synthesis, pharmacology, and docking studies, this research has developed a deeper and more nuanced

understanding of lactam inhibitors of FAAH. Each research domain contributed unique and complementary perspectives, creating a virtuous cycle where progress in one area informs and enhances the others.

The interdisciplinary nature of this project has enabled the overcoming of complex challenges and the opening of new research avenues. For example, docking studies guided the design of new compounds and explained the variations in efficacy observed during pharmacological tests. Similarly, pharmacological results helped refine docking models, making these simulations more accurate and predictive.

This integrated approach also identified structural modifications of compounds that do not affect inhibitory activity, such as the reduction of the double bond or the substitution of the ester function. These insights led to the design of new promising inhibitors, such as compound **117**, which demonstrated remarkable efficacy in increasing NAE levels in cells.

In summary, this thesis illustrates the power of interdisciplinarity in scientific research. By combining diverse skills and perspectives, it has achieved significant advances in understanding lactam inhibitors of FAAH and opened up prospects for the development of new drugs. This synergy between chemical synthesis, pharmacology, and docking underscores the importance of a systemic approach to tackling the complex challenges of medicinal chemistry research.

Chapter 10: Experimental part

10.1 Synthesis

10.1.1 General considerations

10.1.1.1 Equipment

Nuclear Magnetic Resonance (NMR) spectroscopy: NMR spectra were recorded on a Bruker avance II 300 operating at 300 MHz for proton-^{1}H and 75 MHz for carbon-^{13}C. Solvents are indicated case-by-case. Chemical shifts (δ) are reported in ppm relative to the reference signal (TMS) and coupling constants are given in Hertz (Hz). For some molecules, the ^{1}H and ^{13}C signals attributions required additional analyses (COSY, HMQC, HMBC, ^{13}C DEPT-Q). NMR multiplicities are abbreviated as follow: s = singlet, bs = broad singlet, d = doublet, t = triplet, q = quartet, sep = septet, m = multiplet. Quantitative ^{13}C NMR analyses were recorded at room temperature (291 K) on a Bruker Avance 500 spectrometer equipped with a BBO probehead and a z-gradient coil, and operating at 500 MHz for ^{1}H and 125 MHz for ^{13}C NMR experiments. NMR spectra were calibrated using residual non-deuterated $CDCl_3$ signal as an internal reference (7.26 ppm) for ^{1}H and $CDCl_3$ signal (77.16 ppm) for ^{13}C NMR spectra. Standard zg programs were employed for ^{1}H NMR experiments. Relaxation delay was 15 sec and NS was 16. For the quantitative acquisition of ^{13}C NMR spectra, the inverse gated decoupled pulse program zgig was used with a long relaxation delay (D1 = 20 sec) and a NS of 1440. Processing of NMR data was performed using MestReNova program (10.01 Version, Mestrelab Research S.L.). Integrations of ^{1}H and ^{13}C NMR resonances were carried out with a deconvolution module of MestReNova, after phase and baseline corrections. All mathematical fits employed during the deconvolution procedure were 100% Lorentzian in nature.

Mass spectrometry: Mass spectra and high-resolution mass spectra were recorded by the ASM plateform on a Thermo Orbitrap Exactive device.

The mass values are given in Dalton. The ionisation methods used are either electrospray ionisation (ESI) or atmospheric-pressure chemical ionisation (APCI).

IR spectrophotometry: IR spectra were recorded with an infrared spectrophotometer PerkinElmer Spectrum UATR Two. The wave numbers are given in cm^{-1}.

High-Performance Liquid Chromatography (HPLC): HPLC analyses were carried out using a quaternary pump Waters 600 controller equipped with a Waters 996 PDA photodiode array detector and a Waters 717 plus autosampler. The two columns used (CHIRALPAK IC and CHIRALPAK IB) were purchased from Daicel Chemical Industries. The particles size is 5 μm and the dimensions of the columns are 4.6 mm x 250 mm.

Optical rotation: The optical rotation measurements were measured on an Atago Polax-2L semi-automatic polarimeter equipped with a 1 mL sample cell (1 dm length).

Melting points: Melting points were obtained on a Büchi B-540 apparatus.

Circular dichroism (CD): Spectra were recorded between 220 and 300 nm with a MOS-500 spectropolarimeter at 20 °C in chloroform, using a 1 mm pathlength quartz Suprasil cell (Hellma). Four scans were averaged, solvent baseline was subtracted, and resulting corrected spectra were smoothed. For each scan, the following parameters were used: 30 nm/min scanning rate, 2 nm bandwidth, 0.5 nm data pitch, and 1 s digital integration time. Data are presented as the ellipticity (θ).

10.1.1.2 Laboratory practice

Reactions: All reactions were carried out under magnetic stirring.

Anhydrous conditions: Reactions requiring anhydrous conditions were carried out under argon atmosphere using glassware previously heated *via* Bunsen burner under reduced pressure, followed by a cooling under argon atmosphere. Anhydrous solvents were purchased as anhydrous grade from Merck Sigma-Aldrich company.

Solvents: All solvents (for reactions, extractions and purification by chromatography) were used without further purification.

Reactants and reagents: Commercially available reagents were used as purchased, unless mentioned otherwise.

Low temperature reactions: Reactions requiring a temperature of -78°C were carried out using a bath of dry ice and isopropanol. Those requiring a temperature of -40°C were carried out using a bath of acetonitrile cooled down by liquid N_2, those requiring a temperature of -10°C were carried out using a bath of ice and brine, and those requiring a temperature of 0°C were carried out using an ice bath.

High temperature reactions: Reactions requiring a temperature >25°C were carried out using a silicon bath (with a magnetic stirring bar), installed on a heating plate equipped with a temperature probe.

Thin layer chromatography (TLCs): TLCs were carried out on Merck Silica gel 60 F254 aluminium backed plates. UV light, potassium permanganate or p-anisaldehyde solution were used for detection.

Flash chromatography: Flash chromatography was performed using Merck Silica gel 60Å (40-63 μm).

10.1.2 Synthesis of bicycle 56

*10.1.2.1 Allylation of azetidinone **32***

Reference: S.-K. Kang, T.-G. Baik, X.-H Jiao, K.-J. Lee, C. H. Lee, *Synlett* **1999**, *4*, 447-450.

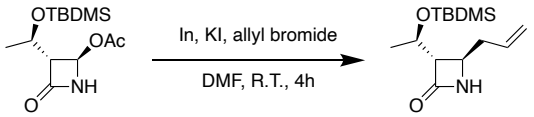

Procedure: In a dried three-neck round-bottom flask under inert conditions, KI (3.1 g, 18.7 mmol, 3.0 eq.) and indium (1.435 g, 12.5 mmol, 2.0 eq.) were added to 50 mL of DMF, followed by allyl bromide (1.618 mL, 18.7 mmol, 3.0 eq.). After 1 hour, the commercially available azetidinone **32** derivative (1.782 g, 6.2 mmol, 1.0 eq.) was introduced into the solution. The mixture was stirred for 4 hours, then diluted with diethyl ether. The organic phase was washed with a saturated NH_4Cl solution, then with brine, and concentrated under reduced pressure.

IUPAC name: (3*S*,4*R*)-4-allyl-3-((*R*)-1-((tert-butyldimethylsilyl)oxy)ethyl) azetidin-2-one

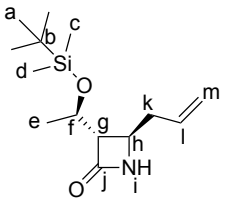

Yield: 98%

Mol. formula: $C_{14}H_{27}NO_2Si$

Mol. Wt.: 269.18 g.mol^{-1}

Aspect: white powder

CAS: 80433-47-2

^{1}H NMR (300 MHz, $CDCl_3$) δ (ppm): 6.12-5.97 (bs, 1H, i), 5.89-5.65 (m, 1H, l), 5.21-5.05 (m, 2H, m), 4,16 (qd, *J* = 6.3; 4.9 Hz, f), 3.69 (ddd, *J* = 7.7, 7.0, 5.0 Hz, 1H, h), 2.77 (ddd, *J* = 5.0, 2.2, 0.9 Hz, 1H, g), 2.48-2.24 (m, 2H, k), 1.20 (d, *J* = 6.2 Hz, 3H, e), 0.87 (s, 9H, a), 0.061 (s, 3H, c or d), 0.058 (s, 3H, c or d).

^{13}C NMR (75 MHz, $CDCl_3$) δ (ppm): 168.5 (j), 133.8 (l), 118,0 (m), 65.4 (f), 63.8 (g), 50.1 (h), 39.4 (k), 25,7 (a), 22.7 (e), 17.9 (b), -4.3 (c or d), -5.0 (c or d).

HRMS (APCI): *m/z found* = 270.18838; calcd. for $[M+H]^+$: 270.18819.

FT-IR (cm^{-1}): 3082, 2928, 2856, 1751, 1250, 1136, 1053, 968, 828, 776, 722.

m.p.: 83°C.

The data align with literature (see above).

*10.1.2.2 N-acylation of **62** under pyridine conditions*

Reference: M. Feledziak, C. Michaux, A. Urbach, G. Labar, G. G. Muccioli, D. M. Lambert, J. Marchand-Brynaert, *J. Med. Chem.* **2009**, *52*, 7054-7068.

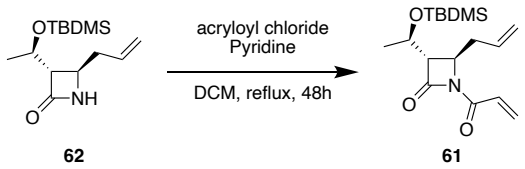

62 **61**

Procedure: In a dried three-neck round-bottom flask under inert conditions, acryloyl chloride (1.464 mL,18.1 mmol, 1.8 eq.) and pyridine (1.299 mL, 16.1 mmol, 1.6 eq.) were added. Meanwhile, compound **62** (2.719 g, 10.1 mmol, 1 eq.) was dissolved in 70 mL of DCM. This solution was added to the mixture and stirred at 40°C for 48 hours. Three additional portions of acryloyl chloride (each 1.5 eq.) were added at 3, 20, and 36 hours. The solution was then washed with a saturated $NaHCO_3$ solution, followed by 1 M HCl solution, then with brine, and dried over $MgSO_4$. The product was concentrated under reduced pressure. The crude product was purified by flash chromatography on silica gel using cyclohexane/AcOEt (90/10).

IUPAC name: (3*S*,4*R*)-1-acryloyl-4-allyl-3-((*R*)-1-((tert-butyldimethylsilyl)oxy)ethyl)azetidin-2-one

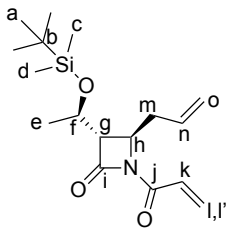

Yield: 12%

Mol. formula: $C_{17}H_{29}NO_3Si$

Mol. Wt.: 323.19 g.mol−1

Aspect: Yellow oil

^{1}H NMR (300 MHz, $CDCl_3$) δ (ppm): 7.01 (dd, *J* = 17.1, 10.4 Hz, 1H, k), 6.52 (dd, *J* = 17.1, 1.7 Hz, 1H, l), 5.84 (dd, *J* = 10.4, 1.7 Hz, 1H, l'), 5.81-5.68 (m, 1H, n), 5.22-5.11 (m, 2H, o), 4.35-4.19 (m, 2H, f, h), 2.96-2.80 (m, 2H, g, m (1H)), 2.55-2.38 (m, 1H, m), 1.17 (d, *J* = 6.3 Hz, 3H, e), 0.80 (s, 9H, a), 0.05 (s, 3H, c or d), 0.01 (s, 3H, c or d).

^{13}C NMR (75 MHz, $CDCl_3$) δ (ppm): 166.9 (i), 163.1 (j), 132.7 (n), 131.4 (l), 129.6 (o), 65.2 (f), 61.9 (g), 52.0 (h), 36.5 (m), 25.9 (a), 22.8 (e), 18.1 (b), -3.9 (c or d), -4.9 (c or d).

*10.1.2.3 N-acylation of **62** under nBuLi conditions*

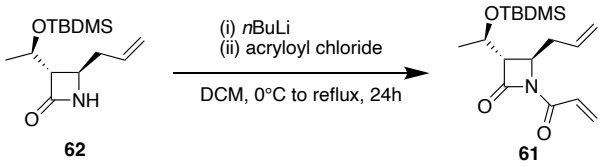

Procedure: In a dried three-neck round-bottom flask under inert conditions, **62** (3.038 g, 9.4 mmol, 1.0 eq.) was dissolved in 100 mL of DCM at 0°C. *n*BuLi (11.3 mmol, 1.2 eq.) was added to the solution, which was stirred for 30 minutes at 0°C. Then, acryloyl chloride (2.281 mL, 28.2 mmol, 3.0 eq.) was added. The mixture was stirred for 24 hours at 45°C. The solution was washed with a saturated NH_4Cl solution, followed by brine, and dried over $MgSO_4$. The product was concentrated under reduced pressure. The

crude product was purified by flash chromatography on silica gel using cyclohexane/AcOEt (90/10).

Yield: 77%

See section 10.1.2.2 for characterisation.

*10.1.2.4 Cycling metathesis of **61***

Reference: J. Caruano, UCLouvain, **2017**.

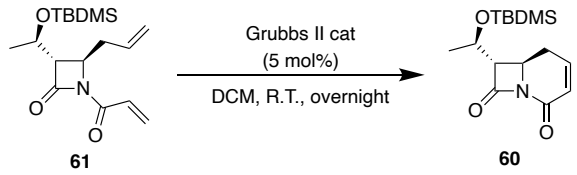

Procedure: In a dried round-bottom flask under inert conditions, Grubbs II catalyst (51 mg, 0.06 mmol, 0.05 eq.) was added, followed by a solution of **61** (420 mg, 1.3 mmol, 1.0 eq.) in 2.5 mL of DCM. The mixture was stirred at room temperature for 16 hours. The product was concentrated under reduced pressure, and the crude product was purified by flash chromatography on silica gel using cyclohexane/AcOEt (50/50).

IUPAC name: (6*R*,7*S*)-7-((*R*)-1-((tert-butyldimethylsilyl)oxy)ethyl)-1-azabicyclo[4.2.0]oct-3-ene-2,8-dione

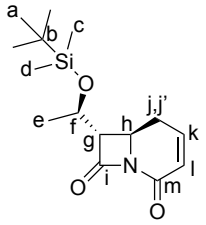

Yield: 62%
Mol. formula: $C_{15}H_{25}NO_3Si$
Mol. Wt.: 295.16 g.mol^{-1}
Aspect: brown oil

^{1}H NMR (300 MHz, $CDCl_3$) δ (ppm): 6.75 (ddd, *J* = 10.2, 6.4, 2.2 Hz, 1H, k), 6.03 (ddd, *J* = 10.2, 3.0, 1.1 Hz, 1H, l), 4.50-4.08 (m, 2H, f, h), 3.15 (dd, *J* = 4.6,

3.1 Hz, 1H, g), 2.66 (dddd, *J* = 17, 6.7, 5.7, 1.1 Hz, 1H, j), 2.58-2.36 (m, 1H, j'), 1.22 (d, *J* = 6.2 Hz, 3H, e), 0.86 (s, 9H, a), 0.08 (s, 3H, c or d), 0.08 (s, 3H, c or d).

^{13}C NMR (75 MHz, $CDCl_3$) δ (ppm): 164.5 (i), 158.3 (m), 143.3 (k), 125.3 (l), 67.8 (g), 65.2 (f), 50.1 (h), 28.8 (j), 26.0 (a), 22.7 (e), 18.2 (b), -3.9 (c or d), -4.7 (c or d).

HRMS (APCI): *m/z found* = 296.16762; calcd. for $[M+H]^+$:296.16765.

FT-IR (cm^{-1}): 2930, 2857, 1794, 1683, 1373, 1325, 1090, 1044, 1000, 834, 814, 775.

m.p.: 127 - 128°C.

*10.1.2.5 Hydrogenation of **60***

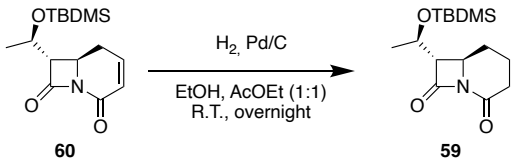

60 **59**

Procedure: In a dried round-bottom flask under inert conditions, Pd/C 10% (85 mg, 0.8 mmol, 1.0 eq.) was added, followed by a solution of **60** (236 mg, 0.8 mmol, 1.0 eq.) in 30 mL of EtOH and 30 mL of AcOEt. The mixture was stirred at room temperature for 16 hours under a hydrogen atmosphere. The solution was filtered through a pad of Celite and concentrated under reduced pressure.

IUPAC name: (6*R*,7*S*)-7-((*R*)-1-((tert-butyldimethylsilyl)oxy)ethyl)-1-azabicyclo[4.2.0]octane-2,8-dione

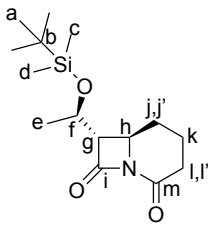

Yield: 87%

Mol. formula: $C_{15}H_{27}NO_3Si$

Mol. Wt.: 297.18 g.mol^{-1}

Aspect: beige powder

^{1}H NMR (300 MHz, $CDCl_3$) δ (ppm): 4.27 (qd, *J* = 6.3, 4.3 Hz, 1H, f), 4.02 (dt, *J* = 11.6, 3.7 HZ, 1H, h), 3.15 (dd, *J* = 4.3, 3.6 Hz, 1H, g), 2.63, 2.26 (m, 2H, k), 2.17 (m, 1H, j), 2.06 (ddd, *J* = 14.1, 7.0, 3.3 Hz, 1H, l), 1.94, 1.76 (m, 1H, l'), 1.52-1.40 (m,1H, j'), 1.20 (d, *J* = 6.3 Hz, 3H, e), 0.90-0.80 (m, 9H, a), 0.06 (s, 6H, c, d).

^{13}C NMR (75 MHz, $CDCl_3$) δ (ppm): 165.8 (m), 165.4 (i), 67.9 (g), 65.1 (f), 54.0 (h), 31.3 (k), 27.8 (j), 26.1 (a), 22.8 (e), 18.3 (b), -4.0 (c or d), -4.7 (c or d).

HRMS (APCI): *m/z found* = 298.18331; calcd. for $[M+H]^+$:298.18330.

FT-IR (cm^{-1}): 3672, 2971, 1810, 1683, 1074, 834, 776.

*10.1.2.6 Allylation of **59***

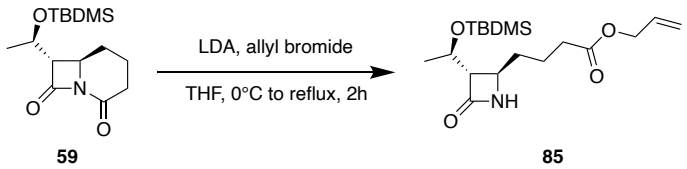

59 **85**

Procedure: In a dried three-neck round-bottom flask under inert conditions, **59** (10 mg, 0.03 mmol, 1.0 eq.) was dissolved in 3 mL of THF at 0°C. LDA (0.04 mmol, 1.2 eq.) was added to the solution, which was stirred for 30 minutes at 0°C. Then, allyl bromide (6 µL, 0.06 mmol, 2.0 eq.) was added. The mixture was stirred for 2 hours at 70°C. The solution was washed with a saturated NH_4Cl solution, followed by brine, and dried over $MgSO_4$. The product was concentrated under reduced pressure. The crude product

was purified by flash chromatography on silica gel using cyclohexane/AcOEt (1/1).

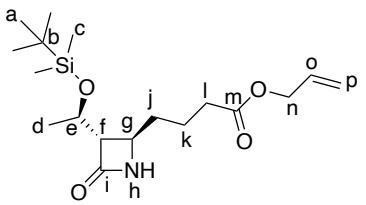

Yield: not determined

Mol. formula: $C_{18}H_{33}NO_4Si$

Mol. Wt.: 355.55 g.mol^{-1}

Aspect: yellow oil

^{1}H NMR (300 MHz, $CDCl_3$) δ (ppm): 6.17 (bs, 1H, h), 6.01 – 5.77 (m, 1H, o), 5.37 – 5.23 (m, 2H, p), 4.60 (d, *J* = 6 Hz, 2H, n), 4.26 (q, *J* = 6.2 Hz, 1H, e), 3,86 (m, 1H, g), 2.48 (dd, *J* = 6.0, 4.5 Hz, 1H, f), 2.44 – 2.18 (m,2H, l), 1.87 (m, 2H, k), 1.72 (m, 2H, J), 1.29 – 1.15 (m, 3H, d), 0,88 (s, 9H, a), 0,09 (s, 6H, c).

10.1.3 Synthesis of bicycle 91

10.1.3.1 Saponification of diethyl n-propylmalonate

Reference: C. F. Riber, A. H. F. Andersen, L. A Rolskov, K. Zuwala, P. Gajda, K. B. Lovschal, F. Dagnaes-Hansen, D. H, T. Pietschmann, M. Tolstrup, A. N. Zelikin, *ACS Macro Lett.* **2017,** *6*, 935-940.

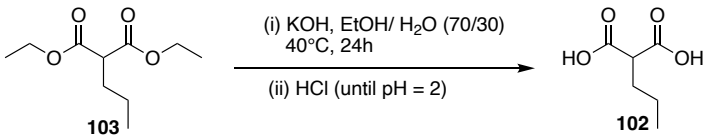

Procedure: In a round-bottom flask, diethyl n-propylmalonate (5 mL, 24.4 mmol, 1.0 eq.) was added to 70 mL of EtOH and 30 mL of H_2O. KOH (4.791 g, 85.4 mmol, 3.5 eq.) was then added, and the mixture was stirred at 40°C for 24 hours. The solution was acidified by dropwise addition of 12 M HCl until reaching a pH of 2. The product was extracted six times with 20 mL of Et_2O, dried over Na_2SO_4, and concentrated under reduced pressure.

IUPAC name: 2-propylmalonic acid

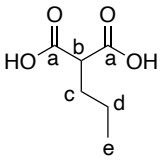

Yield: 97%

Mol. formula: $C_6H_{10}O_4$

Mol. Wt.: 146.06 g.mol^{-1}

Aspect: white powder

CAS: 616-62-6

^{1}H NMR (300 MHz, $CDCl_3$) δ (ppm): 3.46 (t, *J* = 7.4 Hz, 1H, b), 2.04-1.85 (m, 2H, c), 1.53-1.32 (m, 2H, d), 0.96 (t, *J* = 7.3 Hz, 3H, e).

^{13}C NMR (75 MHz, $CDCl_3$) δ (ppm): 174.4 (a), 51.1 (b), 31.0 (c), 20.6 (d), 13.7 (e).

HRMS (ESI): *m/z found* = 145.04948; calcd. for [M-H]$^-$: 145.04954.

FT-IR (cm^{-1}): 2966, 1699, 1410, 1257, 1197, 1108, 906, 673, 536.

Data align with literature (see above).

*10.1.3.2 Decarboxylation of **102***

Reference: L. Wu, F. Wang, P. Chen, G. Liu, *J. Am. Chem. Soc.* **2019**, *141*, 1887-1892.

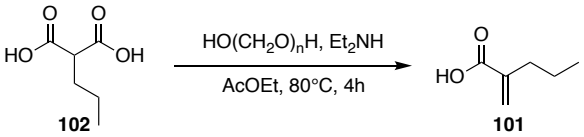

Procedure: In a round-bottom flask, diethylamine (3.310 mL, 32.0 mmol, 1.5 eq.) was added dropwise to a solution of 2-propylmalonic acid **102** (3.111 g, 21.3 mmol, 1.0 eq.) in 150 mL of AcOEt. Paraformaldehyde (1.282 g, 42.7 mmol, 2.0 eq.) was then added. The mixture was stirred at 80°C for 4 hours. The solution was acidified by dropwise addition of 12 M HCl until a pH of 2 was reached. The product was extracted with AcOEt and washed with

brine. It was then dried over Na_2SO_4 and concentrated under reduced pressure.

IUPAC name: 2-methylenepentanoic acid

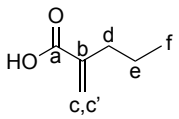

Yield: 94%
Mol. formula: $C_6H_{10}O_2$
Mol. Wt.: 114.14 $g.mol^{-1}$
Aspect: colourless oil
CAS: 5650-75-9

^{1}H NMR (300 MHz, $CDCl_3$) δ (ppm): 6.29 (d, *J* = 1.4 Hz, 1H, c), 5.64 (d, *J* = 1.4 Hz, 1H c'), 2.28 (t, *J* = 8.4 Hz, 2H, d), 167-1.37 (m, 2H, e), 0.93 (t, *J* = 7.4 Hz, 3H, f).

^{13}C NMR (75 MHz, $CDCl_3$) δ (ppm): 173.0 (a), 140.1 (b), 127,2 (c), 33.7 (d), 21.7 (e), 13.8 (f).

HRMS (ESI): *m/z found* = 113.05967; calcd. for $[M-H]^-$: 113.05971.

FT-IR (cm^{-1}): 2962, 2874, 1691, 1627, 1438, 1235, 1187, 947.

The data align with literature (see above).

*10.1.3.3 N-acylation of **62***

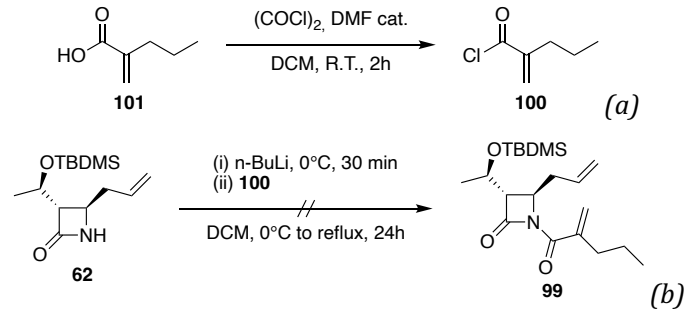

Procedure: In a dried three-neck round-bottom flask under inert conditions, oxalyl chloride (0.283 mL, 3.3 mmol, 3.0 eq.) was added to a solution of 2-methylenepentanoic acid (377 mg, 3.3 mmol, 3.0 eq.) in 15 mL of DCM. One drop of DMF was then added. The mixture was stirred at room temperature for 2 hours until the off gassing ceased. Meanwhile, in another three-neck round-bottom flask under inert conditions, **62** (269 mg, 1.1 mmol, 1.0 eq.) was dissolved in 15 mL of DCM. *n*BuLi (1.3 mmol, 1.3 eq.) was added dropwise at 0°C to the **62** solution. The mixture was stirred at 0°C for 30 minutes. The solution of 2-methylenepentanoic chloride was then added dropwise at 0°C *via* cannulation between the three-neck round-bottom flasks. The mixture was stirred at 40°C for 24 hours. The solution was washed with a saturated NH_4Cl solution, followed by brine, and dried over $MgSO_4$. The product was concentrated under reduced pressure. The crude product was purified by flash chromatography on silica gel using hexane/AcOEt (95/5).

IUPAC name: (3*S*,4*R*)-4-allyl-3-((*R*)-1-((tert-butyldimethylsilyl)oxy)ethyl)-1-(2-methylenepentanoyl)azetidin-2-one

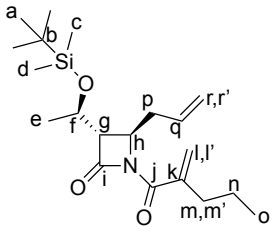

Yield: 67%

Mol. formula: $C_{20}H_{35}NO_3Si$

Mol. Wt.: 365.24 g.mol^{-1}

Aspect: colourless oil

^{1}H NMR (300 MHz, $CDCl_3$) δ (ppm): 5.91 (s, 1H,l), 5.84-5.69 (m, 1H, q), 5.67 (s, 1H, l'), 5.19-5.14 (m, 1H, r), 5.12 (d, *J* = 1.2 Hz, 1H, r'), 4.27 (m, 2H, f, h), 2.88 (t, *J*=3.4 Hz, 1H, m), 2.82-2.66 (m, 1H, g), 2.56-2.04 (m, 3H, p, m' (1H)), 1.55-1.40 (m, 2H, n), 1.16 (d, *J* = 6.3 Hz, 3H, e), 0.92 (t, *J* = 7.4 Hz, 3H, o), 0.81 (s, 9H, a), 0.04 (s,3H, c or d), 0.00 (s, 3H, c or d).

^{13}C NMR (75 MHz, $CDCl_3$) δ (ppm): 167.5 (i), 165.3 (j), 143.0 (k), 132.6 (q), 124.2 (l), 119.3 (r), 63.0 (f), 60.4 (m), 51.2 (h), 36.4 (g), 34.4 (p), 25.8 (a), 22.6 (e), 21.3 (n), 17.9 (b), 13.8 (o), -4.1 (c or d), -5.0 (c or d).

HRMS (ESI): *m/z found* = 366.24591; calcd. for $[M+H]^+$: 366.24590.

*10.1.3.4 Cycling metathesis of **99***

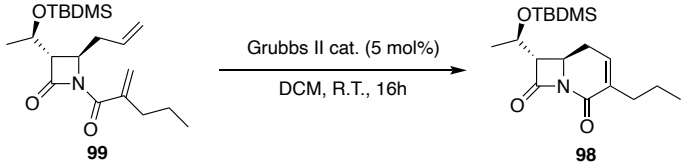

Procedure: In a dried round-bottom flask under inert conditions, Grubbs II catalyst (25 mg, 0.03 mmol, 0.05 eq.) was added, followed by a solution of **99** (219 mg, 0.6 mmol, 1.0 eq.) in 2.5 mL of DCM. The mixture was stirred at 40°C for 16 hours. The product was concentrated under reduced pressure, and the crude product was purified by flash chromatography on silica gel using hexane/AcOEt (80/20).

IUPAC name: (6*R*,7*S*)-7-((*R*)-1-((tert-butyldimethylsilyl)oxy)ethyl)-3-propyl-1-azabicyclo[4.2.0]oct-3-ene-2,8-dione

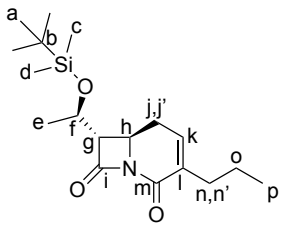

Yield: 83%

Mol. formula: $C_{18}H_{31}NO_3Si$

Mol. Wt.: 337.21 g.mol^{-1}

Aspect: white powder

^{1}H NMR (300 MHz, $CDCl_3$) δ (ppm): 6.43-6.34 (m, 1H, k), 4.28-4.20 (m, 1H, f), 4.16 (m, 1H, h), 3.07 (dd, *J* = 4.9, 3.0 Hz, 1H, g), 2.67-2.58 (m, 1H, j), 2.48 (m, 1H, j'), 2.42-2.30 (m, 1H, n), 2.18 (m, 1H, n'), 1.47 (m, 2H, o), 1.22 (d, *J* = 6.2 Hz, 3H, e), 0.91 (t, *J* = 7.3, 3H, p), 0.86 (s, 9H, a), 0.08 (2s, 6H, c, d).

^{13}C NMR (75 MHz, $CDCl_3$) δ (ppm): 200.5 (i), 159.3 (m), 136.1 (k), 110.1 (l), 66.9 (g), 65.2 (f), 5.2 (h), 28.9 (j), 25.8 (a), 22.6 (e), 21.7 (o), 18.0 (b), 13.8 (p), -4.1 (c or d), -4.9 (c or d).

HRMS (APCI): *m/z found* = 338.21460; calcd. for $[M+H]^+$:338.21460.

FT-IR (cm^{-1}): 2956, 2928, 2853, 1798, 1681, 1291, 834, 777.

m.p.: 84°C.

*10.1.3.5 Hydrogenation of **98***

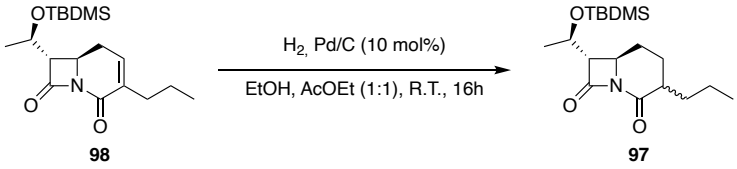

Procedure: In a dried round-bottom flask under inert conditions, Pd/C 10% (0.3 mmol, 1.0 eq.) was added, followed by a solution of **98** (101 mg, 0.3 mmol, 1.0 eq.) in 10 mL of EtOH and 10 mL of AcOEt. The mixture was

stirred at room temperature for 16 hours under a hydrogen atmosphere. The solution was filtered through a pad of celite and concentrated under reduced pressure.

IUPAC name: (6*R*,7*S*)-7-((*R*)-1-((tert-butyldimethylsilyl)oxy)ethyl)-3-propyl-1-azabicyclo[4.2.0]octane-2,8-dione

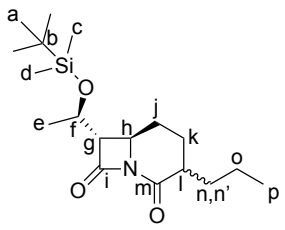

Yield: 99%

dr: 51/49

Mol. formula: $C_{18}H_{33}NO_3Si$

Mol. Wt.: 339.22 g.mol^{-1}

Aspect: white powder

^{1}H NMR (300 MHz, $CDCl_3$) δ (ppm): 4.25 (m, 1H, f), 4.06-3.95 (m, 1H, h), 3.12 (dd, *J* = 4.3, 3.6 Hz, 1H (dia 1), g), 3.00 (dd, *J* = 4.5, 3.2 Hz, 1H (dia 2), g), 2.37 (m, 1H (dia 1), l), 2.23 (m, 1H (dia 2), l), 2.18-2.05 (m, 2H, k), 1.91-1.77 (m, 1H, n), 1.76-1.66 (m, 1H, n'), 1.56-1.48 (m, 2H, j), 1.45-1.23 (m, 2H, o), 1.19 (d, *J* = 6.3 Hz, 3H, e), 0.94-0.88 (m, 3H, p), 0.86 (d, *J* = 1.7 Hz, 9H, a), 0.06 (2 s, 6H, c, d).

^{13}C NMR (75 MHz, $CDCl_3$) δ (ppm): 170.2 (dia 1, g), 169.5 (dia 2, g), 165.8 (dia 1, m), 165.4 (dia 2, m), 67.4 (dia 1, g), 67.3 (dia 2, g), 65.0 (dia 1, f), 64.9 (dia 2, f), 54.1 (dia 1, h), 52.5 (dia 2, h), 41.9 (dia 1, l), 39.9 (dia 2, l), 34.6 (dia 1, n), 32.5 (dia 2, n), 28.0 (dia 1, o), 27.1 (dia 2, o), 26.1 (dia 1, k), 26.0 (dia 2, k), 22.8 (a), 22.6 (c), 20.5 (dia 1, j), 19.9 (dia 2, j), 18.0 (b), 14.2 (p), -4.6 (c or d), -4.9 (c or d).

HRMS (ESI): *m/z found* = 362.21085; calcd. for $[M+Na]^+$: 362.21204.

10.1.3.6 Deprotection of ***97***

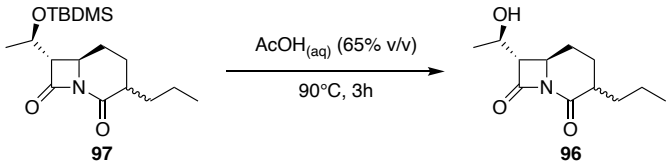

Procedure: In a round-bottom flask, **97** (68 mg, 0.2 mmol, 1.0 eq.) was added to 1.4 mL of AcOH and 0.5 mL of H_2O. The solution was heated to 90°C and stirred for 3 hours. The product was then concentrated under reduced pressure.

IUPAC name: (6*R*,7*S*)-7-((*R*)-1-hydroxyethyl)-3-propyl-1-azabicyclo[4.2.0]octane-2,8-dione

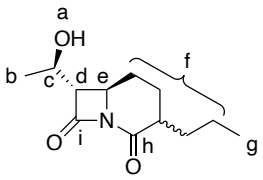

Yield: 91%

dr: 61/39

Mol. formula: $C_{12}H_{19}NO_3$

Mol. Wt.: 225.14 g.mol^{-1}

Aspect: yellow oil

^{1}H NMR (500 MHz, $CDCl_3$) δ (ppm): 4.27 (m, 1H, c), 4.07-3.99 (m, 1H, e), 3.87 (bs, 1H, a), 3.20 (dd, *J* = 5.3, 3.6 Hz, 1H (dia 1),d), 3.07 (dd, *j* = 5.3, 3.2 Hz, 1H (dia 2), d), 2.39-1.93 (m, 2H, f), 1.92-1.68 (m, 2H, f), 1.66-1.33 (m, 2H, f), 1.31-1.22 (m, 3H, f), 1.20 (d, *J* = 6.4, 3H, b), 0.95-0,84 (m, 3H, g).

^{13}C NMR (125 MHz, $CDCl_3$) δ (ppm): 170.4 (dia 1, i), 169.6 (dia 2, i), 165.6 (dia 1, h), 165.2 (dia 2, h), 66.8 (d), 64.7 (c), 53.6 (dia 1, e), 52.8 (dia 2, e), 42.0 (f), 39.9 (f), 32.5 (f), 29.8 (f), 28.0 (f), 27.1 (f), 26.1 (f), 21.8 (f), 20.5 (f), 20.0 (b), 14.0 (g).

HRMS (APCI): *m/z found* = 226.14366; calcd. for $[M+H]^+$: 226.14377.

FT-IR (cm^{-1}): 3327, 2958, 2928, 2872, 1802, 1697, 1638, 1301.

*10.1.3.7 Esterification of **96***

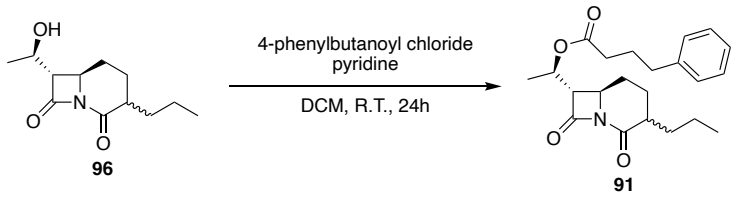

Procedure: In a dried three-neck round-bottom flask under inert conditions, 4-phenylbutanoyl chloride (256 mg, 1.4 mmol, 1.6 eq.) and pyridine (0.161 mL, 2.0 mmol, 2.3 eq.) were added to a solution of **96** (203 mg, 0.9 mmol, 1.0 eq.) in 20 mL of DCM. The mixture was stirred at room temperature for 24 hours. The solution was washed with a saturated $NaHCO_3$ solution, followed by 1M HCl, then with brine, and dried over $MgSO_4$. The product was concentrated under reduced pressure. The crude product was purified by flash chromatography on silica gel using cyclohexane/AcOEt (80/20). The two diastereomers were successfully separated completely.

IUPAC names: (*R*)-1-((3*R*,6*R*,7*S*)-2,8-dioxo-3-propyl-1-azabicyclo[4.2.0]octan-7-yl)ethyl 4-phenylbutanoate *and* (*R*)-1-((3*S*,6*R*,7*S*)-2,8-dioxo-3-propyl-1-azabicyclo[4.2.0]octan-7-yl)ethyl 4-phenylbutanoate

Yield for both diastereomers: 42%

Mol. formula: $C_{22}H_{29}NO_4$

Mol. Wt.: 371.21 $g.mol^{-1}$

Aspect: yellow oil for both products

The two diastereomers were identified by NOESY analysis.

Diastereomer 1 – (3*R*)

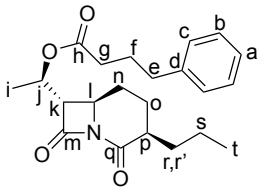

^{1}H NMR (500 MHz, $CDCl_3$) δ (ppm): 7.30-7.26 (m, 2H, a/b/c), 7.22-7.15 (m, 3H, a/b/c), 5.26 (q, *J* = 6.4 Hz, 1H, j), 3.95 (m, 1H, l), 3.16 (dd, *J* = 6.6, 3.3 Hz, 1H, k), 2.69-2.51 (t, *J* = 7.6 Hz, 2H, e), 2.35-2.28 (t, *J* = 7.5 Hz, 2H, g), 2.27-2.20 (m, 1H, p), 2.19-2.04 (m, 2H, o), 1.98-1.89 (m, 2H, f), 1.85 (m, 1H, r), 1.76-1.67 (m, 1H, r'), 1.60 (m, 2H, n), 1.46-1.31 (m, 5H, i, s), 0.92 (t, *J* = 7.4 Hz, 3H, t).

^{13}C NMR (125 MHz, $CDCl_3$) δ (ppm): 172.6 (h), 170.2 (m), 163.3 (q), 141.3 (d), 128.3 (a/b/c), 128.2 (a/b/c), 126.2 (a/b/c), 67.3 (j), 64.5 (k), 54.0 (l), 39.9 (p), 35.2 (e), 33.7 (g), 32.5 (r), 26.5 (f), 26.1 (n), 25.9 (o), 20.5 (s), 18.6 (i), 14.1 (t).

HRMS (ESI): *m/z found* = 372.21688; calcd. for $[M+H]^+$: 372.21693.

FT-IR (cm^{-1}): 2957, 2936, 2872, 1804, 1733, 1700, 1298, 1135.

Diastereomer 2 – (3*S*)

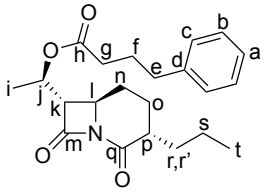

^{1}H NMR (500 MHz, $CDCl_3$) δ (ppm): 7.30-7.26 (m, 2H, a/b/c), 7.21-7.15 (m, 3H, a/b/c), 5.25 (q, *J* = 6.4 Hz, 1H, j), 3.92 (dt, *J* = 11.1, 3.7 Hz, 1H, l), 3.30 (dd, *J* = 6.5, 3.7 Hz, 1H, k), 2.70-2.61 (m, 2H, e), 2.39-2.33 (m, 1H, p), 2.33-2.28 (m,

2H, g), 2.14 (m, 2H, n), 1.99-1.90 (m, 2H, f), 1.83 (m, 1H, r), 1.56-1.47 (m, 3H, o, r' (1H)), 1.46-1.31 (m, 5H, i, s), 0.92 (t, J = 7.3 Hz, 3H, t).

^{13}C NMR (125 MHz, $CDCl_3$) δ (ppm): 172.6 (h), 169.4 (m), 163.7 (q), 141.3 (d), 128.6 (a/b/c), 128.5 (a/b/c), 126.2 (a/b/c), 67.2 (j), 64.4 (k), 55.8 (l), 42.0 (p), 35.1 (e), 34.3 (r), 33.7 (g), 28.0 (o), 26.9 (f), 26.5 (n), 19.9 (s), 18.5 (i), 14.0 (t).

HRMS (ESI): *m/z found* = 372.21685; calcd. for $[M+H]^+$: 372.21693.

FT-IR (cm^{-1}):2957, 2931, 1804, 1735, 1687, 1298, 1137.

10.1.4 Synthesis of bicycle 104

*10.1.4.1 Deprotection of **98***

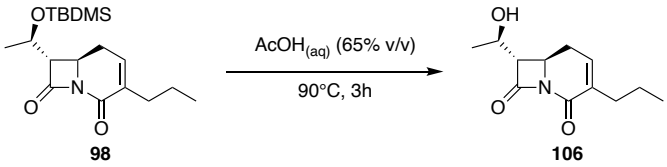

Procedure: In a round-bottom flask, **98** (371 mg, 1.1 mmol, 1.0 eq.) was added to 7.6 mL of AcOH and 3.0 mL of H_2O. The solution was heated to 90°C and stirred for 3 hours. The product was then concentrated under reduced pressure.

IUPAC name: (6*R*,7*S*)-7-((*R*)-1-hydroxyethyl)-3-propyl-1-azabicyclo[4.2.0]oct-3-ene-2,8-dione

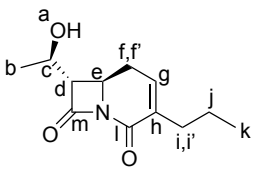

Yield: 99%

Mol. formula: $C_{12}H_{17}NO_3$

Mol. Wt.: 223.14 g.mol^{-1}

Aspect: yellow oil

^{1}H NMR (300 MHz, $CDCl_3$) δ (ppm): 6.41 (m, 1H, g), 4.37-4.11 (m, 2H, c, e), 3.14 (dd, *J* = 5.7, 3.0 Hz, 1H, d), 2.66 (ddd, *J* = 17.1, 6.5, 5.6 Hz, 1H, f), 2.51 (m, 1H, f'), 2.45-2.30 (m, 1H, i), 2.21-2.09 (m, 1H, i'), 1.56-1.42 (m, 2H, j), 1.31 (d, *J*, 6.3, 3H, b), 0.90 (t, *J* = 7.3 Hz, 3H, k).

^{13}C NMR (75 MHz, $CDCl_3$) δ (ppm): 164.1 (m), 159.4 (l), 136.8 (g, h), 66.2 (d), 64.8 (c), 50.5 (e), 32.0 (i), 27.1 (j), 21.8 (h), 13.8 (k).

HRMS (APCI): *m/z found* = 224.12819; calcd. for $[M+H]^+$: 224.12812.

FT-IR (cm^{-1}): 3451, 2963, 1792, 1673, 1377, 1288.

*10.1.4.2 Esterification of **106***

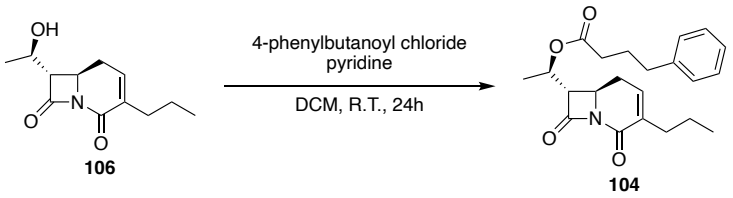

Procedure: In a dried three-neck round-bottom flask under inert conditions, 4-phenylbutanoyl chloride (274 mg, 1.5 mmol, 1.3 eq.) and pyridine (0.169 mL, 2.1 mmol, 2.0 eq.) were added to a solution of **106** (268 mg, 1.2 mmol, 1.0 eq.) in 20 mL of DCM. The mixture was stirred at room temperature for 24 hours. The solution was washed with a saturated $NaHCO_3$ solution, followed by 1 M HCl, then with brine, and dried over $MgSO_4$. The product was concentrated under reduced pressure. The crude product was purified by flash chromatography on silica gel using cyclohexane/AcOEt (80/20).

IUPAC name: (*R*)-1-((6*R*,7*S*)-2,8-dioxo-3-propyl-1-azabicyclo[4.2.0]oct-3-en-7-yl)ethyl 4-phenylbutanoate

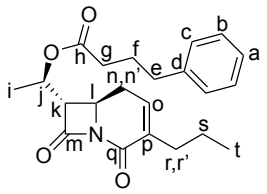

Yield: 49%

Mol. formula: $C_{22}H_{27}NO_4$

Mol. Wt.: 369.19 g.mol^{-1}

Aspect: yellow oil

^{1}H NMR (300 MHz, $CDCl_3$) δ (ppm): 7.29 (m, 2H, a/b/c), 7.23-7.14 (m, 3H, a/b/c), 6.39 (m, 1H, o), 5.25 (q, *J* = 6.4 Hz, 1H, j), 4.18-4.04 (m, 1H, l), 3.24 (dd, *J* = 6.7, 3.1 Hz, 1H, k), 2.71-2.55 (m, 3H, e, n (1H)), 2.53-2.43 (m, 1H, n'), 2.37 (t, *J* =7.5 Hz, 1H, r), 2.34-2.29 (m, 2H, g), 2.22-2.09 (m, 1H, r'), 2.02-1.87 (m, 2H, f), 1.55-1.40 (m, 2H, s), 1.36 (d, *J* = 6.3 Hz, 3H, i), 0.91 (t,*J* = 7.3 Hz, 3H, t).

^{13}C NMR (75 MHz, $CDCl_3$) δ (ppm): 172.6 (h), 162.3 (m), 159.2 (q), 141.3 (d), 136.5 (p), 136.1 (o), 128.6 (a/b/c), 128.5 (a/b/c), 126.2 (a/b/c), 67.4 (j), 64.0 (k), 51.6 (l), 35.1 (e), 33.7 (g), 31.9 (r), 28.9 (n), 26.5 (f), 21.7 (s), 18.5 (i), 13.8 (t).

HRMS (APCI): *m/z found* = 370.20128; calcd. for $[M+H]^+$: 370.20128.

FT-IR (cm^{-1}): 2247, 2972, 1801, 1736, 1681, 1379, 1281, 1081.

10.1.5 Synthesis of diastereomer 63 (first strategy)

*10.1.5.1 Substitution by thiophenolate on azetidinone **32***

Reference: M. Feledziak, C. Michaux, A. Urbach, G. Labar, G. G. Muccioli, D. M. Lambert, J. Marchand-Brynaert, *J. Med. Chem.* **2009**, *52*, 7054-7068.

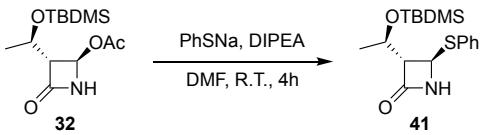

Procedure: In a dried three-neck round-bottom flask under inert conditions, PhSNa (925 mg, 7.0 mmol, 2.0 eq.) was added to a solution of the

commercially available azetidinone **32** (1.0 g, 3.5 mmol, 1.0 eq.) in 20 mL of DMF. DIPEA (0.731 mL, 4.3 mmol, 1.2 eq.) was then added, and the mixture was stirred at room temperature for 4 hours. The mixture was then diluted with 40 mL of water and washed with brine. The product was concentrated under reduced pressure. The crude product was purified by flash chromatography on silica gel using cyclohexane/AcOEt (80/20).

IUPAC name: (3*S*,4*R*)-3-((*R*)-1-((tert-butyldimethylsilyl)oxy)ethyl)-4-(phenylthio)azetidin-2-one

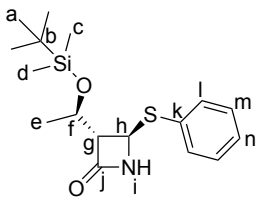

Yield: 87%

dr: 100/0

Mol. formula: $C_{17}H_{27}NO_2SSi$

Mol. Wt.: 337.15 g.mol^{-1}

Aspect: yellow powder

CAS: 85281-73-8

^{1}H NMR (300 MHz, $CDCl_3$) δ (ppm): 7.51-7.31 (m, 5H, l, m, n), 6.00 (bs, 1H, i), 5.07 (dd, *J* = 2.3, 0.5 Hz, 1H, h), 4.22 (qd, *J* = 6.3, 3.4 Hz, 1H, f), 3.02 (ddd, *J* = 3.3, 2.3, 0.9 Hz, 1H, g), 1.20 (d, *J* = 6.3 Hz, 3H, e), 0.86 (s, 9H, a), 0.06 (s, 3H, c or d), 0.05 (s, 3H, c or d).

^{13}C NMR (75 MHz, $CDCl_3$) δ (ppm): 134.1 (l/m/n), 129.7 (l/m/n) 129.0 (l/m/n), 65.9 (g) 64.9 (f), 56.5 (h), 26.1 (a), 22.6 (e), 18.3 (b), -4.0 (c or d), -4.8 (c or d). 2 quaternary C could not be observed.

HRMS (APCI): *m/z found* = 338.16047; calcd. for $[M+H]^+$: 338.16045.

Data align with literature (see above).

*10.1.5.2 Thiophenolate abstraction on **41***

Reference: M. Feledziak, C. Michaux, A. Urbach, G. Labar, G. G. Muccioli, D. M. Lambert, J. Marchand-Brynaert, *J. Med. Chem.* **2009**, *52*, 7054-7068.

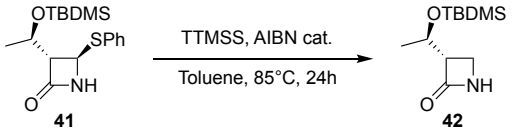

Procedure: In a dried three-neck round-bottom flask under inert conditions, 50 mL of toluene were heated to 85°C. **41** (508 mg, 1.5 mmol, 1 eq.) was dissolved in 10 mL of toluene. Meanwhile, AIBN (33 mg, 0.2 mmol, 0.2 eq.) and TTMSSH (2.715 mL, 8.8 mmol, 6.0 eq.) were added to the main solution. The **41** solution was then added to the mixture, which was stirred at 85°C for 24 hours. The product was concentrated under reduced pressure. The crude product was purified by flash chromatography on silica gel using cyclohexane/AcOEt (75/25).

IUPAC name: (*S*)-3-((*R*)-1-((tert-butyldimethylsilyl)oxy)ethyl)azetidin-2-one

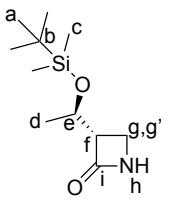

Yield: 50%

Mol. formula: $C_{11}H_{23}NO_2Si$

Mol. Wt.: 229.15 g.mol^{-1}

Aspect: white powder

CAS: 109323-90-2

^{1}H NMR (300 MHz, $CDCl_3$) δ (ppm): 5.66 (s, 1H, h), 4.21 (qd, J = 6.2, 4.4 Hz, 1H, e), 3.35 (dd, J = 4.9, 2.5 Hz, 1H, g), 3.29 (t, J = 5.1 Hz, 1H, g'), 3.25-3.19 (m, 1H, f), 1.19 (d, J = 6.2 Hz, 3H, d), 0.87 (s, 9H, a), 0.07 (s, 6H, c).

HRMS (APCI): *m/z found* = 230.15701; calcd. for $[M+H]^+$: 230.14708.

Data align with literature (see above).

*10.1.5.3 Direct reduction of azetidinone **32***

Reference: C. Crauste, M. Froyen, J. Anné, P. Herderwijn, *Eur. J. Org. Chem.* **2011**, 3437-3449.

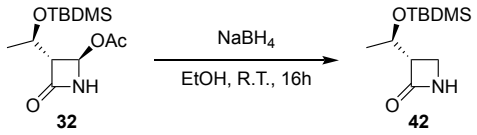

Procedure: In a round-bottom flask, $NaBH_4$ (806 mg, 31.3 mmol, 1.5 eq.) was added to a solution of commercially available azetidinone **32** (6.0 g, 20.9 mmol, 1.0 eq.) in 30 mL of absolute ethanol at 10°C. The mixture was then stirred at room temperature for 16 hours. Subsequently, acidic Amberlite™ resin (18 g) was added and stirred for 30 minutes before being filtered and washed with EtOAc. The crude product was concentrated under reduced pressure. The product was then dissolved in DCM, purified with a pad of silica, and concentrated under vacuum.

See section 10.1.5.2 for characterisation.

*10.1.5.4 N-acylation of **42***

Reference: M. Feledziak, C. Michaux, A. Urbach, G. Labar, G. G. Muccioli, D. M. Lambert, J. Marchand-Brynaert, *J. Med. Chem.* **2009**, *52*, 7054-7068.

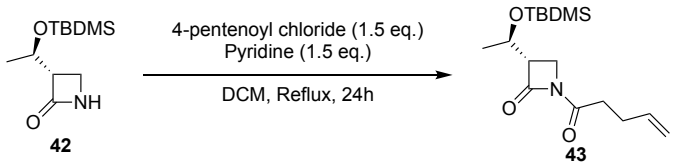

Procedure: In a dried three-neck round-bottom flask under inert conditions, **42** (252 mg, 1.1 mmol, 1.0 eq.) was dissolved in 10 mL of DCM. Pent-4-enoyl chloride (0.188 mL, 1.7 mmol, 1.5 eq.) was added to the solution, followed by pyridine (0.137 mL, 1.7 mmol, 1.5 eq.). The mixture was

stirred at 45°C for 24 hours. The product was washed with 10 mL of 10% Na_2CO_3 solution, then the organic layer was washed with 2 M HCl, followed by brine, and dried over $MgSO_4$. The crude product was purified by flash chromatography on silica gel using cyclohexane/AcOEt (90/10).

IUPAC name: (*S*)-3-((*R*)-1-((tert-butyldimethylsilyl)oxy)ethyl)-1-(pent-4-enoyl)azetidin-2-one

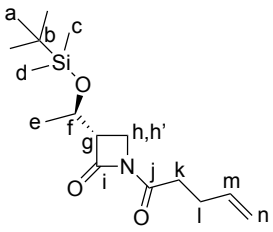

Yield: 75%

Mol. formula: $C_{16}H_{29}NO_3Si$

Mol. Wt.: 311.19 g.mol^{-1}

Aspect: yellow oil

CAS: 1197422-27-7

^{1}H NMR (300 MHz, $CDCl_3$) δ (ppm): 5.83 (ddt, *J* = 16.8, 10.2, 6.5 Hz, 1H, m), 5.17-4.89 (m, 2H, n), 4.30 (qd, *J* = 6.3, 3.3 Hz, 1H, f), 3.68 (dd, *J* = 7.2, 3.6 Hz, 1H, h), 3.54 (dd, *J* = 7.2, 6.5 Hz, 1H, h'), 3.23 (dt, 6.4, 3.5, 1H, g), 2.89-2.64 (m, 2H, k), 2.49-2.31 (m, 2H, l), 1.18 (d, *J* = 6.3 Hz, 3H, e), 0.83 (s, 9H, a), 0.06, (s, 3H, c or d), 0.04 (s, 3H, c or d).

^{13}C NMR (75 MHz, $CDCl_3$) δ (ppm): 170.6 (j), 166.8 (i), 136.9 (m), 116.0 (n), 65.0 (f), 56.7 (g), 38.6 (h), 36.1 (k), 28.3 (l), 25.9 (a), 22.5 (e), 18.2 (b), -3.9 (c or d), -4.9 (c or d).

HRMS (APCI): *m/z found* = 312.19896; calcd. for $[M+H]^+$: 312.19895.

Data align with literature (see above).

*10.1.5.5 Deprotection of **43***

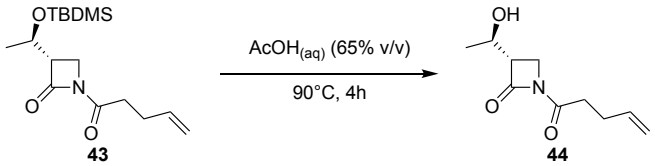

Procedure: A solution of **43** (62 mg, 0.2 mmol, 1 eq.) in 2 mL of AcOH and 1 mL of water was prepared in a round-bottom flask and heated to 90°C for 4 hours. The product was concentrated under reduced pressure and purified by flash chromatography on silica gel using cyclohexane/AcOEt (50/50).

UPAC name: (*S*)-3-((*R*)-1-hydroxyethyl)-1-(pent-4-enoyl)azetidin-2-one

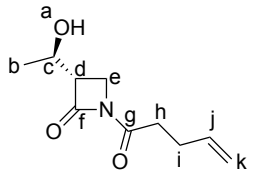

Yield: 99%

Mol. formula: $C_{10}H_{15}NO_3$

Mol. Wt.: 197.11 g.mol^{-1}

Aspect: yellow powder

CAS: 1197422-03-9

^{1}H NMR (300 MHz, $CDCl_3$) δ (ppm): 6.13 (ddt, *J* = 16.8, 10.2, 6.5 Hz, 1H, j), 5.44-5.21 (m, 2H, j), 4.58 (qd, *J* = 6.3, 5.0 Hz, 1H, c), 3.93 (q, *J* = 5.1 Hz, 1H, d), 3.60-3.41 (m, 2H, e), 3.23-3.02 (m, 2H, h), 2.80-2.60 (m, 2H, i), 2.36 (d, *J* = 13.1 Hz, 1H, a), 1.61 (d, *J* = 6.4 Hz, 3H, b).

^{13}C NMR (75 MHz, $CDCl_3$) δ (ppm): 1170.7 (g), 166.3 (f), 136.7 (j), 116.0 (k), 65.0 (c), 55.9 (d), 39.3 (e), 36.0 (h), 31.2 (i), 21.8 (b).

HRMS (APCI): *m/z found* = 198.11264; calcd. for $[M+H]^+$: 198.11247.

FT-IR (cm^{-1}): 3361, 2971, 1784, 1698, 1642, 1380, 1314, 917.

Data align with M. Feledziak, C. Michaux, A. Urbach, G. Labar, G. G. Muccioli, D. M. Lambert, J. Marchand-Brynaert, *J. Med. Chem.* **2009**, *52*, 7054-7068.

10.1.6 Synthesis of diastereomer 63 (second strategy)

*10.1.6.1 Deprotection of **42***

Reference: inspired from C. Crauste, M. Froyen, J. Anné, P. Herderwijn, *Eur. J. Org. Chem.* **2011**, 3437-3449.

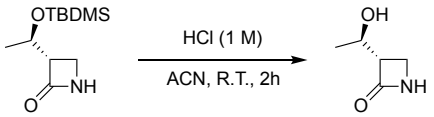

Procedure: In a round-bottom flask, **42** (3.048 g, 13.3 mmol, 1.0 eq.) was dissolved in 70 mL of ACN. To this solution, 13 mL of 1 M HCl were added, and the mixture was stirred at room temperature for 1 hour and 30 minutes. An additional 6.5 mL of 1 M HCl were then added. After 30 minutes, the mixture was diluted with water, and the remaining HCl was neutralised with 1 M NaOH until the pH reached 7. The product was concentrated under reduced pressure. A minimum amount of iced MeOH was added to dissolve the product. The solution was centrifuged, and the supernatant was collected. This process was repeated until small yellow crystals appeared.

IUPAC name: (*S*)-3-((*R*)-1-hydroxyethyl)azetidin-2-one

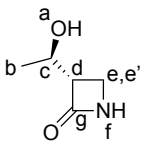

Yield: 95%

Mol. formula: $C_5H_9NO_2$

Mol. Wt.: 115.13 g.mol^{-1}

Aspect: yellow oil

CAS: 120236-28-4

^{1}H NMR (300 MHz, DMSO) δ (ppm): 7.66 (bs, 1H, f), 4.80 (bs, 1H, a), 3.86-3.69 (m, 1H, c), 3.09 (t, *J* = 5.3 Hz, 1H, e), 3.04-2.98 (m, 2H, d, e' (1H)), 1.05 (d, *J* = 6.3 Hz, 3H, b).

^{13}C NMR (75 MHz, DMSO) δ (ppm): 168.8 (g), 64.4 (c), 58.5 (d), 37.5 (e), 22.0 (b).

FT-IR (cm^{-1}): 3166, 1723, 1377, 1214, 1141, 1097, 1067, 897, 704.

Data align with literature (see above).

*10.1.6.2 Mitsunobu reaction on **109***

Reference: C. Crauste, M. Froyen, J. Anné, P. Herderwijn, *Eur. J. Org. Chem.* **2011**, 3437-3449.

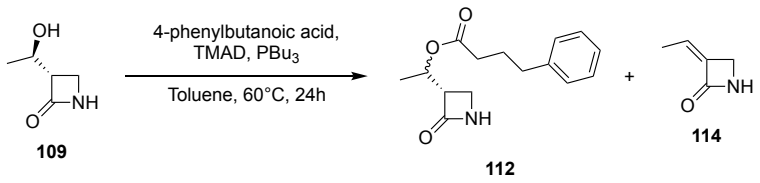

Procedure: In a dried three-neck round-bottom flask under inert conditions, **109** (196 mg, 1.7 mmol, 1.0 eq.) was dissolved in 6 mL of toluene. At 0°C, PBu_3 (0.658 mL, 2.6 mmol, 1.5 eq.) was added to the solution, followed by 4-phenylbutanoic acid (279 mg, 1.7 mmol, 1.0 eq.). TMAD (448 mg, 2.6 mmol, 1.5 eq.) was then added, and the mixture was stirred at 0°C for 10 minutes before being heated to 60°C for 24 hours. A large volume of hexane was added, and the resulting suspension was filtered. The solution was concentrated under reduced pressure. The crude product was purified by flash chromatography on silica gel using hexane/AcOEt (30/70).

IUPAC name: **A** 3-ethylideneazetidin-2-one and **B** (*R*)-1-((*S*)-2-oxoazetidin-3-yl)ethyl 4-phenylbutanoate

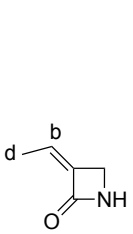

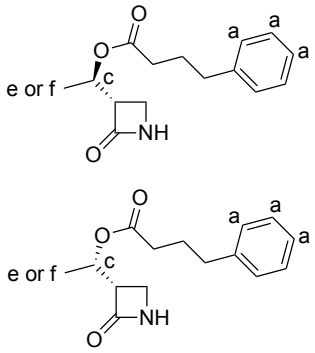

Mol. formula: C_5H_7NO Mol. formula: $C_{15}H_{19}NO_3$

Mol. Wt.: 97.05g.mol^{-1} Mol. Wt.: 261.14g.mol^{-1}

Aspect: yellow oil

A mixture of 3 products was obtained. This can be confirmed *via* HRMS analysis. We were not able to separate them and the mixture was used for the following step. The results of the N-acylation suggest us that two diastereomers were obtained during the Mitsunobu reaction. Some characteristic NMR signals can be observed for the mixture:

^{1}H NMR (300 MHz, $CDCl_3$) δ (ppm) (only the characteristic peaks): 7.36 – 7.08 (m, 5H, a); 6.28 – 6.13 (m, 1H, b), 5.30 – 5.17 (m, 1H, c), 1.75 (d, *J* = 7.1 Hz, 3H, d), 1.39 (d, *J* = 6.5 Hz, 3H, e or f), 1.36 (d, *J* = 6.3 Hz, 3H, e or f).

HRMS (APCI) A: m/z found = 98.06049; calcd. for [M+H]+: 98.06004.

HRMS (APCI) B: m/z found = 284.12571; calcd. for [M+Na]+: 284.12571.

FT-IR (cm−1): 2957, 2931, 2872, 1696, 1133, 700.

*10.1.6.3 Esterification of **112***

Reference: M. Feledziak, C. Michaux, A. Urbach, G. Labar, G. G. Muccioli, D. M. Lambert, J. Marchand-Brynaert, *J. Med. Chem.* **2009**, *52*, 7054-7068.

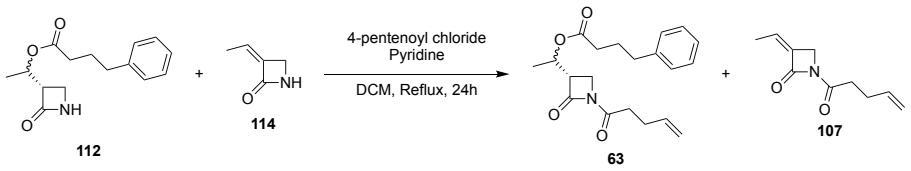

Procedure: In a dried three-neck round-bottom flask under inert conditions, **112** (418 mg, 1.6 mmol, 1.0 eq.) was dissolved in 10 mL of DCM. Pent-4-enoyl chloride (344 mg, 2.9 mmol, 2 eq.) was added to the solution, followed by pyridine (0.178 mL, 2.2 mmol, 1.5 eq.). The mixture was stirred at 45°C for 24 hours. The product was washed with 10 mL of 10% Na_2CO_3 solution, then the organic layer was washed with 2 M HCl, followed by brine, dried over $MgSO_4$ and concentrated under reduced pressure. The crude product was purified by flash chromatography on silica gel using cyclohexane/AcOEt (70/30).

After purification, two fractions were obtained: **fraction 1**, containing the enantiomer of the lead compound, and **fraction 2**, containing three products: the elimination product, the enantiomer of the lead compound, and the target diastereomer. This mixture was further purified by semi-preparative HPLC, which removed the elimination product (**107**); however, the two diastereomers could not be separated.

Fraction 1

IUPAC name: ((*S*)-1-((*R*)-2-oxo-1-(pent-4-enoyl)azetidin-3-yl)ethyl 4-phenylbutanoate and ((*R*)-1-((*S*)-2-oxo-1-(pent-4-enoyl)azetidin-3-yl)ethyl 4-phenylbutanoate

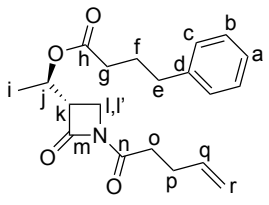

Mol. formula: $C_{20}H_{25}NO_4$
Mol. Wt.: 343.18 g.mol^{-1}
Aspect: yellow oil

^{1}H NMR (300 MHz, $CDCl_3$) δ (ppm): 7.37 – 7.10 (m, 5H, a, b, c), 5.81 (ddt, *J* = 16.9, 10.2, 6.5 Hz, 1H, q), 5.37 – 5.18 (m, 1H, j), 5.14 – 4.93 (m, 2H, r), 3.66 (dd, *J* = 7.7, 6.6 Hz, 1H, l), 3.53 (dd, *J* = 7.7, 3.6 Hz, 1H, l'), 3.40 (td, *J* = 6.4, 3.6 Hz, 1H, k), 2.77 (t, *J* = 7.6 Hz, 2H, o), 2.63 (t, *J* = 7.6 Hz, 2H, g), 2.48 – 2.33 (m, 2H, p), 2.30 (t, *J* = 7.5 Hz, 2H, e), 2.01 – 1.83 (m, 2H, f), 1.35 (d, *J* = 6.4 Hz, 3H, i).

^{13}C NMR (75 MHz, $CDCl_3$) δ (ppm): 172.4 (h), 170.3 (n), 162.4 (m), 141.2 (d), 136.5 (q), 128.6 (a/b/c), 126.2 (a/b/c), 115.9 (r), 67.2 (j), 53.7 (k), 39.6 (l), 35.9 (o), 35.2 (g), 33.8 (e) , 28.0 (p), 26.6 (f), 18.0 (i).

HRMS (APCI): *m/z found* = 366.16768; calcd. for $[M+Na]^+$: 366.16758.

FT-IR (cm^{-1}): 2975, 2935, 2913, 1790, 1713, 1704, 1315.

Fraction 2

IUPAC name: (*S*)-1-((*R*)-2-oxo-1-(pent-4-enoyl)azetidin-3-yl)ethyl 4-phenylbutanoate and (*S*)-1-((*S*)-2-oxo-1-(pent-4-enoyl)azetidin-3-yl)ethyl 4-phenylbutanoate

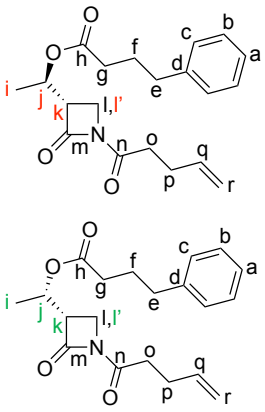

Mol. formula: $C_{16}H_{29}NO_3Si$

Mol. Wt.: 311.19 $g.mol^{-1}$

Aspect: yellow oil

^{1}H NMR (300 MHz, $CDCl_3$) δ (ppm): 7.47 – 7.03 (m, 5H, a, b, c), 5.92 – 5.70 (m, 1H, q), 5.34 – 5.18 (m, 1H, j, j), 5.14 – 4.94 (m, 2H,r), 3.65 (ddd, *J* = 9.8, 7.7,

6.5 Hz, 1H, l), 3.53 (dd, J = 7.8, 3.7 Hz, 1H, l'), 3.49 – 3.30 (m, 2H, l', f), 2.86 – 2.71 (m, 2H, o), 2.69 – 2.55 (m, 2H, g), 2.47 – 2.22 (m, 4H, e, p), 2.01 – 1.86 (m, 2H, f), 1.40 (d, J = 6.5 Hz, 3H, i), 1.35 (d, J = 6.4 Hz, 3H, i).

^{13}C NMR (75 MHz, $CDCl_3$) δ (ppm): 172.4 (h), 170.3 (n), 162.4 (m), 141.2 (d), 136.5 (q), 128.6 (a/b/c), 126.2 (a/b/c), 115.9 (r), 67.3 (j), 67.2 (j), 53.7 (k), 52.8 (k), 39.6 (l), 35.9 (o), 35.2 (g), 33.8 (e) , 28.0 (p), 26.6 (f), 18.5 (i), 18.0 (i).

HRMS (APCI): *m/z found* = 366.16768; calcd. for $[M+H]^+$: 366.16758.

FT-IR (cm^{-1}): 2974, 2912, 1788, 1735, 1703, 1312.

10.1.7 Synthesis of γ-lactam 65

*10.1.7.1 Preparation of γ-lactam **71***

Reference: W. Yang, X. Sun, W. Yu, R. Rai, J. R. Deschamps, L. A. Mitchell, C. Jiang, A. D. MacKerell, Jr., F. Xue, *Org. Lett.* **2015**, *17*, 3070-3073.

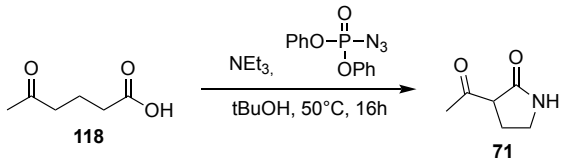

Procedure: In a dried three-neck round-bottom flask under inert conditions, compound **118** (130 mg, 1.0 mmol, 1.0 eq.) was dissolved in 5 mL of tBuOH. DPPA (0.237 mL, 1.1 mmol, 1.1 eq.) was added to the solution at room temperature, followed by triethylamine (0.270 mL, 2.0 mmol, 2.0 eq.). The mixture was stirred at 50°C for 16 hours. The product was then concentrated under reduced pressure and purified by flash chromatography on silica gel using hexane/AcOEt (2/1).

IUPAC name: 3-acetylpyrrolidin-2-one

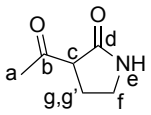

Yield: 11%

Mol. formula: $C_6H_9NO_2$

Mol. Wt.: 127.14 g.mol^{-1}

Aspect: orange powder

CAS: 31536-38-6

^{1}H NMR (300 MHz, $CDCl_3$) δ (ppm): 6.54 (bs, 1H, e), 3.51 (dd, *J* = 9.2, 6.3 Hz, 1H, c), 3.46 – 3.28 (m, 2H, f), 2.70 – 2.55 (m, 1H, g), 2.39 (s, 3H, a), 2.23 – 2.07 (m, 1H, g').

^{13}C NMR (75 MHz, $CDCl_3$) δ (ppm): 203.6 (b), 173.8 (d), 54.9 (c), 40.6 (f), 30.1 (a), 22.5 (g).

HRMS (ESI): *m/z found* = 150.05259; calcd. for $[M+Na]^+$: 150.05255.

Data align with lite*rature (see above).*

*10.1.7.2 Acetylation of **119***

Reference: Y. Lou, Y. Hu, J. Lu, F. Guan, G. Gong, Q. Yin, X. Zhang, *Angew. Chem. Int. Ed. Engl.* **2018**, *57*, 14193-14197.

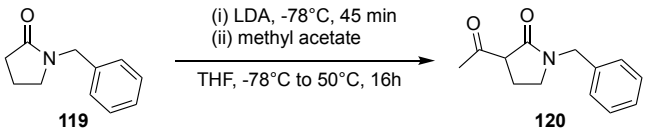

Procedure: In a dried three-neck round-bottom flask under inert conditions, commercially available 1-benzyl-2-pyrrolidinone **119** (1.051 g, 6.0 mmol, 1.0 eq.) was dissolved in 10 mL of THF. LDA (7.0 mmol, 1.2 eq.) was added to the solution, which was stirred for 40 minutes at -78°C. Methyl acetate (0.548 mL, 6.9 mmol, 1.2 eq.) was then added, and the mixture was stirred at room temperature for 12 hours. The reaction was quenched with a saturated NH_4Cl solution and then extracted with 3 x 10 mL of EtOAc, washed with brine, and dried over Na_2SO_4. The product was concentrated under

reduced pressure, and the crude product was purified by flash chromatography on silica gel using cyclohexane/AcOEt (90/10).

IUPAC name: 3-acetylpyrrolidin-2-one

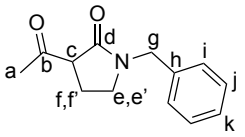

Yield: 98%
Mol. formula: $C_{13}H_{15}NO_2$
Mol. Wt.: 217.27 g.mol^{-1}
Aspect: colourless oil
CAS: 143129-53-7

^{1}H NMR (300 MHz, $CDCl_3$) δ (ppm): 7.36 – 7.15 (m, 5H, i, j, k), 4.51 – 4.33 (m, 2H, g), 3.63 (dd, *J* = 9.3, 6.1 Hz, 1H, c), 3.29 (ddd, *J* = 9.7, 8.8, 5.4 Hz, 1H e), 3.18 (ddd, *J* = 9.6, 8.7, 5.5 Hz, 1H, e'), 2.57 – 2.46 (m, 1H, f), 2.44 (s, 3H, a), 1.99 (dddd, *J* = 13.2, 9.3, 8.7, 5.5 Hz, 1H, f').

^{13}C NMR (75 MHz, $CDCl_3$) δ (ppm): 203.9 (b), 169.9 (d), 136.1 (h), 128.9 (i/j/k), 128.1 (i/j/k), 127.9 (i/j/k), 55.8 (c), 47.0 (g), 45.0 (e), 30.1 (a),19.6 (f).

Data align with literature (see above).

*10.1.7.3 Bromination of alcohol **124***

Reference: A. K. Ghosh, D. D. Anderson, *Org. Lett.* **2012**, *14*, 4730-4733.

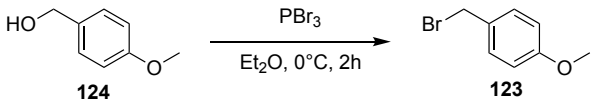

Procedure: In a dried three-neck round-bottom flask under inert conditions, commercially available para-methoxybenzyl alcohol **124** (5.400 mL, 43.5 mmol, 2.0 eq.) was dissolved in 50 mL of Et_2O. PBr_3 (2.068 mL, 22.0 mmol, 1.0 eq.) was added to the solution at 0°C. The mixture was stirred at

0°C for 2 hours. The solution was then washed three times with saturated $NaHCO_3$ solution, followed by brine. The organic layer was dried over $MgSO_4$, and the product was concentrated under reduced pressure.

IUPAC name: 1-(bromomethyl)-4-methoxybenzene

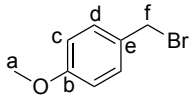

Yield: 88%
Mol. formula: C_8H_9BrO
Mol. Wt.: 201.06 g.mol^{-1}
Aspect: orange oil
CAS: 2746-25-0

^{1}H NMR (300 MHz, $CDCl_3$) δ (ppm): 7.37 – 7.27 (m, 2H, d), 6.91 – 6.81 (m, 2H, c), 4.50 (s, 2H, f), 3.81 (s, 3H, a).

Data align with M. Gonzalez, Y. Ellahioui, L. Gallego, A. Vicente-Blazquez, R. Alvarez, M. Medarde, R. Pelaez, *Bioorg. Chem.* **2023**, *131*, 106282.

*10.1.7.4 Protection of pyrrolidin-2-one **122***

Reference: C. Curti, B. Ranieri, L. Battistini, G. Rassu, V. Zambrano, G. Pelosi, G. Casiraghi, F. Zanardi, *Adv. Synth. Catal.* **2010**, *352*, 2011-2022.

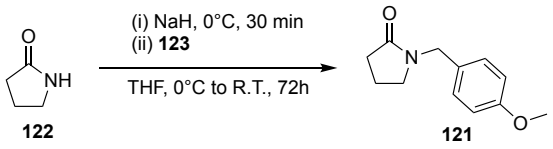

Procedure: In a dried three-neck round-bottom flask under inert conditions, NaH (in paraffin oil, 35%, 42.2 mmol, 1.1 eq.) was dissolved in 45 mL of THF, and the suspension was cooled to 0°C. Meanwhile, pyrrolidine-2-one **122** (2.884 mL, 38.4 mmol, 1.0 eq.) was dissolved in 30 mL of THF. The latter solution was added dropwise to the suspension, and the mixture was stirred at 0°C for 30 minutes. Then, 1-(bromomethyl)-4-methoxybenzene

123 (7.721 g, 38.4 mmol, 1.0 eq.) was added, and the reaction was stirred at room temperature for 3 days. The solvent was removed under reduced pressure, and 80 mL of AcOEt and 80 mL of water were added. The organic layer was washed with brine and dried over $MgSO_4$. The product was concentrated under reduced pressure, and the crude product was purified by flash chromatography on silica gel using cyclohexane/AcOEt (60/40).

IUPAC name: 1-(4-methoxybenzyl)pyrrolidin-2-one--pyrrolidin-2-one

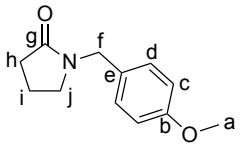

Yield: 70%

Mol. formula: $C_{12}H_{15}NO_2$

Mol. Wt.: 205.36 g.mol^{-1}

Aspect: orange oil

CAS: 60737-65-7

^{1}H NMR (300 MHz, $CDCl_3$) δ (ppm): 7.21 – 7.14 (m, 2H, d), 6.89 – 6.82 (m, 2H, c), 4.39 (s, 2H, f), 3.80 (s, 3H, a), 3.24 (t, *J* = 7.1 Hz, 2H,j), 2.43 (t, *J* =8.1 Hz, 2H, h), 2.07 – 1.90 (m, 2H, i).

HRMS (ESI): *m/z found* = 228.09981; calcd. for $[M+Na]^+$: 228.09950.

Data align with D. Hayrapetyan, V. Stepanova, *Eur. J. Org. Chem.* **2021**, *2021*, 2121-2125.

*10.1.7.5 Acetylation of **121***

Reference: Y. Lou, Y. Hu, J. Lu, F. Guan, G. Gong, Q. Yin, X. Zhang, *Angew. Chem. Int. Ed. Engl.* **2018**, *57*, 14193-14197.

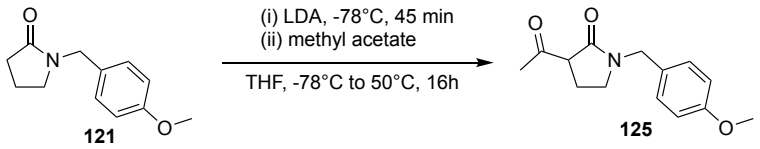

Procedure: In a dried three-neck round-bottom flask under inert conditions, compound **121** (1.499 g, 7.3 mmol, 1.0 eq.) was dissolved in 12 mL of THF. LDA (8.0 mmol, 1.1 eq.) was added to the solution, which was stirred for 40 minutes at -78°C. Methyl acetate (0.668 mL, 8.4 mmol, 1.2 eq.) was then added, and the mixture was stirred at room temperature for 16 hours. The reaction was quenched with a saturated NH_4Cl solution and then extracted with 3 x 10 mL of EtOAc, washed with brine, and dried over Na_2SO_4. The product was concentrated under reduced pressure, and the crude product was purified by flash chromatography on silica gel using cyclohexane/AcOEt (70/30).

IUPAC name: 3-acetyl-1-(4-methoxybenzyl)pyrrolidin-2-one

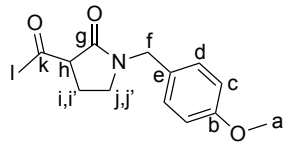

Yield: 70%
Mol. formula: $C_{14}H_{17}NO_3$
Mol. Wt.: 247.29 $g.mol^{-1}$
Aspect: yellow oil
CAS: 2247025-10-9

^{1}H NMR (300 MHz, $CDCl_3$) δ (ppm): 7.17 – 7.07 (m, 2H, d), 6.88 – 6.80 (m, 2H, c), 4.36 (q, *J* = 14.5 Hz, 2H, f), 3.79 (s, 3H, a), 3.62, (dd, *J* = 9.3, 6.0 Hz, 1H, h), 3.34 – 3.23 (m, 1H, j), 3.23 – 3.10 (m, 1H, j'), 2.55 – 2.46 (m, 1H, i), 2.45 (s, 3H, l), 2.06 – 1.90 (m, 1H, i').

^{13}C NMR (75 MHz, $CDCl_3$) δ (ppm): 204.0 (k), 169.8 (g), 159.3 (b), 129.6 (d), 128.2 (e), 114.3 (c), 55.9 (h), 55.4 (a), 46.4 (f), 45.0 (j), 30.2 (l), 19.5 (i).

Data align with D. Hayrapetyan, V. Stepanova, *Eur. J. Org. Chem.* **2021**, *2021*, 2121-2125.

*10.1.7.6 Reduction of **125***

Reference: D. Lynch, R. E. Deasy, L. A. Clarke, C. N. Slattery, U. B. Khandavilli, S. E. Lawrence, A. R. Maguire, N. A. Magnus, H. A. Moynihan, *Org. Lett.* **2016**, *18*, 4978-4981.

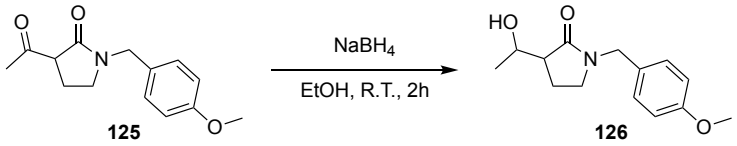

Procedure: In a round-bottom flask, $NaBH_4$ (26 mg, 0.7 mmol, 1.1 eq.) was dissolved in 3 mL of EtOH and cooled to 0°C. Meanwhile, compound **125** (148 mg, 0.6 mmol, 1.0 eq.) was dissolved in 11 mL of EtOH. This solution was added to the $NaBH_4$ solution over 15 minutes. The reaction mixture was stirred at 0°C for 2 hours and then at room temperature for an additional 2 hours. The reaction was quenched by the dropwise addition of 5 M HCl. The solvent was then evaporated under reduced pressure. To the residue, 10 mL of DCM and 10 mL of water were added. After separation, the aqueous layer was extracted with an additional 10 mL of DCM. The combined organic layers were washed with brine and dried over $MgSO_4$.

IUPAC name: 3-(1-hydroxyethyl)-1-(4-methoxybenzyl)pyrrolidin-2-one

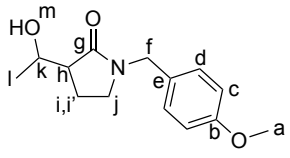

Yield: 97%

dr:63/37

Mol. formula: $C_{14}H_{19}NO_3$

Mol. Wt.: 249.31 g.mol^{-1}

Aspect: colourless oil

^{1}H NMR (300 MHz, $CDCl_3$) δ (ppm): 7.15 (d,*J* =8.6 Hz, 2H, d), 6.85 (d, *J* = 88 Hz, c), 5.23 (bs, 1H, m), 4.43 – 4.36 (m, 2H, f), 3.89 – 3.75 (m, 4H, a, k), 3.19 (ddd, *J* = 9.6, 6.4, 2.4 Hz, 2H, j), 2.65 (td, *J* = 9.3, 3.4 Hz, 1H (dia 1), h), 2.37 (q,

J = 9.6 Hz, 1H (dia 2), h), 2.16 – 1.85 (m, 1H, i), 1.69 – 1.47 (m, 1H, i'), 1.24 – 1.12, m, 3H, l)

HRMS (ESI): *m/z found* = 250.14395; calcd. for $[M+H]^+$ 250.14377.

*10.1.7.7 Esterification of **126***

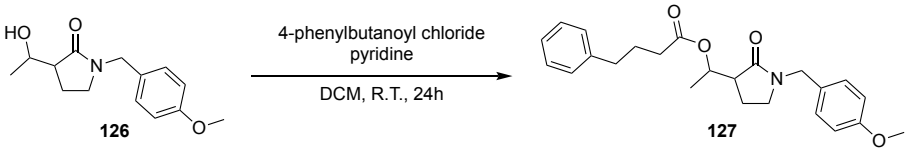

Procedure: In a dried three-neck round-bottom flask under inert conditions, 4-phenylbutanoyl chloride (183 mg, 1.0 mmol, 1.6 eq.) and pyridine (0.113 mL, 1.4 mmol, 2.3 eq.) were added to a solution of **126** (150 mg, 0.6 mmol, 1.0 eq.) in 14 mL of DCM. The mixture was stirred at room temperature for 24 hours. The solution was washed with a saturated $NaHCO_3$ solution, followed by 1M HCl, then with brine, and dried over $MgSO_4$. The product was concentrated under reduced pressure. The crude product was purified by flash chromatography on silica gel using cyclohexane/AcOEt (80/20).

IUPAC name: 1-(1-(4-methoxybenzyl)-2-oxopyrrolidin-3-yl)ethyl 4-phenylbutanoate

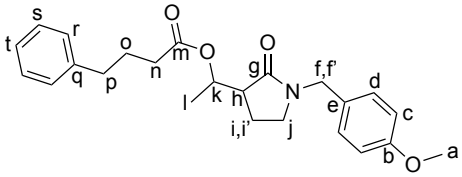

Yield: 58%
dr: not determined
Mol. formula: $C_{24}H_{29}NO_4$
Mol. Wt.: 395.50 $g.mol^{-1}$
Aspect: yellow oil

^{1}H NMR (300 MHz, $CDCl_3$) δ (ppm): 7.32 – 7.12 (m, 7H, d, r, s, t), 6.89 – 6.76 (m, 2H, c), 5.28 (qd, *J* = 6.5, 4.3 Hz, k), 4.49 (d, *J* = 14.4 Hz, f), 4.26 (d, *J* = 14.4 Hz, f'), 3.78 (s, 3H, a), 3.15 (t, *J* = 7.4 Hz, 2H, j), 2.80 (ddd, *J* = 9.6,7.3, 4.3 Hz,

1H, h), 2,62, (t, *J* =7.5 Hz, 2H, p), 2.27 (t, *J* = 7.4 Hz, 2H, n), 2.16 – 2.01 (m, 1H, i), 1.99 – 1.74 (m, 3H,o, i' (1H)), 1.33 (d, *J* = 6.5 Hz, 3H, l).

HRMS (ESI): *m/z found* = 396.21690; calcd. for $[M+H]^+$: 396.21693.

10.1.8 Synthesis of δ-lactam 66

*10.1.8.1 Protection of δ-valerolactam **78***

Reference: U. Ragnarsson, L. Grehn, *RSC Advances*, **2013**, *3*, 18691-18697.

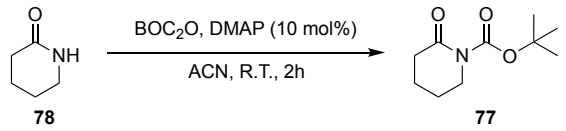

Procedure: In a dried round-bottom flask under inert conditions, commercially available δ-valerolactam **78** (991 mg, 10.0 mmol, 1.0 eq.) was dissolved in 30 mL of ACN. DMAP (122 mg, 1.0 mmol, 0.1 eq.) was added to the solution, followed by BOC_2O (2.532 g, 11.6 mmol, 1.2 eq.). The mixture was stirred at room temperature for 2 hours. The solution was then concentrated under reduced pressure. Then, 20 mL of Et_2O were added, and the product was washed with 1 M HCl and brine. The aqueous phase was extracted with 2 × 20 mL of Et_2O. The organic layer was dried over Na_2SO_4, and the solvent was finally removed under reduced pressure.

IUPAC name: tert-butyl 2-oxopiperidine-1-carboxylate

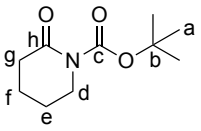

Yield: 60%

Mol. formula: $C_{10}H_{17}NO_3$

Mol. Wt.: 199.24 $g.mol^{-1}$

Aspect: yellow oil

CAS: 85908-96-9

^{1}H NMR (300 MHz, $CDCl_3$) δ (ppm):3.66 (t, J = 8.6 Hz, 2H, d), 2.52 (t, J = 7.2 Hz, 2H, g), 1.88-1.74 (m, 4H, e, f), 1.52 (s, 9H, a).

^{13}C NMR (75 MHz, $CDCl_3$) δ (ppm): 171.4 (h), 152.8 (c), 82.9 (b), 46.3 (d), 34.9 (g), 28.0 (a), 22.8 (e or f), 20.5 (e or f).

HMRS (ESI): *m/z found* = 200.12810; calcd. for $[M+H]^+$: 200.12812.

FT-IR (cm^{-1}): 1713, 1144, 1160, 1297, 1249.

Data align with J. Lee, J. W. Ban, J. Kim, S. Yang, G. Lee, L. P. Dhorma, M. H. Kim, M. W. Ha, S. Hong, H. G. Park, *Org. Lett.* **2022**, *24*, 1647-1651.

*10.1.8.2 Acetylation of **77***

Reference: M. Kenny, J. Christensen, S. J. Coles, V. Franckevicius, *Org. Lett.*, **2015**, *17*, 3926-3929.

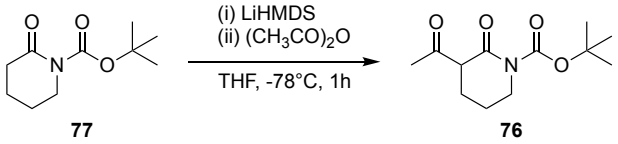

77 **76**

Procedure: In a dried three-neck round-bottom flask under inert conditions, compound **77** (1.036 g, 5.2 mmol, 1.0 eq.) was dissolved in 100 mL of THF at -78°C. LiHMDS (10.5 mmol, 2.0 eq.) was added to the solution, which was stirred for 15 minutes at -78°C. Acetic anhydride (0.473 mL, 5.0 mmol, 1.0 eq.) was then added, and the mixture was stirred for 1 hour at -78°C. The solution was allowed to return to room temperature, after which 10 mL of saturated NH_4Cl solution was added. The mixture was extracted with 3 × 15 mL of EtOAc, washed with brine, and dried over $MgSO_4$. The product was concentrated under reduced pressure, and the crude product was purified by flash chromatography on silica gel using cyclohexane/AcOEt (80/20) with 1% Et_3N.

IUPAC names: tert-butyl 3-acetyl-2-oxopiperidine-1-carboxylate *and* tert-butyl (Z)-3-(1-hydroxyethylidene)-2-oxopiperidine-1-carboxylate

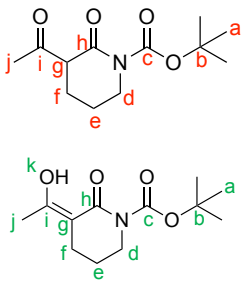

Yield for both tautomers: 14%

Mol. formula: $C_{12}H_{19}NO_4$

Mol. Wt.: 241.13 g.mol^{-1}

Aspect: colourless oil

^{1}H NMR (300 MHz, $CDCl_3$) δ (ppm): 14.83 (s, 1H, k), 3.61 – 3.54 (m, 2H, d, d), 3.51 (t, J = 8.9 Hz, 1H, g), 2.31 (s, 3H, j), 2.30 – 2.25 (t, J = 3.2 Hz, 2H, f), 1.93 (s, 3H, j), 1.84 – 1.72 (m, 2H, e, e, f), 1.47 (s, 9H, a), 1.45 (s, 9H, a).

^{13}C NMR (75 MHz, $CDCl_3$) δ (ppm): 178.3 (c), 175.7 (i), 175.6 (i),172.3 (c), 152.6 (h), 152.5 (h), 97.7 (g), 83.8 (b), 83.3 (b), 58.3 (g), 46.5 (d), 46.4 (d), 30.3 (f), 28.4 (a), 28.3 (a), 24.2 (j), 23.1 (f), 22.9 (f), 21.4 (e), 21.3 (e), 20.0 (j).

HMRS (ESI): *m/z found* = 242.13852; calcd. for $[M+H]^+$: 242.13868.

FT-IR (cm^{-1}): 1688, 1134, 1298, 1756, 911.

*10.1.8.3 Deprotection of **76***

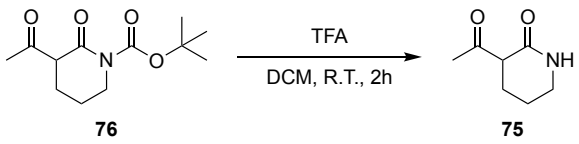

Procedure: In a round-bottom flask, compound **76** (96 mg, 0.4 mmol, 1.0 eq.) was dissolved in 2.2 mL of DCM. To this solution, TFA (0.115 mL, 1.5 mmol, 1.6 eq.) was added, and the mixture was stirred at room temperature for 2 hours. The product was concentrated under reduced

pressure, then a minimum amount of a chloroform/isopropanol (90/10) mixture was added. The solution was washed with saturated $NaHCO_3$ solution, followed by brine, and dried over $MgSO_4$. Finally, the product was concentrated under reduced pressure.

IUPAC names: 3-acetylpiperidin-2-one *and* (Z)-3-(1-hydroxyethylidene)piperidin-2-one

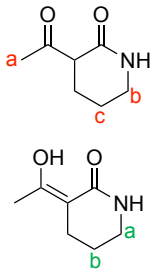

Yield for both tautomers: 55%

Mol. formula: $C_7H_{11}NO_2$

Mol. Wt.: 141.08 g.mol^{-1}

Aspect: beige powder

^{1}H NMR (300 MHz, $CDCl_3$) δ (ppm) (only characteristic peaks): 3.43 (b), 3.26 (a), 2.30 (a), 1.88 (c), 1.78 (b).

HMRS (ESI): *m/z found* = 142.08635; calcd. for $[M+H]^+$: 142.08626.

FT-IR (cm^{-1}): 1144, 1251, 1285, 1716, 1623.

*10.1.8.4 N-acylation of **75***

Reference: M. Feledziak, C. Michaux, A. Urbach, G. Labar, G. G. Muccioli, D. M. Lambert, J. Marchand-Brynaert, *J. Med. Chem.* **2009**, *52*, 7054-7068.

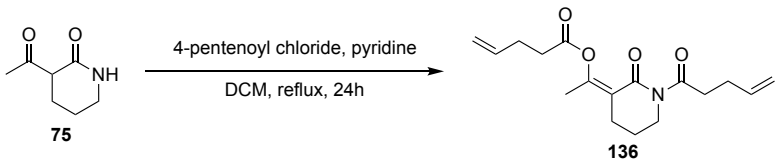

Procedure: In a dried three-neck round-bottom flask under inert conditions, **75** (127 mg, 0.9 mmol, 1.0 eq.) was dissolved in 10 mL of DCM.

Pent-4-enoyl chloride (190 mg, 1.6 mmol, 1.8 eq.) was added to the solution, followed by pyridine (0.153 mL, 1.9 mmol, 2.1 eq.). The mixture was stirred at 45°C for 24 hours. The product was washed with 10 mL of 10% Na_2CO_3 solution, then the organic layer was washed with 2 M HCl, followed by brine, and dried over $MgSO_4$. The crude product was purified by flash chromatography on silica gel using cyclohexane/AcOEt (70/30).

IUPAC name: (Z)-1-(2-oxo-1-(pent-4-enoyl)piperidin-3-ylidene)ethyl pent-4-enoate

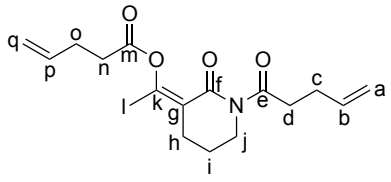

Yield: 45%

Mol. formula: $C_{17}H_{23}NO_4$

Mol. Wt.: 305.16 g.mol^{-1}

Aspect: beige powder

^{1}H NMR (300 MHz, $CDCl_3$) δ (ppm): 5.90 – 5.69 (m, 2 H, b, p), 5.10 – 4.85 (m, 4H, a, q), 3.71 – 3.63 (m, 2H, j), 3.01 (t, J = 7.4 Hz, 2H, h), 2.49 (m, 4H, d, n), 2.42 – 2.27 (m, 4H, c, o), 1.92 (s, 3H, l), 1.79 (m, 2H, i).

^{13}C NMR (75 MHz, $CDCl_3$) δ (ppm): 175.6 (e), 171.0 (m), 165.7 (f), 153.4 (g), 137.5 (p), 136.5 (b), 118.1 (k), 115.6 (a), 115.1 (q), 42.4 (j), 38.5 (h), 33.4 (d), 29.0 (c), 28.5 (o), 25.3 (n), 22.1 (i), 19.0 (l).

HMRS (ESI): *m/z found* = 306.16994; calcd. for $[M+H]^+$: 306.16998.

FT-IR (cm^{-1}): 1690, 1147, 1757, 1299, 164.

10.1.9 Preparation of β-lactam 117

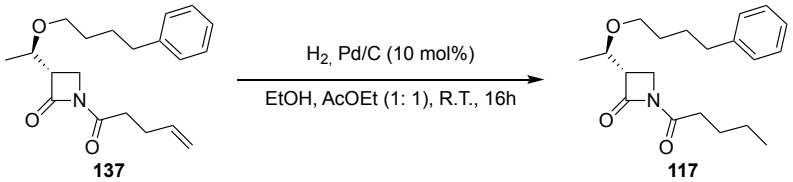

Procedure: In a dried round-bottom flask under inert conditions, Pd/C 10% (0.03 mmol, 1.0 eq.) was added, followed by a solution of **137** (10 mg, 0.03 mmol, 1.0 eq.), previously obtained by M. Feledziak,[3] in 1 mL of EtOH and 1 mL of AcOEt. The mixture was stirred at room temperature for 16 hours under a hydrogen atmosphere. The solution was filtered through a pad of celite and concentrated under reduced pressure.

IUPAC name: (*S*)-1-pentanoyl-3-((*R*)-1-(4-phenylbutoxy)ethyl)azetidin-2-one

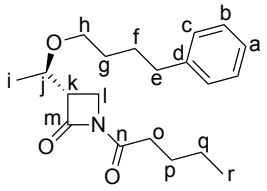

Yield: quantitative
Mol. formula: $C_{20}H_{29}NO_3$
Mol. Wt.: 331.46g.mol^{-1}
Aspect: yellow oil

^{1}H NMR (300 MHz, $CDCl_3$) δ (ppm): 7.35 – 7.05 (m, 5H,a, b, c), 3.88 – 3.74 (m, 1H, j), 3.66 – 3.52 (m, 2H, l), 3.43 -3.28 (m, 2H, h), 3.27 – 3.20 (m, 1H, k), 2.93 – 2.52 (massif, 4H, e, o), 1.70 – 1.51 (m, 4H, f, n), 1.45 – 1.14 (massif, 7H, g, i, q), 0.90 (t *J* = 7.4 Hz, 3H, r).

^{13}C NMR (75 MHz, $CDCl_3$) δ (ppm): 171.3 (n), 166.2 (m), 142.4 (d), 128.5 (a/b/c), 125,9 (a/b/c), 72.0 (j or k), 69.1, 55.0 (j or k), 39.6, 16.4, 35.8, 29.9, 28.2, 26.4, 22.4, 18.1 (i), 13.9 (r).

10.2 Pharmacology

10.2.1 Determination of IC_{50} values

10.2.1.1 General procedure

Mouse brain homogenates are obtained by homogenising mice brains (4°C, PBS, pH 7.4) and then centrifuging the resulting homogenate at 15 000g for 20 min. The resulting pellet was recovered, resuspended in PBS and centrifuged again (15 000g, 20 min). The resulting pellet was finally resuspended, the protein content determined, and the resulting membrane preparation stored at -80°C until use.

Tubes containing mouse brain homogenates (10 mM Tris-HCl, 1 mM EDTA, 0.1% (w/v) BSA, pH 7.4, 165 µL), the test compound (at concentrations ranging from 10^{-11} to 10^{-4} M) or DMSO alone for controls (10 µL) and the substrate (2 µM of AEA, 25µL) are incubated at 37°C for 10 minutes. The substrate consisted in unlabelled AEA and 1'[^{3}H]-AEA (50,000 dpm) used as tracer. The reactions are stopped by quickly placing the tubes on ice and adding 400 µL of a pre-cooled chloroform/methanol mixture (1:1 v/v). The tubes are then vigorously shaken, and the phases are separated by centrifugation at 850 g. The supernatant (200 µL of methanol/buffer) containing the released ethanolamine is collected and quantified by liquid scintillation counting (LSC). In all assays, tubes containing only the buffer are used as controls for 1'[^{3}H]-AEA non-enzymatic hydrolysis ("blank"). This value is systematically subtracted from the other results.

*10.2.1.2 Lead **35***

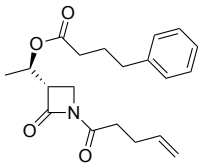

35

IC_{50}: 4.9 nM [3.8 – 6.4]

Calculated log P: 3.04

Calculated tPSA: 63.68

Log [inhibitor]	Compound 35 (lead) (% of activity)					
-11	104.08	103.82	109.71	107.39	92.2	92.73
-10	100.15	107.39	68.81	108.31	106.06	100.08
-9	92.1	86.51	92.83	92.97	84.1	104.28
-8	34.72	32.51	32.1	25.92	32	27.52
-7	4.95	4.69	5.5	4.9	7.44	12.24
-6	0.93	1.13	1.72	3.23	0.21	4.97
-5	1.23	1.06	1.08	2.17	-0.79	-0.58

*10.2.1.3 Bicycle **91a***

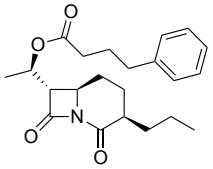

91a

IC_{50}: 55.0 nM [42.1 – 72.2]

Calculated log P: 3.76

Calculated tPSA: 63.68

Log [inhibitor]	Compound 91a (% of activity)					
-11	98,53	101,28	n.d.	n.d.	n.d.	n.d.
-10	101,46	102,76	104,82	142,04*	105,06	235,24*
-9	96,73	95,08	123,95	127,44	112,98	111,3
-8	83,89	85,83	111	107,66	103,15	110,77
-7,5	n.d.	n.d.	75,27	80,9	75,45	72,76
-7	22,38	21,65	37,2	35,22	21,34	33,32
-6	1,49	2,59	5,38	1,49	2,8	6,47
-5	1,57	0,74	-1,14	-0,29	0,85	0,62

*10.2.1.4 Bicycle **91b***

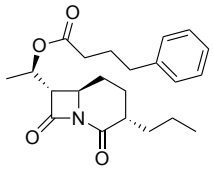

91b

IC_{50}: 197 nM [157 – 247]

Calculated log P: 3.76

Calculated tPSA: 63.68

Log [inhibitor]	Compound 91b (% of activity)					
-11	104.09	102.81	n.d.	n.d.	n.d.	n.d.
-10	99.71	101.2	104.82	110.31	88.57	-16.95*
-9	103.11	100.21	106.85	94.76	103.09	105.98
-8	97.16	100.71	110.85	104.07	104.88	79.75
-7	69.67	71.56	86.44	71.94	73.59	68.15
-6,5	n.d.	n.d.	25.53	24.4	39.41	28.41
-6	5.37	4.35	2.29	2.4	5.29	3.75
-5	1.62	2.03	-1.13	-3.57	-1.2	-0.5

*10.2.1.5 Bicycle ***104***

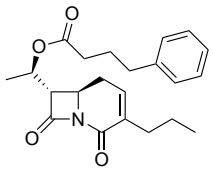

104

IC_{50}: 171 nM [122 – 240]

Calculated log P: 3.53

Calculated tPSA: 63.68

Log [inhibitor]	Compound 104 (% of activity)					
-11	105.14	104.53	109.84	109.6	94.07	106.49
-10	106.43	104.45	101.25	110.74	98.77	107.22
-9	99.9	105.57	81.71	103.47	98.36	99.59
-8	97.16	61.97	101.71	97.25	104.98	98.12
-7	65.68	47.24	64.89	68.61	77.42	81.31
-6	3.41	5.29	4.8	7.23	10.01	13.88
-5	1.19	1.54	3.6	7.56	2.11	6.27

*10.2.1.6 Mixture of enantiomers **35** and **116** (Fraction 1)*

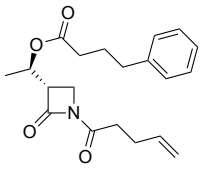

35

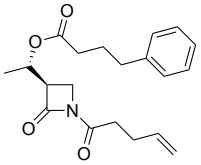

116

IC_{50}: 10.4 nM [8.6 – 12.9]

Calculated log P: 3.04 for both

Calculated tPSA: 63.68 for both

Log [inhibitor]	Mixture of compounds 35 and 116 (% of activity)					
-11	98.32	101.23	106.64	107.47	102.43	106.66
-10	100.41	100.32	115.15	112.77	104.18	109.02
-9	94.01	92.65	93.81	110.89	89.55	82.63
-8	52.89	51.1	60.83	55.36	47.68	66.88
-7	7.93	7.82	4.17	8.71	13.72	9.55
-6	0.74	0.77	0.98	-0.78	3.39	10.48
-5	1.24	0.77	2.13	0.22	7.35	1.02

*10.2.1.7 Mixture of stereoisomers **35**, **63**, **116** (and likely **115**)*

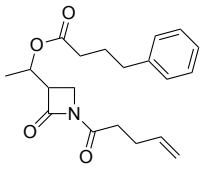

35, **63**, **115**, **116**

IC_{50}: 14.0 nM [12.1 – 16.2]

Calculated log P: 3.53 for all

Calculated tPSA: 63.68 for all

Log [inhibitor]	Mixture of compounds 35, 63, 116 (and 115) (% of activity)					
-11	103.22	103.3	105.73	106.06	99.79	104.58
-10	100.99	106.02	102.81	107.25	101.57	94.88
-9	96.17	109.95	94.85	100.59	95.79	103.28
-8	57.66	60.65	73.53	55.1	65.73	56.09
-7	9.71	9.43	9.56	7.66	8.69	8.98
-6	2.99	2.27	2.1	1.43	-0.22	4.95
-5	0.78	1.31	-0.39	0.02	-1.92	1.02

10.2.2 Cell studies

10.2.2.1 General procedure

The general procedure for the study of inhibitors in J774 macrophage cells, described below, is directly taken from M. Alhouayek, P. Bottemanne, A. Makriyannis, G. G. Muccioli, *Biochim. Biophys. Acta. Mol. Cell. Biol. Lipids* **2017**, *1862*, 474-484.

Cell culture

The murine macrophage cell line J774 was routinely cultured under standard conditions (37 °C in a humidified 5% CO_2 incubator) in RPMI 1640 medium containing 10% fetal bovine serum and antibiotics (100 units·mL^{-1} of penicillin and 100 µg·mL^{-1} of streptomycin).

NAE quantification by UPLC-MS/MS

Cells (10^7 cells/condition) were seeded in 10% FBS media for 16 h prior to the experiment. Then cells were incubated in media containing 1% FBS and the molecules of interest (10 μM) or vehicle (DMSO, 0.4%). At the end of the incubation, the media was removed and the cells recovered using PBS (2 mL) followed by methanol (MeOH, 4 mL) and transferred to dichloromethane (CH_2Cl_2) containing the internal standards (d_4-PEA; d_4-AEA; d_4-OEA; d_4-SEA; d_5-2-AG). Following vigorous mixing and sonication, the samples were centrifuged and the organic layer was recovered and then dried under a stream of N_2. The resulting lipid fraction was pre-purified by solid-phase extraction (SPE) over silica. Following a first step with hexane – iPOH (99 :1), the lipids of interest were eluted using hexane – iPOH (7: 3). the resulting lipid fractions were quantified according to the protocol used in previous studies, by using an UPLC system coupled to a Xevo-TQ-S Mass Spectrometer (Waters Corporation, Milford, Massachusetts, USA).[115] Analyte separation was achieved by using an Acquity UPLC BEH C18 column (1.7 mm, 2.1 × 50 mm; Waters Corporation) connected to an in-line filter unit and maintained at 40°C. Mobile phases A and B were composed of methanol-water-acetic acid (75:24.9:0.1, v/v/v) and methanol-acetic acid (99.9:0.1, v/v), respectively. The injection volume was 1 mL and the gradient 0.2 mL/min. An electrospray ionisation source in positive mode was used. For data acquisition and processing, the software MassLynx was used. For each compound of interest, the ratio between the analyte and the respective internal standard was determined. Calibration curves were established using similar conditions. The amounts of each compound were determined by linear interpolation from the calibration curve.

Materials

PF-3845 (N-3-pyridinyl-4-[[3-[[5-(trifluoromethyl)-2-pyridinyl]-oxy]phenyl]methyl]-1-piperidinecarboxamide) was purchased from Tocris

bioscience (R&D Systems Europe Ltd., Abingdon, UK). Deuterated NAE's were synthesised in the laboratory of Dr Muccioli following well established procedures.[116]

*10.2.2.2 2-AG **7** levels*

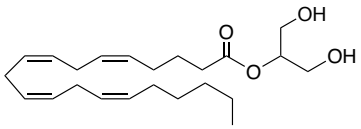

2-arachidonylglycerol (2-AG) **7**

2-AG levels (pmol/sample)					
Vehicle	**35 (lead)**	**91a**	**54**	**117**	**PF-3845**
28,09	29,04	24,41	37,07	29,39	26,34
24,62	29,47	24,50	31,51	28,56	27,31
22,14	24,61	26,18	31,34	27,64	25,36
18,97	29,19	20,34	24,27	20,82	28,11
17,33	24,59	21,38	19,98	21,33	26,12
18,47	22,98	23,51	25,79	22,81	28,10
18,48	20,85	n.d.	23,91	22,35	25,20
22,43	26,24	n.d.	26,74	26,04	25,07
22,99	30,19	n.d.	27,68	25,85	26,48

*10.2.2.3 AEA **6** levels*

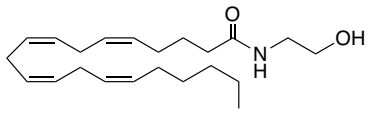

N-arachidonoylethanolamine (anandamide) **6**

AEA levels (pmol/sample)					
Vehicle	**35 (lead)**	**91a**	**54**	**117**	**PF-3845**
2,66	4,79	3,76	3,88	5,65	7,38
2,08	4,54	3,28	3,51	5,56	6,29
2,31	4,12	4,67	4,34	5,25	6,69
1,30	2,40	1,87	2,74	4,23	2,87
1,35	2,67	3,05	1,52	4,21	4,12
1,64	1,84	2,55	2,84	3,30	4,37
1,41	2,92	n.d.	1,76	4,90	4,40
2,17	3,20	n.d.	3,06	4,57	3,99
1,00	3,19	n.d.	3,14	3,89	4,03

*10.2.2.4 PEA **10** levels*

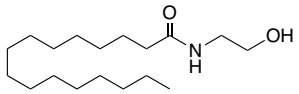

N-palmitoylethanolamine **10**

PEA levels (pmol/sample)					
Vehicle	**35 (lead)**	**91a**	**54**	**117**	**PF-3845**
1,02	1,20	1,86	1,81	4,27	16,58
0,34	0,68	1,00	1,18	4,25	17,91
0,68	0,94	0,98	1,36	3,19	15,64
2,52	2,54	3,60	4,58	7,26	16,62
2,40	2,95	3,80	3,85	6,30	16,30
2,43	2,55	5,01	2,93	5,57	16,34
3,21	3,22	n.d.	3,73	7,00	14,63
2,90	2,39	n.d.	3,98	6,48	13,37
2,28	2,40	n.d.	3,25	5,37	14,19

*10.2.2.5 SEA **12** levels*

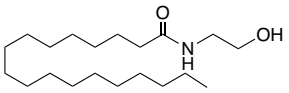

N-stearoylethanolamine **12**

SEA levels (pmol/sample)					
Vehicle	**35 (lead)**	**91a**	**54**	**117**	**PF-3845**
0,00	0,86	0,25	0,76	2,48	3,72
0,00	0,85	0,00	1,34	2,41	3,68
0,00	0,76	0,28	0,35	1,23	3,45
1,09	1,72	1,63	2,58	4,04	4,39
1,10	1,96	2,03	2,13	3,51	4,29
1,57	1,80	2,01	1,66	3,14	4,08
1,01	2,44	n.d.	2,06	3,77	4,06
1,38	1,72	n.d.	2,36	3,86	3,29
1,24	1,91	n.d.	1,53	3,40	3,79

*10.2.2.6 OEA **11** levels*

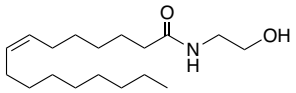

N-oleoylethanolamine **11**

SEA levels (pmol/sample)					
Vehicle	**35 (lead)**	**91a**	**54**	**117**	**PF-3845**
5,48	8,39	7,15	7,79	12,75	45,87
4,90	6,89	6,85	7,75	12,73	48,73
5,35	6,38	7,56	7,34	11,21	43,41
3,28	4,39	5,23	5,36	9,22	28,74
3,05	4,65	4,78	5,58	8,80	29,67
3,38	4,09	4,81	4,70	8,84	29,04
4,48	5,56	n.d.	6,06	11,04	34,56
4,36	5,15	n.d.	6,37	10,99	34,30
4,02	4,91	n.d.	5,53	10,18	32,02

10.3 Computational details

10.3.1 *Syn*/*trans* equilibrium

Calculations were performed using the Jaguar 8.5 suite of programs.[117] Density Functional Theory (DFT) was applied by the means of the B3LYP hybrid functional corrected for dispersion as proposed by Grimme (D3 correction). The 6-31+G(d) basis set was used for all atoms. Frequency calculations were performed to obtain free energy corrections. Solvent effects were modelled by using the polarisable continuum-Poisson method as incorporated in Jaguar, using the parameters for dichloromethane.

10.3.2 CD spectrum simulation of lead 35

First, the geometry of the molecule **35** was optimized with the DFT method using the ωB97X D exchange-correlation function and the 6-311G(d) basis set. Second, a conformer ensemble was generated at the GFN2-xTB//ALPB(chloroform) level of theory using the CREST algorithm.[118-122] Third, CENSO sorted out the conformers with respect to their free-energy,[123] and reoptimized their geometry with the r^2 SCAN 3c//COSMO-RS(chloroform) scheme.[124-125] For each conformer, the molecular orbitals and their energies were computed at the PBE0/6 31+G(d)//C-PCM Level of theory.[126] Finally, circular dichroism spectra for each conformer were computed at the XsTD DFT method (XsPBE0/6 31+G(d)).[127] Spectra were shifted by -0.93 eV and convoluted with Gaussians considering a droping factor of 0.20 eV at full width at half maximum, to best match experiment. The spectrum of the Boltzmann weighted sum over all conformers at 0 K, 50 K, 100 K, and 298.15 K were drawn and compared to experiment.

The geometry optimizations were performed using Turbomole 7.7.1,[128] CREST 3.0, xTB 6.7.0,[129] and CENSO 1.2.0 were used. Molecular

orbitals for XsTD-DFT calculations were computed with Q Chem 6.0.[130] XsTD-DFT calculations were computed with stda.[131]

10.3.3 Keto/enol equilibrium

Calculations were performed using the Jaguar 8.5 suite of programs.[117] Optimisation was performed at the M06-2X/6-31+G(d) level of theory. Solvent effects were modelled by using the polarisable continuum-Poisson method as incorporated in Jaguar, using the parameters for chloroform. Frequency calculations were carried out at the same level of theory to obtain free energy corrections. Gas phase electronic energies were recomputed at the M06-2X/6-311+G(d,p) level.

10.3.4 Docking

A model of the mouse FAAH was built, using SWISSMODEL, by homology with the crystal structure of the humanised-rat FAAH (pdb code:2VYA), as template. Docking of the inhibitors into the active site of the mouse FAAH was performed using GOLD. It is based on a genetic algorithm (GA), performing docking of flexible ligands into proteins with partial flexibility in the neighbourhood of the active site. The binding region was defined as a 17A° radius sphere centred on Leu_{192}. For the 20 GA runs performed, a total of 100 000 genetic operations were carried out on 5 islands, each containing 100 individuals. The solutions were ranked by the GOLD score. The GOLD fitness function is made up of four components: protein-ligand hydrogen bond energy, protein-ligand van der Waals energy, ligand internal van der Waals energy and ligand torsional strain energy. The figures were produced, and the H-bond lengths calculated using PyMOL.[132-133]

Bibliography

[1] M. Feledziak, Université catholique de Louvain (Louvain-La-Neuve), **2012**.

[2] J. Caruano, UCLouvain **2017**.

[3] M. Feledziak, G. G. Muccioli, D. M. Lambert, J. Marchand-Brynaert, *J. Med. Chem.* **2011**, *54*, 6812-6823.

[4] R. Mechoulam, in *Cannabinoids as Therapeutic Agents* (Ed.: ed. R Mechoulam), CRC Press, **2019**, pp. 1–20.

[5] D. P. Finn, S. Haroutounian, A. G. Hohmann, E. Krane, N. Soliman, A. S. C. Rice, *Pain* **2021**, *162*, S5-S25.

[6] D. M. Lambert, C. J. Fowler, *J. Med. Chem.* **2005**, *48*, 5059-5087.

[7] Y. Gaoni, R. Mechoulam, *J. Am. Chem. Soc.* **1964**, *86*, 1646-1647.

[8] H. Isbell, C. W. Gorodetzsky, D. Jasinski, U. Claussen, F. von Spulak, F. Korte, *Psychopharmacologia* **1967**, *11*, 184-148.

[9] R. Mechoulam, *Br. J. Pharmacol.* **2005**, *146*, 913-915.

[10] G. F. Mangiatordi, M. M. Cavalluzzi, P. Delre, G. Lamanna, M. C. Lumuscio, M. Saviano, J. P. Majoral, S. Mignani, A. Duranti, G. Lentini, *Biomedicines* **2023**, *11*, 469-487.

[11] A. J. Hill, C. M. Williams, B. J. Whalley, G. J. Stephens, *Pharmacol. Ther.* **2012**, *133*, 79-97.

[12] S. E. Turner, C. M. Williams, L. Iversen, B. J. Whalley, *Prog. Ch. Org. Nat. Prod.* **2017**, *103*, 61-101.

[13] D. A. Kendall, G. A. Yudowski, *Front. Cell. Neurosci.* **2017**, *10*, 294.

[14] A. C. Howlett, F. Barth, T. I. Bonner, G. Cabral, P. Casellas, W. A. Devane, C. C. Felder, M. Herkenham, K. Mackie, B. R. Martin, R. Mechoulam, R. G. Pertwee, *Pharmacol. Rev.* **2002**, *54*, 161-202.

[15] V. Di Marzo, M. Bifulco, L. De Petrocellis, *Nat. Rev. Drug. Discov.* **2004**, *3*, 771-784.

[16] C. Benito, R. M. Tolon, M. R. Pazos, E. Nunez, A. I. Castillo, J. Romero, *Br. J. Pharmacol.* **2008**, *153*, 277-285.

[17] L. A. Matsuda, S. J. Lolait, M. J. Brownstein, A. C. Young, T. I. Bonner, *Nature* **1990**, *346*, 561-564.

[18] K. Mackie, *Handb. Exp. Pharmacol.* **2005**, 299-325.

[19] S. Munro, K. L. Thomas, M. Abu-Shaar, *Nature* **1993**, *365*, 61-65.

[20] J. P. Alexander, B. F. Cravatt, *J. Am. Chem. Soc.* **2006**, *128*, 9699-9704.

[21] V. Lucas-Andrzejak, PhD, Université de Lille Norde de France (Lille), **2010**.

[22] A. Ulugol, *Balk. Med. J.* **2014**, *31*, 115-120.

[23] S. M. Stout, N. M. Cimino, *Drug Metab. Rev.* **2014**, *46*, 86-95.

[24] R. Christensen, P. K. Kristensen, E. M. Bartels, H. Bliddal, A. Astrup, *Lancet* **2007**, *370*, 1706-1713.

[25] *New Tools to Interrogate Endocannabinoid Signalling*, **2020**.

[26] N. van Egmond, V. M. Straub, M. van der Stelt, *Annu. Rev. Pharmacol. Toxicol.* **2021**, *61*, 441-463.

[27] A. Ward, B. Holmes, *Drugs* **1985**, *30*, 127-144.

[28] D. Piomelli, A. Mabou Tagne, *Annu. Rev. Pharmacol. Toxicol.* **2022**, *62*, 483-507.

[29] W. A. Devane, L. Hanus, A. Breuer, R. G. Pertwee, L. A. Stevenson, G. Griffin, D. Gibson, A. Mandelbaum, A. Etinger, R. Mechoulam, *Science* **1992**, *258*, 1946-1949.

[30] R. Mechoulam, S. Ben-Shabat, L. Hanus, M. Ligumsky, N. E. Kaminski, A. R. Schatz, A. Gopher, S. Almog, B. R. Martin, D. R. Compton, et al., *Biochem. Pharmacol.* **1995**, *50*, 83-90.

[31] A. C. Porter, J. M. Sauer, M. D. Knierman, G. W. Becker, M. J. Berna, J. Bao, G. G. Nomikos, P. Carter, F. P. Bymaster, A. B. Leese, C. C. Felder, *J. Pharmacol. Exp. Ther.* **2002**, *301*, 1020-1024.

[32] T. H. Burkey, R. M. Quock, P. Consroe, F. J. Ehlert, Y. Hosohata, W. R. Roeske, H. I. Yamamura, *Eur. J. Pharmacol.* **1997**, *336*, 295-298.

[33] C. L. Waldemar Gonsiorek, Xuedong Fan, Satwant Narula, Daniel Lundell, R. William Hipkin, *Mol. Pharmacol.* **2000**, *57*, 1045-1050.

[34] J. R. Savinainen, T. Jarvinen, K. Laine, J. T. Laitinen, *Br. J. Pharmacol.* **2001**, *134*, 664-672.

[35] H. S. Hansen, V. Vana, *Br. J. Pharmacol.* **2019**, *176*, 1443-1454.

[36] H. S. Hansen, *Pharmacol. Res.* **2014**, *86*, 18-25.

[37] J. Giacobbe, A. Marrocu, M. G. Di Benedetto, C. M. Pariante, A. Borsini, *Brain. Behav. Immun.* **2021**, *93*, 353-367.

[38] S. S. Hu, H. B. Bradshaw, V. M. Benton, J. S. Chen, S. M. Huang, A. Minassi, T. Bisogno, K. Masuda, B. Tan, R. Roskoski, Jr., B. F. Cravatt, V. Di Marzo, J. M. Walker, *Prostag. Leukotr. Ess.* **2009**, *81*, 291-301.

[39] D. M. Lambert, V. Di Marzo, *Curr. Med. Chem.* **1999**, *6*, 757-773.

[40] M. Feledziak, PhD, UCLouvain (Louvain-La-Neuve), **2012**.

[41] M. Kaczocha, S. T. Glaser, D. G. Deutsch, *Proc. Natl. Acad. Sci. U. S. A.* **2009**, *106*, 6375-6380.

[42] N. Ueda, K. Tsuboi, D. M. Lambert, *Neuropharmacology* **2005**, *48*, 1079-1085.

[43] J. L. Blankman, G. M. Simon, B. F. Cravatt, *Chem. Biol.* **2007**, *14*, 1347-1356.

[44] P. C. Schmid, M. L. Zuzarte-Augustin, H. H. Schmid, *J. Biol. Chem.* **1985**, *260*, 14145-14149.

[45] K. Katayama, N. Ueda, Y. Kurahashi, H. Suzuki, S. Yamamoto, I. Kato, *Biochim. Biophys. Acta.* **1997**, *1347*, 212-218.

[46] F. Desarnaud, H. Cadas, D. Piomelli, *J. Biol. Chem.* **1995**, *270*, 6030-6035.

[47] D. K. Giang, B. F. Cravatt, *Proc. Natl. Acad. Sci. U. S. A.* **1997**, *94*, 2238-2242.

[48] M. H. Bracey, M. A. Hanson, K. R. Masuda, R. C. Stevens, B. F. Cravatt, *Science* **2002**, *298*, 1793-1796.

[49] A. Morelle, J. Caruano, M. Feledziak, C.Michaux, E. A. Perpete, G. G. Muccioli, J. Marchand-Brynaert, R. Robiette, *Chimie Nouvelle* **2020**, *134*, 41-49.

[50] M. K. McKinney, B. F. Cravatt, *J. Biol. Chem.* **2003**, *278*, 37393-37399.

[51] M. Seierstad, J. G. Breitenbucher, *J. Med. Chem.* **2008**, *51*, 7327-7343.

[52] T. M. Gomes, D. Dias da Silva, H. Carmo, F. Carvalho, J. P. Silva, *Pharmacol. Res.* **2020**, *162*, 105237.

[53] D. Parolaro, N. Realini, D. Vigano, C. Guidali, T. Rubino, *Exp. Neurol.* **2010**, *224*, 3-14.

[54] T. Bisogno, N. Sepe, L. De Petrocellis, R. Mechoulam, V. Di Marzo, *Biochem. Bioph. Res. Co.* **1997**, *239*, 473-479.

[55] A. Stasiulewicz, K. Znajdek, M. Grudzien, T. Pawinski, A. J. I. Sulkowska, *Int. J. Mol. Sci.* **2020**, *21*, 2778-2824.

[56] G. Labar, C. Michaux, *Chem. Biodivers.* **2007**, *4*, 1882-1902.

[57] H. Lowe, N. Toyang, B. Steele, J. Bryant, W. Ngwa, *Int. J. Mol. Sci.* **2021**, *22*, 9472-9514.

[58] M. Mileni, J. Garfunkle, J. K. DeMartino, B. F. Cravatt, D. L. Boger, R. C. Stevens, *J. Am. Chem. Soc.* **2009**, *131*, 10497-10506.

[59] D. G. Deutsch, S. A. Chin, *Biochem. Pharmacol.* **1993**, *46*, 791-796.

[60] D. G. Deutsch, M. S. Goligorsky, P. C. Schmid, R. J. Krebsbach, H. H. Schmid, S. K. Das, S. K. Dey, G. Arreaza, C. Thorup, G. Stefano, L. C. Moore, *J. Clin. Invest.* **1997**, *100*, 1538-1546.

[61] S. Vandevoorde, D. Lambert, *Chimie Nouvelle* **2004**, *87*, 102-105.

[62] D. G. Deutsch, R. Omeir, G. Arreaza, D. Salehani, G. D. Prestwich, Z. Huang, A. Howlett, *Biochem. Pharmacol.* **1997**, *53*, 255-260.

[63] D. G. Deutsch, S. Lin, W. A. Hill, K. L. Morse, D. Salehani, G. Arreaza, R. L. Omeir, A. Makriyannis, *Biochem. Bioph. Res. Co.* **1997**, *231*, 217-221.

[64] D. L. Boger, H. Miyauchi, W. Du, C. Hardouin, R. A. Fecik, H. Cheng, I. Hwang, M. P. Hedrick, D. Leung, O. Acevedo, C. R. Guimaraes, W. L. Jorgensen, B. F. Cravatt, *J. Med. Chem.* **2005**, *48*, 1849-1856.

[65] A. H. Lichtman, D. Leung, C. C. Shelton, A. Saghatelian, C. Hardouin, D. L. Boger, B. F. Cravatt, *J. Pharmacol. Exp. Ther.* **2004**, *311*, 441-448.

[66] G. Tarzia, A. Duranti, A. Tontini, G. Piersanti, M. Mor, S. Rivara, P. V. Plazzi, C. Park, S. Kathuria, D. Piomelli, *J. Med. Chem.* **2003**, *46*, 2352-2360.

[67] M. Mor, S. Rivara, A. Lodola, P. V. Plazzi, G. Tarzia, A. Duranti, A. Tontini, G. Piersanti, S. Kathuria, D. Piomelli, *J. Med. Chem.* **2004**, *47*, 4998-5008.

[68] P. Bar-On, C. B. Millard, M. Harel, H. Dvir, A. Enz, J. L. Sussman, I. Silman, *Biochemistry* **2002**, *41*, 3555-3564.

[69] K. Otrubova, C. Ezzili, D. L. Boger, *Bioorg. Med. Chem. Lett.* **2011**, *21*, 4674-4685.

[70] D. Zhang, A. Saraf, T. Kolasa, P. Bhatia, G. Z. Zheng, M. Patel, G. S. Lannoye, P. Richardson, A. Stewart, J. C. Rogers, J. D. Brioni, C. S. Surowy, *Neuropharmacology* **2007**, *52*, 1095-1105.

[71] T. Matsumoto, M. Kori, J. Miyazaki, Y. Kiyota*, Vol. EP1813606A1* (Ed.: T. Pharmaceuticals), **2006**.

[72] K. Ahn, D. S. Johnson, L. R. Fitzgerald, M. Liimatta, A. Arendse, T. Stevenson, E. T. Lund, R. A. Nugent, T. K. Nomanbhoy, J. P. Alexander, B. F. Cravatt, *Biochemistry* **2007**, *46*, 13019-13030.

[73] A. Minkkila, S. M. Saario, H. Kasnanen, J. Leppanen, A. Poso, T. Nevalainen, *J. Med. Chem.* **2008**, *51*, 7057-7060.

[74] H. R. Chobanian, Y. Guo, P. Liu, M. D. Chioda, S. Fung, T. J. Lanza, L. Chang, R. K. Bakshi, J. P. Dellureficio, Q. Hong, M. McLaughlin, K. M. Belyk, S. W. Krska, A. K. Makarewicz, E. J. Martel, J. F. Leone, L. Frey, B. Karanam, M. Madeira, R. Alvaro, J. Shuman, G. Salituro, J. L. Terebetski, N. Jochnowitz, S. Mistry, E. McGowan, R. Hajdu, M. Rosenbach, C. Abbadie, J. P. Alexander, L. L. Shiao, K. M. Sullivan, R. P. Nargund, M. J. Wyvratt, L. S. Lin, R. J. DeVita, *ACS Med. Chem. Lett.* **2014**, *5*, 717-721.

[75] X. Wang, K. Sarris, K. Kage, D. Zhang, S. P. Brown, T. Kolasa, C. Surowy, O. F. El Kouhen, S. W. Muchmore, J. D. Brioni, A. O. Stewart, *J. Med. Chem.* **2009**, *52*, 170-180.

[76] A. Saha, A. Y. Shih, T. Mirzadegan, M. Seierstad, *J. Chem. Theory Comput.* **2018**, *14*, 5815-5822.

[77] R. Apodaca, J. G. Breitenbucher, A. Chambers, X. Deng, N. Hawryluk, J. Keith, N. Mani, J. Merit, J. Pierce, M. Seierstad, W. Xiao, *Vol. WO-2009105220-A1* (Ed.: J. P. NV), **2008**.

[78] C. S. S. T. (CSST), **2016**.

[79] D. C. D'Souza, J. Cortes-Briones, G. Creatura, G. Bluez, H. Thurnauer, E. Deaso, K. Bielen, T. Surti, R. Radhakrishnan, A. Gupta, S. Gupta, J. Cahill, M. A. Sherif, A. Makriyannis, P. T. Morgan, M. Ranganathan, P. D. Skosnik, *Lancet Psychiatry* **2019**, *6*, 35-45.

[80] M. E. Klein, A. Bangerter, R. J. Halter, K. Cooper, Z. Aguilar, C. M. Canuso, W. C. Drevets, M. E. Schmidt, G. Pandina, *Neuropsychopharmacology* **2024**.

[81] A. Urbach, Université catholique de Louvain (Louvain-La-Neuve), **2006**.

[82] M. Feledziak, C. Michaux, A. Urbach, G. Labar, G. G. Muccioli, D. M. Lambert, J. Marchand-Brynaert, *J. Med. Chem.* **2009**, *52*, 7054-7068.

[83] R. K. P. Tripathi, *Eur. J. Med. Chem.* **2020**, *188*, 111953-111993.

[84] J. E. Hugonnet, J. S. Blanchard, *Biochemistry* **2007**, *46*, 11998-12004.

[85] M. Lee, D. Hesek, M. Suvorov, W. Lee, S. Vakulenko, S. Mobashery, *J. Am. Chem. Soc.* **2003**, *125*, 16322-16326.

[86] D. L. Boger, H. Sato, A. E. Lerner, M. P. Hedrick, R. A. Fecik, H. Miyauchi, G. D. Wilkie, B. J. Austin, M. P. Patricelli, B. F. Cravatt, *Proc. Natl. Acad. Sci. U. S. A.* **2000**, *97*, 5044-5049.

[87] D. Leung, C. Hardouin, D. L. Boger, B. F. Cravatt, *Nat. Biotechnol.* **2003**, *21*, 687-691.

[88] J. Caruano, M. Feledziak, G. Labar, C. Michaux, E. A. Perpete, G. G. Muccioli, R. Robiette, J. Marchand-Brynaert, *J. Enzym. Inhib. Med. Ch.* **2014**, *29*, 654-662.

[89] M. Feledziak, C. Michaux, D. M. Lambert, J. Marchand-Brynaert, *Eur. J. Med. Chem.* **2013**, *60*, 101-111.

[90] C. H. Di Tomaso E., Gaillet S., Beltramo M., Desarnaud F., Venance L., Piomelli D., in *Eicosanoids and other bioactive lipids in cancer, inflamation and radiation injury 3, Vol. 407* (Ed.: M. L. J. Honn K.. V., Nigam S., Jones R. L., Wong P. Y.-K.), Advances in experimental medicine and biology, **1997**, pp. 335-340.

[91] O. Vander Auwera, Master, UCLouvain (Louvain-La-Neuve), **2015**.

[92] S.-K. Kang, T.-G. Baik, X.-H. Jiao, K.-J. Lee, C. H. Lee, *Synlett* **1999**, 447-449.

[93] M. E. Geherty, PhD, University of Pittsburgh (Pittsburgh), **2012**.

[94] T. Tsuda, H. Satomi, T. Hayashi, T. Saegusa, *J. Org. Chem.* **1987**, *52*, 439-443.

[95] P. Y. Bruice, in *Chimie organique* (Ed.: Pearson), **2012**, p. 720.

[96] G. Sabitha, G. Chandrashekhar, K. Yadagiri, J. S. Yadav, *Tetrahedron-Asymmetr.* **2011**, *22*, 1729-1735.

[97] J. Dechenne, Master, UCLouvain (Louvain-La-Neuve), **2020**.

[98] C. F. Riber, A. H. F. Andersen, L. A. Rolskov, K. Zuwala, P. Gajda, K. B. Lovschall, F. Dagnaes-Hansen, D. H. Banda, T. Pietschmann, M. Tolstrup, A. N. Zelikin, *ACS Macro Lett.* **2017**, *6*, 935-940.

[99] L. Wu, F. Wang, P. Chen, G. Liu, *J. Am. Chem. Soc.* **2019**, *141*, 1887-1892.

[100] A. Morelle, Master, UCLouvain (Louvain-La-Neuve), **2018**.

[101] P. B. Finn, B. P. Derstine, S. M. Sieburth, *Angew. Chem. Int. Ed. Engl.* **2016**, *55*, 2536-2539.

[102] C. Crauste, M. Froeyen, J. Anné, P. Herdewijn, *Eur. J. Org. Chem.* **2011**, *2011*, 3437-3449.

[103] R. J. Cherney, L. Wang, *J. Org. Chem.* **1996**, *61*, 2544-2546.

[104] G. Huang, S. Schramm, J. Heilmann, D. Biedermann, V. Kren, M. Decker, *Beilstein J. Org. Chem.* **2016**, *12*, 662-669.

[105] W. Yang, X. Sun, W. Yu, R. Rai, J. R. Deschamps, L. A. Mitchell, C. Jiang, A. D. MacKerell, Jr., F. Xue, *Org. Lett.* **2015**, *17*, 3070-3073.

[106] Y. Lou, Y. Hu, J. Lu, F. Guan, G. Gong, Q. Yin, X. Zhang, *Angew. Chem. Int. Ed. Engl.* **2018**, *57*, 14193-14197.

[107] K. Moriyama, Y. Nakamura, H. Togo, *Org. Lett.* **2014**, *16*, 3812-3815.

[108] F. Rombouts, D. Franken, C. Martínez-Lamenca, M. Braeken, C. Zavattaro, J. Chen, A. A. Trabanco, *Tetrahedron Lett.* **2010**, *51*, 4815-4818.

[109] S. Degueldre, Master, UCLouvain (Louvain-La-Neuve), **2021**.

[110] D. K. Winter, A. Drouin, J. Lessard, C. Spino, *J. Org. Chem.* **2010**, *75*, 2610-2618.

[111] U. Ragnarsson, L. Grehn, *RSC Adv.* **2013**, *3*, 18691-18697.

[112] M. Kenny, J. Christensen, S. J. Coles, V. Franckevicius, *Org. Lett.* **2015**, *17*, 3926-3929.

[113] M. Alhouayek, P. Bottemanne, A. Makriyannis, G. G. Muccioli, *Biochim. Biophys. Acta* **2017**, *1862*, 474-484.

[114] P. Tsoungas, N. Assimomytis, Y. Sariyannis, G. Stavropoulos, G. Varvounis, P. Cordopatis, *Synlett* **2009**, *2009*, 2777-2782.

[115] A. Romano, M. Friuli, B. Eramo, C. A. Gallelli, J. B. Koczwara, E. K. Azari, A. Paquot, M. Arnold, W. Langhans, G. G. Muccioli, T. A. Lutz, S. Gaetani, *Front. Endocrinol. (Lausanne)* **2023**, *14*, 1158287-1159299.

[116] G. G. Muccioli, C. Xu, E. Odah, E. Cudaback, J. A. Cisneros, D. M. Lambert, M. L. Lopez Rodriguez, S. Bajjalieh, N. Stella, *J. Neurosci.* **2007**, *27*, 2883-2889.

[117] *Jaguar 8.5, Schrodinger, Inc., New York, NY,* **2014**.

[118] C. Bannwarth, S. Ehlert, S. Grimme, *J. Chem. Theory Comput.* **2019**, *15*, 1652-1671.

[119] S. Ehlert, M. Stahn, S. Spicher, S. Grimme, *J. Chem. Theory Comput.* **2021**, *17*, 4250-4261.

[120] P. Pracht, S. Grimme, C. Bannwarth, F. Bohle, S. Ehlert, G. Feldmann, J. Gorges, M. Muller, T. Neudecker, C. Plett, S. Spicher, P. Steinbach, P. A. Wesolowski, F. Zeller, *J. Chem. Phys.* **2024**, *160*, 114110-114138.

[121] P. Pracht, F. Bohle, S. Grimme, *Phys. Chem. Chem. Phys.* **2020**, *22*, 7169-7192.

[122] S. Grimme, *J. Chem. Theory Comput.* **2019**, *15*, 2847-2862.

[123] S. Grimme, F. Bohle, A. Hansen, P. Pracht, S. Spicher, M. Stahn, *J. Phys. Chem. A.* **2021**, *125*, 4039-4054.

[124] S. Grimme, A. Hansen, S. Ehlert, J. M. Mewes, *J. Chem. Phys.* **2021**, *154*, 064103.

[125] A. Klamt, F. Eckert, W. Arlt, *Annu. Rev. Chem. Biomol. Eng.* **2010**, *1*, 101-122.

[126] B. Mennucci, J. Tomasi, R. Cammi, J. R. Cheeseman, M. J. Frisch, F. J. Devlin, S. Gabriel, P. J. Stephens, *J. Phys. Chem. A.* **2002**, *106*, 6102-6113.

[127] M. de Wergifosse, S. Grimme, *J. Chem. Phys.* **2024**, *160*, 204110.

[128] TURBOMOLE V7.7 2022, a development of University of Karlsruhe and Forchungszentrum Karlsruhe GmbH, 1989-2007, TURBOMOLE GmbH, since 2007, available from https://www.turbomole.org.

[129] The development of the xtb code can be obtained from https://github.com/grimme-lab/xtb.

[130] E. Epifanovsky, A. T. B. Gilbert, X. Feng, J. Lee, Y. Mao, N. Mardirossian, P. Pokhilko, A. F. White, M. P. Coons, A. L. Dempwolff, Z. Gan, D. Hait, P. R. Horn, L. D. Jacobson, I. Kaliman, J. Kussmann, A. W. Lange, K. U. Lao, D. S. Levine, J. Liu, S. C. McKenzie, A. F. Morrison, K. D. Nanda, F. Plasser, D. R. Rehn, M. L. Vidal, Z. Q. You, Y. Zhu, B. Alam, B. J. Albrecht, A. Aldossary, E. Alguire, J. H. Andersen, V. Athavale, D. Barton, K. Begam, A. Behn, N. Bellonzi, Y. A. Bernard, E. J. Berquist, H. G. A. Burton, A. Carreras, K. Carter-Fenk, R. Chakraborty, A. D. Chien, K. D. Closser, V. Cofer-Shabica, S. Dasgupta, M. de Wergifosse, J. Deng, M. Diedenhofen, H. Do, S. Ehlert, P. T. Fang, S. Fatehi, Q. Feng, T. Friedhoff, J. Gayvert, Q. Ge, G. Gidofalvi, M. Goldey, J. Gomes, C. E. Gonzalez-Espinoza, S. Gulania, A. O. Gunina, M. W. D. Hanson-Heine, P. H. P. Harbach, A. Hauser, M. F. Herbst, M. Hernandez Vera, M. Hodecker, Z. C. Holden, S. Houck, X. Huang, K. Hui, B. C. Huynh, M. Ivanov, A. Jasz, H. Ji, H. Jiang, B. Kaduk, S. Kahler, K. Khistyaev, J. Kim, G. Kis, P. Klunzinger, Z. Koczor-Benda, J. H. Koh, D. Kosenkov, L. Koulias, T. Kowalczyk, C. M. Krauter, K. Kue, A. Kunitsa, T. Kus, I. Ladjanszki, A. Landau, K. V.

Lawler, D. Lefrancois, S. Lehtola, et al., *J. Chem. Phys.* **2021**, *155*, 084801.

[131] The stda program can be obtained from https://github.com/grimme-lab/stda.

[132] G. Jones, P. Willett, R. C. Glen, A. R. Leach, R. Taylor, *J. Mol. Biol.* **1997**, *267*, 727-748.

[133] *The PyMOL Molecular Graphics System, Version 3.0.2, Schrödinger, LLC.*